Effects of Electric Fields on Forces between Dielectric Particles in Air

Ching-Wen Chiu

Thesis submitted to the faculty of the Virginia Polytechnic Institute and State University in partial fulfillment of the requirements for the degree of

Master of Science
In
Chemical Engineering

William A. Ducker
James R. Heflin
Chang Lu
Stephen M. Martin

May 1st, 2013
Blacksburg, VA

Keywords: Electric field-induced force, dielectrophoresis, Maxwell-Wagner interfacial relaxation, AFM

Effects of Electric Fields on Forces between Dielectric Particles in Air

Ching-Wen Chiu

Abstract

We developed a quantitative measurement technique using atomic force microscopy (AFM) to study the effects of both DC and AC external electric fields on the forces between two dielectric microspheres. In this work we measured the DC and AC electric field-induced forces and adhesion force between two barium titanate ($BaTiO_3$) glass microspheres in a low humidity environment by this technique. The objective here is to find out the correlation between these measured forces and applied field strength, frequency, and the separation distance between the two spheres was studied. Since the spheres would oscillate under an AC field, the AC field-induced force was divided into dynamic component (i.e., time-varying term) and static component (i.e., time-averaged term) to investigate. The oscillatory response occurs at a frequency that is twice the drive frequency since the field-induced force is theoretically proportional to the square of the applied field. This behavior can be observed in the fast Fourier transformation (FFT) spectra of the time series of the deflection signal. The magnitude of the vibration response increases when the frequency of the drive force is near resonant frequency of the particle-cantilever probe. The amplitude of this vibration increases with proximity of the two particles, and ultimately causes the particles to repeatedly hit each other as in tapping mode AFM.

The effect of the Maxwell-Wagner interfacial relaxation on the DC electric field-induced force was discovered by monitoring the variation of the field-induced force with time. The static component of the AC electric field-induced force does not vary with the applied frequency in the range from 1 to 100 kHz, suggesting that the crossover frequency may equal to or less than 1 kHz and the permittivities of the $BaTiO_3$ glass microspheres and medium dominate the field-

induced force. The AC field-induced force is proportional to the square of the applied electric field strength. This relationship persists even when the separation between the spheres is much smaller than the diameter of the microspheres. The large magnitude of the force at small separations suggests that the local field is distorted by the presence of a second particle, and the continued dependence on the square of the field but the measured force is much larger than the theoretical results, suggesting that the local electric field around the closely spaced spheres is distorted and enhanced but the effects of the local field distortion may have not much to with the applied electric field. Compared with the calculated results from different models, our results demonstrate that the field-induced force is much more long-range than expected in theory. In addition, the DC field-induced adhesion force is larger than the AC field-induced one due to the interfacial charge accumulation, agreeing with the discovery of the Maxwell-Wagner interfacial relaxation effect on the DC field-induced force. No obvious correlation between the field-induced adhesion and the applied frequency is found. However, both the DC and AC field-induced adhesion forces display the linearity with the square of the applied electric field strength as well.

Acknowledgements

I would like to thank Dr. William Ducker for his guidance and generous funding from ACS PRF. In addition, I would like to thank Diane, Tina, and Nora for the help with the school and administrative matters. Thanks my labmates and Riley for the help and assistance with the experimental matters. Last I would like to thank my friends and parents for their support during these years.

Table of Contents

List of symbols

A, B	coefficients of dipole solution for potential in Eq. (3.5) and Eq. (3.6)
A'	area of the electrode plate and the cantilever in Eq. (6.2)
A_c	effective capacitance area
C	capacitance of capacitor
C_c	contact capacitance at the interface between particles
C_p	self-particle capacitance
$\vec{D}$	electric flux density vector or electric displacement vector (unit: Cm^{-2})
D	distance between the two subjects in Eq. (5.7)
$\vec{E}$	electric field vector
E_0	external applied electric field
E_{rms}	root mean square value of electric field
E_{rm}	normal electric field components in fluid
E_{rp}	normal electric field components in particle
$\vec{F}_{DEP}$	dielectrophreitc force vector
F_{DC}	DC electric force
$\vec{F}_{dipole}$	net force vector on an infinitesimal dipole in a non-uniform electric field
F_{el}	electrostatic force
F_{ext}	external force on particle
F_{in}	AC electric field-induced force
$\vec{F}_{ij}$	field-induced force vector between two particles i and j in Maxwell-Wagner model
F_{opt}	force of the optical trap acting the same force with opposite direction to balance the external force
F_{ω}	force at electric pulsation ω
$F_{2\omega}$	force at electric pulsation 2ω
G	gap between the two electrodes
K	Calusius-Mossotti function as defined by Eq. (3.12)
$\underline{K}(\omega)$	complex Calusius-Mossotti function as defined by Eq. (T3.2)
$K^{(n)}$	Calusius-Mossotti function of n^{th} order linear multipole defined by Eq. (T3.6)
K_1, K_2	constants account for effective capacitance area, distributed capacitance, curvature of particles, and the average contact separation distance
R	radius of spherical particle
R_1, R_2	radii of the two subjects respectively
R_c	particle contact resistance (i.e., resistance of the air between the two particles
R_p	single particle resistance
T	Temperature

U_{el}	energy stored in a parallel plated capacitor
V	applied voltage
V_0	equilibrium voltage to levitate particle for DEP levitation
V_1	voltage between the cantilever and the bottom electrode
$V_{1,0}$	maximum voltage between the cantilever and the bottom electrode
V_2	voltage between the cantilever and the top electrode
$V_{2,0}$	maximum voltage between the cantilever and the top electrode
V_c	AC (or DC as $\omega \to 0$) voltage drop across the contact capacitance
V_{CPD}	voltage of contact potential difference (CPD) between the tip and the sample surface
V_{DC}	DC-voltage
V_{AC}	AC-voltage
W	interaction free-energy
a	ratio of radii of spherical shell
$\vec{d}$	vector distance between charges in finite dipole
d	particle diameter
d	separation or distance between the colloidal probe and the surface
$\vec{e}_i$	unit vector in the i direction
f	Frequency
f_0	drive/applied frequency
f_r	resonant frequency
g	gravitational acceleration (9.81 m/s^2)
g'	gap between the cantilever and the bottom electrode
i , j	notations of two identical spheres in Maxwell-Wagner model
j	square root of minus one; $j = \sqrt{-1}$
k	stiffness/spring constant of a AFM cantilever
k_{opt}	optical trap stiffness
m_b	buoyant mass of particle in fluid
$\vec{p}$	electric dipole moment vector
$p^{(n)}$	moment of nth order liner multipole
p_{eff}	effective electric dipole moment
q	electric charge
$\vec{r}$	position vector
r'	radius of effective capacitance area A_c
r_c	particle contact radius
r_{ij}	separation between the centers of the particles i and j in Maxwell-Wagner model
x	displacement of particle from its equilibrium position

x	calibrated and converted deflection signal
x_c	separation distance between the closest apexes of the particles.
z	displacement of the cantilever
Ω	slope of the constant compliance region
α	fluidized bed voidage
α_0 , α_1	coefficients depending on the geometry and spacing of the electrodes in the DEP levitation
δ , β , γ	constants in Eq. (3.36) and Eq. (3.37)
β_{eff}	effective relative polarizability as defined by Eq. (3.21) and Eq. (3.22)
δ_1, δ_2	δ_1 and δ_2 are defined as $\tan\delta_1 = 1/\omega\tau_b$ and $\tan\delta_2 = 1/\omega\tau_p$
ε	Permittivity
$\underline{\varepsilon}$	complex permittivity
ε'	real part f complex permittivity
ε''	negative imaginary part of complex permittivity
ε_0	permittivity of free space (8.854×10^{-12} F/m)
ε_1	permittivity of ohmic dielectric fluid where the particles suspend
ε_2	permittivity of ohmic dielectric spherical particle
ε_m	permittivity of lossless dielectric fluid where the particles suspend
ε_p	permittivity of lossless dielectric spherical particle
$\bar{\varepsilon}_p$	corresponding bulk powder permittivity
θ	polar angle in spherical coordinates
θ_{ij}	angle between the line-of-center of the particles i and j and the electric field in Maxwell-Wagner model
ρ	volume charge density
ρ_b	apparent bulk powder resistivity
ρ_p	apparent (single) particle resistivity
σ	electrical conductivity
σ_1	electrical conductivity of ohmic medium where the particles suspend
σ_2	electrical conductivity of ohmic spherical particle
σ_m	electrical conductivity of lossless dielectric fluid where the particles suspend
σ_p	electrical conductivity of lossless dielectric spherical particle
σ_s	surface electrical conductivity of particle
τ_b	particle-particle relaxation time for transient decay of charge between two particles
τ_{MW}	Maxwell-Wagner relaxation time
τ_p	self-particle charge relaxation time for transient decay of charge within a particle
τ_{pc}	particle contact relaxation time
ϕ	scalar electric potential (unit: volts)

ϕ_{dipole}	dipolar electric potential
ϕ_m	electric potential within fluid
ϕ_p	electric potential within particle
ϕ_{tip}	work function of tip
ϕ_{smaple}	work function of sample
φ	volume fraction of noninteracting spherical particles in a medium
ω	radian frequency of electric field
ω_{AC}	frequency of an AC electric field to excited the tip in a Kelvin Probe Force Microscopy (KPFM)

List of Figures

List of Tables

Chapter 1 – Introduction

1.1 Literature Review and Thesis Motivation

The forces between microparticles induced by an external electric field play an important role in many areas, such as powder contamination in the semiconductor industry, xerography,[1] electric field stabilized fluidized bed,[2] electrostatic separation,[3] electrorheological fluids[4,5] and micro- and nano-electromechanical systems (MEMS and NEMS).[6] Although there are numerous studies on surface and interfacial phenomena of particles, not many are related to the effects of external electric fields, and even fewer studies on the closely spaced microparticles under an electric field where the point-dipole approximation may fail. One of the reasons for the lack of study in this area is the limits of the measurement techniques. So far, the measurement techniques for studying the electric-field induced interactions and/or forces are mainly dielectrophoretic (DEP) levitation, optical tweezers, atomic force microscopy (AFM) and some home-built apparatus.

Dielectrophoretic (DEP) levitation is principally used to study the field-induced effective dipole moment and Calusius-Mossotti function of single microparticles and microparticle chains, which both are proportional to the electric field-induced force (i.e, dielectrophoretic force, which will be introduced in detail in Chapter 3).[7,8] The principle of the DEP levitation is to adjust the applied voltage and frequency so that the electric field induced force would be equal to the buoyant force with opposite direction, levitating the particle(s).[7] The reduced equation of motion for the levitated particle(s) in an equilibrium condition can be expressed as

$$0 = -m_b g + 4\pi R^3 \varepsilon_1 \,\mathrm{Re}[\underline{K}(\omega)]\alpha_0 \alpha_1 V_0^2 \qquad (1.1)$$

where m_b is the buoyant mass of particle(s), g is gravitational acceleration, R is it the radius of the levitated particles, ε_1 is dielectric constant of the medium where the particles suspend, $\underline{K}(\omega)$ is the Calusius-Mossotti function and it is a complex number if the applied field is an AC field, $\mathrm{Re}[\underline{K}(\omega)]$ means the real part of the Calusius-Mossotti function, α_0 and α_1 are the coefficients depending on the geometry and spacing of the electrodes, and V_0 is the applied voltage.[7] Figure 1-1 depicts a typical DEP levitation system. However, the density of individual microparticles used for calculating the buoyant mass is hard to determine due to their small size.[7] Furthermore,

the DEP levitator cannot control the separation between the particles; it is thus not able to study the correlation of the particle chains and the separation between/among the particles.

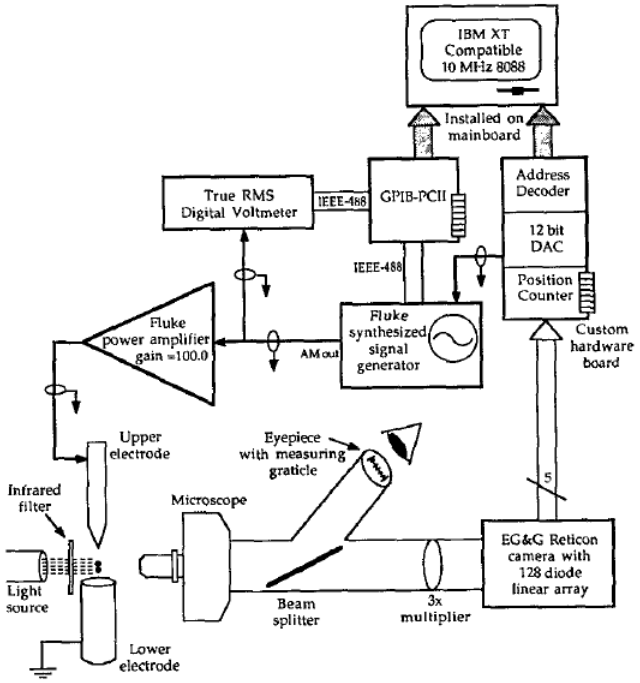

Figure 1-1 Schematic of a digital active feedback controlled DEP levitation system [Tombs, T. N.; Jones, T. B., DIGITAL DIELECTROPHORETIC LEVITATION. *Review of Scientific Instruments* **1991**, *62* (4), 1072-1077.][8] (Used under fair use, 2013)

Wang *et al.* have developed a home-built apparatus to control the separation between the particles and which is able to directly measure the electric field-induced forces between two particles in both liquid and gaseous media as shown in Figure 1-2.[9,10,11] Nevertheless, the size of the particle they used is around 6 mm and the smallest of the separation between the particles is 0.01 mm, which cannot truly show the field-induced interaction between closely spaced microparticles. Rankin *et al.* have modified a rheometer for the application of an electric field so as to study the electric field polarization mechanisms of electrorheological behavior.[12] The parameter they measured is the yield stress of a solution of $BaTiO_3$ with diameters in the range 53-90 μm and silicone oil under an electric field. However, the modified rheometer only can be used to study the collective behavior of microparticles in fluids, not the behavior of individual particles. Besides, the separation between the particles cannot be controlled by this technique.

Therefore, it is very difficult to extract the fundamental force-separation data from their experiment.

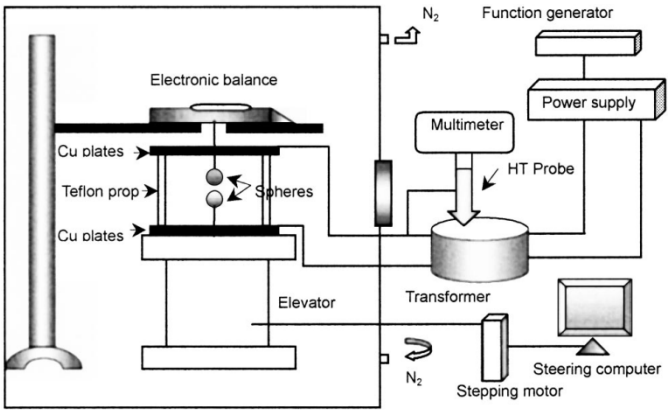

Figure 1-2 Schematic of an apparatus for measuring electric field-induced force between two particles with a computer-controlled elevator to adjust the separation between the particles [Wang, Z. Y.; Peng, Z.; Lu, K. Q.; Wen, W. J., Experimental investigation for field-induced interaction force of two spheres. *Applied Physics Letters* **2003**, *82* (11), 1796-1798.][9] (Used under fair use, 2013)

Several research groups[13,14,15] have adapted optical tweezers to truly investigate the interaction between individual microparticles under an electric field. Optical tweezers basically use a laser beam to manipulate particles ranged in diameter from ~20 nm to several micrometers.[16,17] Because of the dual nature of light, the mechanism of manipulating particles by a laser beam can be explained from the particle and wave viewpoints respectively. From the aspect of the particle nature of light, when light irradiates particles, light would be scattered and absorbed by the particles, depending on the refractive indexes of the particles and the medium. The change in direction and magnitude of photon momentum causes an equal and opposite change in the particle momentum, applying a force to the particle.[16] The displacement of the particles from their own equilibrium position is proportional to the force of the optical trap so the trap can be taken as a linear spring and used to measure external forces on the particles, as shown in Figure 1-3. The "spring constant" of the optical trap (i.e., optical trap stiffness) depends on the optical gradient (i.e., how tightly the laser is focused), the laser power, the size and optical properties of the trapped particles and the optical properties of the medium.[16,17] However, the magnitude of the force that optical tweezers can measure is ranged from femtonewtons to piconewtons.[17] Thus, it is not suitable to use optical tweezers to study strong electric field-induced force. Also, local heating due to the high power laser beam may damage the particles

and affect flow and the viscosity if the medium is liquid, thus causing artificial effects in the measuring results. In addition, the commercial optical tweezers usually do not have the position detection so extra modification and setup are necessary.

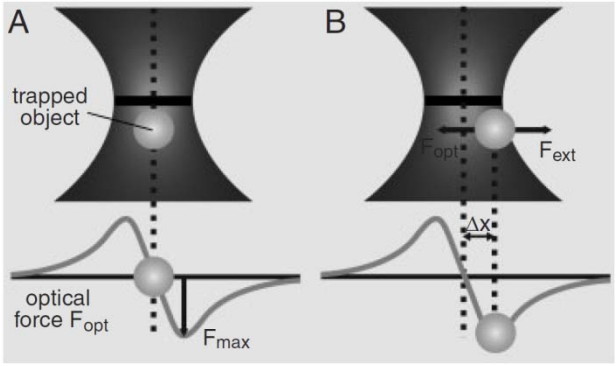

Figure 1-3 The principal of measuring an external force on a particle by an optical trap. (A) There is no external force acting on the particle so the particle is at its equilibrium position and the net force from the optical trap is zero. (B) The particle deviates from its equilibrium position due to an external force (F_{ext}) and the force of the optical trap (F_{opt}) acting the same force with opposite direction to balance the external force. $-F_{ext} = F_{opt} = -k_{opt}\Delta x$, where k_{opt} is the optical trap stiffness. [Jonas, A.; Zemanek, P., Light at work: The use of optical forces for particle manipulation, sorting, and analysis. *Electrophoresis* **2008,** *29* (24), 4813-4851.][16] (Used under fair use, 2013)

Another potential technique able to truly study the polarization and interaction of microparticles under an electric field is atomic force microscopy (AFM). The principle of the surface force measurement by AFM is that a microparticle is glued to a cantilever, creating a "colloidal probe." The forces on the microparticle are determined by measuring the deflection of the spring. A laser beam is reflected from the spring and a built-in photodiode reads the deflection of the spring, which is proportional to the force. The measured force can range from piconewtons to micronewtons, depending on the stiffness of the chosen cantilever, and the force measurement can be employed either in a gaseous medium or in a liquid medium. In contrast to the aforementioned techniques, the separation between particles can be changed in an AFM easily by using its built-in piezo and feedback loop system. Mizes *et al.* at Xerox have modified an AFM to investigate the effects of external direct-current (DC) electric field on the adhesion of different individual microparticles to an electrode (Figure 1-4 (A)) so as to understand the mechanism of toners behaviors in the xerographic process.[18,19] Later on, Kwek *et al.* modified Mizes' setup to study DC electric field-induced force of a charged and a uncharged particle

respectively by varying the position of the microparticles between the parallel condenser electrodes as shown in Figure 1-4 (B).[20] All the measurements by Mizes *et al.* and Kwek *et al.* were in ambient environment, which are strongly influenced by water adsorbed on the particle, and were measured in the presence of a DC field, not an alternating-current (AC) field, which make them strongly influenced by surface conductivity.[21,22,23]

(A) (B)

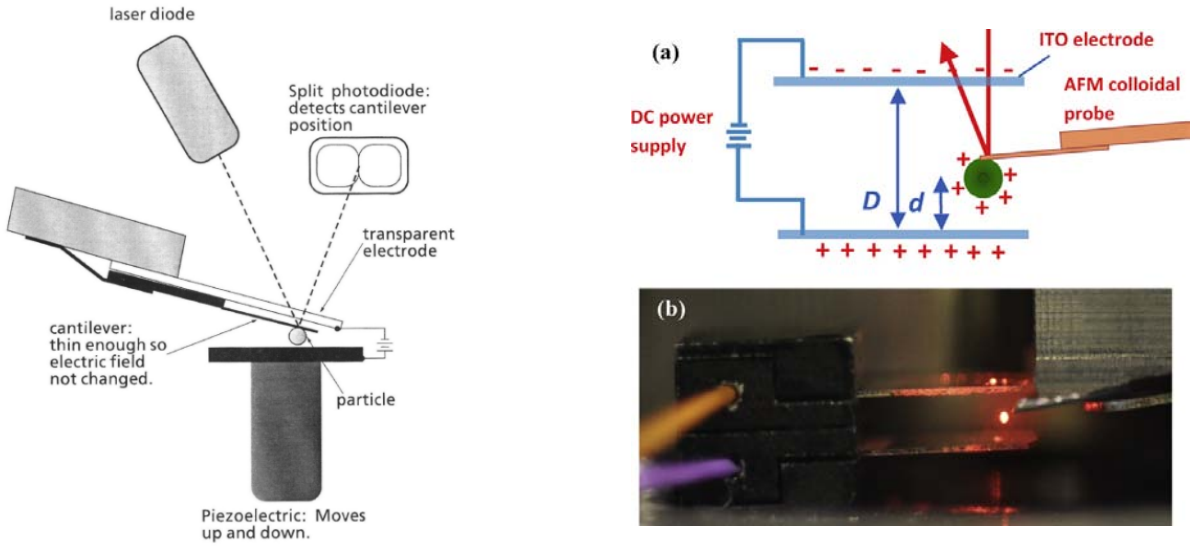

Figure 1-4 (A) Scheme of Mizes' setup to study the electrostatic adhesion of microparticles [Mizes, H. A., ADHESION OF SMALL PARTICLES IN ELECTRIC-FIELDS. *Journal of Adhesion Science and Technology* **1994**, *8* (8), 937-951.][18] (Used under fair use, 2013); (B) The modified setup based on Mizes' setup to study DC electric field-induced force of a microparticle between the parallel condenser electrodes. [Kwek, J. W.; Vakarelski, I. U.; Ng, W. K.; Heng, J. Y. Y.; Tan, R. B. H., Novel parallel plate condenser for single particle electrostatic force measurements in atomic force microscope. *Colloids and Surfaces a-Physicochemical and Engineering Aspects* **2011**, *385* (1-3), 206-212.][20] (Used under fair use, 2013)

Based on the above introduction, we believe that AFM enables to measure the field-induced force between closely spaced microparticles varying with the separation between the particles, thus helping to clarify the real phenomena and mechanisms that the studies by other measurement techniques have simplified and/or overlooked.

1.2 Objectives and Outline of This Thesis

The objective of this work is to study polarization forces between particles, particularly at small separations (less than the particle diameter). To maximize the polarization, we used two $BaTiO_3$ glass microparticles. To minimize the effects of surface conductivity, we used a low

humidity environment. We used an AFM to measure the forces, and built a pair of parallel electrodes in an AFM similar to Mizes' apparatus. In contrast to Mizes' work, we study both AC and DC field-induced forces. The response to a DC field is dominated by surface conductivity whereas the response to an AC field is dominated by polarization. We have three fundament variables: (1) the frequency of the applied field, which explores the frequency dependence of polarization; (2) the applied field strength, which helps to determine the mechanism of the force (as described later, a polarization force should be proportional to the square of the field) and (3) the separation between the particles, which also helps us to understand the perturbation of the applied field by a second particle. The use of high frequency fields induced high frequency forces, which required us to synchronize two different data acquisition methods with different sample rates. Through these experiments, we hope that this study will improve the understanding of the polarization and interaction between microparticles under an electric field, facilitating the development of applications involving field induced forces. This thesis will show that the electrical field-induced forces are much, much larger than the traditionally studied van der Waals and double-layer surface forces and thus offer a greater ability to control microparticles.

In the following chapters of this thesis, we will first introduce basic definitions of solid dielectric materials and some basic dielectric theory in Chapter 2, including the mechanisms of electric polarization and the frequency response of dielectrics under an AC electric field, which are required for the analysis of electric field-induced interactions and forces between dielectrics. Then the theories of polarization and interaction of particles under an electric field will be explained in Chapter 3. Chapter 4 will describe the principles of AFM and the technique of force measurement by AFM in detail. Chapter 5 will describe the home-built apparatus for this work, sample preparation, some experimental methods and methods for data analysis in detail. The experimental and theoretical results accompanying with discussion will be shown in Chapter 6.

Chapter 2 – Electric Polarization and Relaxation of Solid Dielectrics

Ideal dielectrics do not permit the passage of any particles, including electrons (i.e., the conductivity is zero) so they are also referred to ideal insulators and taken as capacitors electrically.[24,25] Nevertheless, real dielectrics always contain some free electrons but far fewer than conductors so that real dielectrics have finite conductivity. The differences between real dielectrics and semiconductor are that semiconductors have higher conductivity and the dominate charge carriers in semiconductor are attributed to thermal excitation (i.e., electron-hole generation) but in dielectrics are due to other sources, such as charge injection and optical excitation.[24] When the dielectrics have finite conductivity, the dielectrics can be said "lossy" and are electrically equivalent to an ideal lossless capacitor in parallel with a resistor.[26] The permittivity, ε, of a lossy dielectric is a complex term expressed as

$$\underline{\varepsilon} = \varepsilon' - j\varepsilon'' - j\frac{\sigma}{\omega} \qquad (2.1)$$

where j represents the positive square root of -1, σ is conductivity of the lossy dielectric and ω is the frequency of external source (e.g., electric field).[7] The real part of the permittivity, ε', in Eq. (2.1) is related to the storage of energy in the electric field and the imaginary part to the energy dissipation.[26] Both ε' and ε'' are a function of frequency.[27] Note that the two imaginary terms in Eq. (2.1) represent two different mechanisms of energy dissipation.[27] The third term on the right hand side of Eq. (2.1) represents that the energy is lost by Joule heating because the lossy dielectric has a finite conductivity[27] and this mechanism is referred to as ohmic loss[7]. The origin of the second term on the right hand side of Eq. (2.1) is that the dipoles or ions dissipate energy during rotation or other motion.[27] Such energy dissipation is called dielectric loss. It is negligible in may circumstances[7], including as we show, in the experiments in this thesis. In the following sections, we will introduce the polarization mechanisms of dielectrics subjected to different frequencies of an AC electric field.

2.1 The Mechanisms of Electric Polarization

When the applied electric field is much lower than the inner atomic or molecular fields and the low conductivity of the dielectric can be neglected, there are three different polarization mechanisms would prevail, depending on the corresponding behavior of electrons or dipoles to an AC electric field.[24] Figure 2-1 shows how the real ε' and the imaginary ε'' parts of the

complex permittivity vary with different frequency due to loss of a series of response mechanisms.[28]

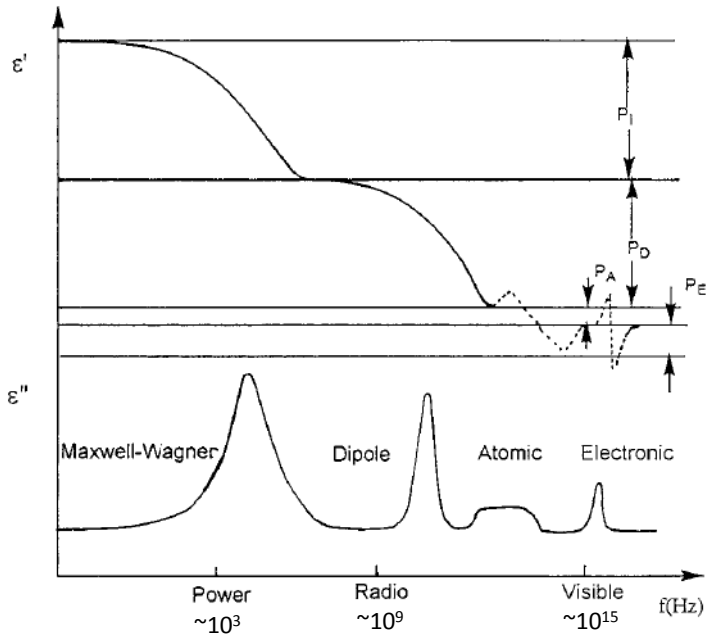

Figure 2-1 Real and imaginary parts of complex permittivity and dielectric dispersion of a heterogeneous lossy dielectric versus the applied frequency [Hao, T.; Kawai, A.; Ikazaki, F., Mechanism of the electrorheological effect: Evidence from the conductive, dielectric, and surface characteristics of water-free electrorheological fluids. *Langmuir* **1998**, *14* (5), 1256-1262.][28] (used under fair use, 2013)

The response mechanisms are:

1. *Electronic polarization*: At UV frequencies (~10^{15} to ~10^{16} Hz), the electron clouds of atoms or molecules are displaced with respect to the inner positive nucleus. This polarization exists in any kind of dielectrics.

2. *Atomic or ionic polarization (vibrational polarization)*: The ions or atoms of a polyatomic molecule are moved relative to each other due to the external electric field, causing a change in dipole moment.

3. *Orientational polarization (or Debye relaxation)*: This polarization only happens in polar dielectric. The electric field would drive the permanent dipoles to align toward the direction of the electric field.

There is a fourth type polarization that occurs when the low conductivity of the dielectric cannot be neglected (or the applied field is high enough): the migration of charge carriers. When the migration of charge carriers is impeded at the interface between two unlike dielectrics and/or grain boundaries of the dielectric, then an accumulation of charge occurs at the interface.[24] This is so-called "interfacial or space charge polarization"[24] and is also referred to as "Maxwell-Wagner interfacial polarization" since the theory was developed by James Clerk Maxwell and later on refined by K.W. Wagner[29]. This polarization exists in amorphous or polycrystalline solids or materials consisting of trapped charges.[24] The movement of charge to the surface takes time, so this mechanism only operates at low frequencies or in a DC electric field. Jones has investigated this time-dependent phenomenon by deriving the time-dependent effective dipole moment of a homogeneous ohmic dielectric sphere with permittivity ε_2, conductivity σ_2, and radius R in a ohmic dielectric fluid with permittivity ε_1 and conductivity σ_1 (Eq. (2.2)).[7]

$$p_{eff}(t) = 4\pi\varepsilon_1 R^3 \left(\frac{\sigma_2 - \sigma_1}{\sigma_2 + 2\sigma_1} \right) E_0 [1 - \exp(-t / \tau_{MW})] + 4\pi\varepsilon_1 R^3 \left(\frac{\varepsilon_2 - \varepsilon_1}{\varepsilon_2 + 2\varepsilon_1} \right) E_0 \exp(-t / \tau_{MW}) \quad (2.2)$$

where $\tau_{MW} = \frac{\varepsilon_2 + 2\varepsilon_1}{\sigma_2 + 2\sigma_1}$ is Maxwell-Wagner charge relaxation time associated with the charge accumulation at the surface of the sphere. When $t << \tau_{MW}$ (i.e., high frequency), the first term on the right hand side of Eq. (2.2) would be negligible and the effective moment is dominate by the permittivities, meaning no charge accumulation at the surface of the sphere. However, when $t >> \tau_{MW}$ (i.e., low frequency), the first term on the right hand side of Eq. (2.2) dominates if charge accumulation can occur at the surface. Since the field-induced force is proportional to the effective dipole moment, we can expect that the field-induced force would have a similar frequency response. The relationship between the field-induced force and the effective moment would be introduced in detail in Chapter 3.

Chapter 3 – Electromechanics of Particles

Every material has its own special electrical properties, thus having different responses, such as polarization and field-induced forces, to an external electric field. In Chapter 2, different electric polarizations and the corresponding mechanisms have been introduced. In this chapter, we focus on the forces that the particles with diameter range from 1 to 1000 μm experience through the action of an external electric field and/or an induced-field by other nearby polarized particles. The forces can be categorized based on the types of the applied electric field and the particles' surroundings (e.g., high conductivity electrolyte or air) as electrophoresis (EP), dielectrophoresis (DEP), electrorotation (ROT), electroosmosis (EO), electrohydrodynamics (EHD), and so forth.[27] Herein we mainly cover DEP since in our study it is the main mechanism and the others do not occur or can be ignored.

First the fundamentals and some equations of the DEP are introduced. Then two analytical models of electric field-induced forces between two identical particles developed from different points of view are reviewed. We will use these models to interpret our experimental observations in Chapter 6.

3.1 General Overview of Dielectrophoresis (DEP)

DEP refers to the translation motion of an uncharged dielectric and/or conductive particle caused by polarization effects in a non-uniform electric field.[7,29] EP is the movement of a charged particle resulted from the Coulomb force between the particle and an electric field.[27] Different from EP, DEP is basically attributed to the interaction of an electric field with the electric field-induced dipole moments.[27] In addition, DEP can occur not only in a DC electric field but also in an AC electric field as long as the electric field is non-uniform, which can be from the directly applied a non-uniform external electric field and/or indirectly generated by other nearby polarized particles[7,27] as is the case in the work described in this thesis. Although a uniform electric field can also induce dipole moments in an uncharged particle, the vector sum of these dipoles is zero, causing no motion of the particle. On the other hand, EP can only occur in a DC electric field since the direction of the EP force depends on the polarity of the electric field and an AC field would cause the charged particle to oscillate around an axis but not move from that average point over time; that is, the EP force is averaged to zero in an AC field.[29] Therefore,

we can conclude different behaviors and forces of a particle under an electric field as follows (Table 3-1).

Table 3-1 Different behaviors and forces for a particle in different conditions

	Uncharged Particle	Charged particle
DC field	Both DEP and EP occur in a non-uniform filed. EP occurs due to the accumulated charges at the interface of the particle. In a uniform field, only EP occurs.	Both DEP and EP occur in a non-uniform field and only EP occurs in a uniform filed.
AC field	Only DEP occurs if the field is non-uniform. Otherwise, neither DEP nor EP will occurs. The particle will oscillate.	Only DEP occurs if the field is non-uniform. Otherwise, neither DEP nor EP will occurs. The particle will oscillate.

One of interesting features of DEP is that the polarized particle is not always attracted to the region of the stronger electric field. It is opposite under certain conditions instead. When the particle is more polarizable than its environment (medium), more induced charge separation takes place in the particle than in the medium, causing higher charge density inside the interface than outside and the effective dipole across the particle is in the same direction as the electric field, as shown in Figure 3-1 (a). If the applied field is non-uniform, then the particle is attracted and to the high-field region, which is termed positive DEP. This is the case in the experiments described in this thesis, where we have a high dielectric particle in air, and the particle is near another particle. On the contrary, if the particle is less polarizable than the medium, the effective dipole across the particle in the opposite direction to the electric field (Figure 3-1 (b)). If the applied field is non-uniform, the particle would be repelled from the high-field region. In other words, the particle is attracted to the low-field region in a non-uniform electric field when the polarizability of the particle is less than the medium. The phenomenon is termed negative DEP.

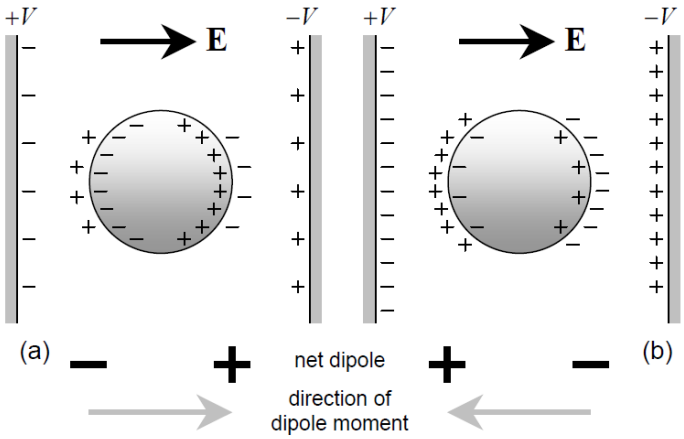

Figure 3-1 Schematic of the polarization of an uncharged particle under an electric field when (a) the polarizability of the particle is greater than the suspending medium or (b) the polariability of the particle is less than the suspending medium. [Morgan, H.; Green, N. G., *AC Electrokinetics: colloids and nanoparticles*. Research Studies Press: Philadelphia, PA, 2003.][27] (Used under fair use, 2013)

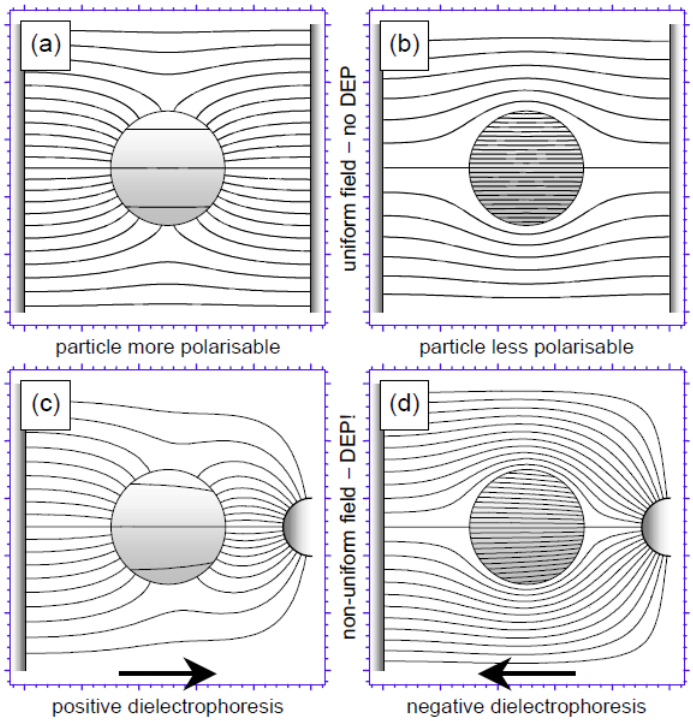

Figure 3-2 Numerically calculated electric field lines of four different situations: (a) the particle is more polarizable than the medium and the field is uniform; (b) the particle is less polarizable than the medium and the field is uniform; (c) the particle is more polarizable than the medium and the field is non-uniform; (d) the particle is less polarizable than the medium and the field is non-uniform. [Morgan, H.; Green, N. G., *AC Electrokinetics: colloids and nanoparticles*. Research Studies Press: Philadelphia, PA, 2003.][27] (Used under fair use, 2013)

Figure 3-2 shows the electric field lines of the above situations. Note that the electric field line on both sides of the particle is symmetric when the electric field is uniform no matter whose polarizability is greater (Figure 3-2 (a) and (b)), meaning the net DEP force exerted on the particle is zero in a uniform field. Further, as the polarizability of the particle greater than the medium, the electric field lines inside the particle is near zero and the lines outside it would bend to and/or be perpendicular to the surface of the particle, just like a metal sphere in an electric field (Figure 3-2 (a) and (c)). By contrast, the particle would act as an insulator as its polarizability less than the medium. The outside electric field lines would bend around the particle and the density of the inside lines is similar to those outside. If the particle and the medium have the same polarizability, there is no effective dipole across the particle and no DEP occurs.

In addition to the electrical properties of the particle and the medium and the non-uniformity and strength of the electric field, the frequency of the applied field can control the direction and the magnitude of the DEP force as well. At low frequencies, the accumulation of the free charge at the interface between the particle and the medium (i.e., a Maxwell-Wagner interfacial polarization as mentioned in Chapter 2) dominates the DEP force. The amount of the accumulated charge on either side of the interface depends on the impedance of these materials and the frequency of the applied field. In other words, the conductivities[I,30] of the particle and the medium dominate the DEP force. At high frequencies, the permittivities of the particle and the medium dominate the DEP force since the charge within the particle is not able to respond to the high frequency field. At the intermediate frequency range, the transition from positive DEP to negative DEP or from negative DEP to positive DEP takes place. This is referred to as dielectric dispersion.[7,27,29] The detail of frequency-dependent DEP would be reviewed in Section 3.2.2.

So far we have discussed DEP on a single particle. But particle-particle interactions are often important in applications, and are the subject of this thesis. Here two cases of particle-particle interactions are stated and their calculated electric field distributions are shown in Figure 3-3 and Figure 3-4, respectively. The first case is that the axis connects the centers of two identical particles (i.e., line-of-centers) parallel to the direction of an applied uniform electric

[I]The more accurate terminology should be “admittance”, not “conductivity.” The admittance in an AC electric field is analogous to the electrical conductance in a DC field.[30] The admittance is complex but usually the real part, which is the electrical conductance, is considered in most discussions. Further, the electrical conductance is proportional to the electrical conductivity so “conductivity” is used in most literatures and models.

field, as shown in Figure 3-3. The darker part in the figures means lower field strength and the lighter part means higher field strength. In Figure 3-3 (a), the particle are more polarizable than the medium so they experience positive DEP. Note that the field strength between the particles is higher than those of the other sides of the particles and the particles would move to high-field region so they would move to each other. On the other hand, the particles are less polarizable than the medium in Figure 3-3 (b) so they experience negative DEP. Interestingly the particle move to each other as well since the field strength between the particles is lower than those of the other sides of the particles. As a result, two identical particles would "attract" to each other when their line-of-centers parallels to the direction of the applied electric field no matter whether

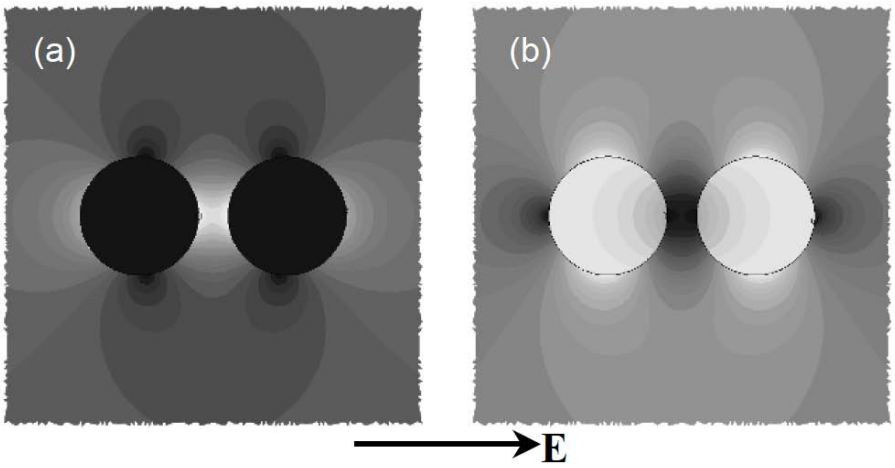

Figure 3-3 Two dimensional electric field distributions around two identical particles align with an axis connecting the centers of the particles parallel to the direction of an applied uniform electric field: (a) particles are more polarizable than the medium so positive DEP occurs; (b) particles are less polarizable than the medium so negative DEP occurs. [Morgan, H.; Green, N. G., *AC Electrokinetics: colloids and nanoparticles*. Research Studies Press: Philadelphia, PA, 2003.][27] (Used under fair use, 2013)

the polarizability of the particles is greater or smaller than the medium. The second case is similar to the first one but the direction of the electric field is perpendicular to the line-of-centers of the particles (Figure 3-4). Contrary to the first case, two identical particles would "repel" each other and move to the region with their favorable field strength (e.g., particles experiencing positive DEP move to high-filed regions) to reach a stable state (i.e., like the arrangement in the first case) no matter whether their polarizability is greater or smaller than the medium. In conclusion, for identical particles under an electric field, the direction of force is determined by the angle between the electric field and the line-of-centers of the particles, not the polarizability.

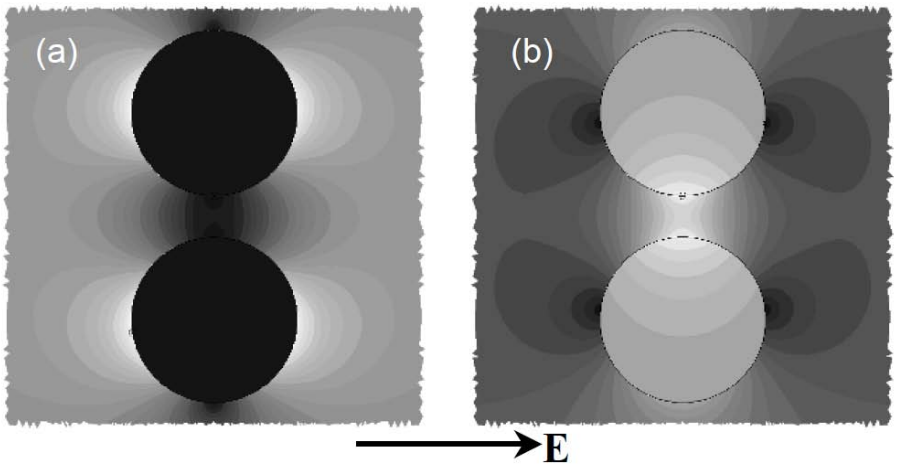

Figure 3-4 Two dimensional electric field distributions around two identical particles align with an axis connecting the centers of the particles perpendicular to the direction of an applied uniform electric field: (a) particles are more polarizable than the medium so positive DEP occurs; (b) particles are less polarizable than the medium so negative DEP occurs. [Morgan, H.; Green, N. G., *AC Electrokinetics: colloids and nanoparticles*. Research Studies Press: Philadelphia, PA, 2003.][27] (Used under fair use, 2013)

We have briefly introduced some features of the DEP from a phenomenological perspective. The following will introduce some related equations of DEP in the electromagnetic and mathematical point of view.

3.2 Analysis of DEP by Effective Moment Method

3.2.1 General Overview of Calculation of DEP force by Effective Moment Method

To derive the equation of the DEP force, first we need to consider a force on an infinitesimal dipole in a non-uniform electric field since the origin of the DEP is the interaction of a non-uniform electric field with the induced field-dipole. As shown in Figure 3-5, a dipole consists of two charges of equal magnitudes and opposite signs separated by a vector distance $\vec{d}$ in an electric field $\vec{E}$. Assume that the charges are stationary or with negligible velocities and accelerations so the movement of the charges does not change the electric field much and thus is negligible, which is referred to as a quasi-electrostatic system.[7]

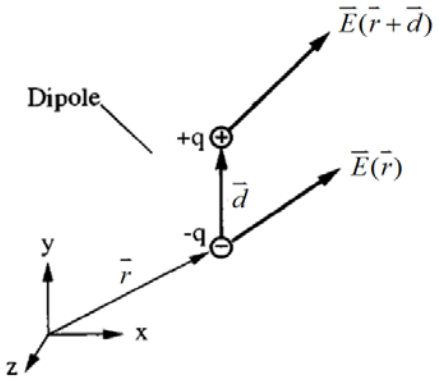

Figure 3-5 The two charges in a dipole experiences different forces in magnitudes of a non-uniform electric field. [Jones, T. B., *Electromechanics of Particles.* Cambridge University Press: New York City, NY, 1995.][7] (Used under fair use, 2013)

Thus, the net force on the dipole is

$$\vec{F} = q\vec{E}(\vec{r}+\vec{d}) - q\vec{E}(\vec{r}) \tag{3.1}$$

where $\vec{r}$ is the position of –q. If $|\vec{d}|$ is smaller than the characteristic dimension of the electric field nonuniformity (i.e., the electric field is nearly uniform across the dipole), the electric field can be expanded around $\vec{r}$ by a vector Taylor series, given by

$$\vec{E}(\vec{r}+\vec{d}) = \vec{E}(\vec{r}) + \vec{d}\cdot\nabla\vec{E}(\vec{r}) + \ldots \tag{3.2}$$

Substituting Eq. (3.2) into Eq. (3.1) gives

$$\vec{F} = q\vec{E}(\vec{r}) + q\vec{d}\cdot\nabla\vec{E}(\vec{r}) - q\vec{E}(\vec{r}) + \ldots \approx q\vec{d}\cdot\nabla\vec{E}(\vec{r}) \tag{3.3}$$

where the higher order terms (i.e., d^2, d^3, and so on) is neglected. For a finite dipole,

$$\vec{F}_{dipole} = \vec{p}\cdot\nabla\vec{E} \tag{3.4}$$

Eq. (3.4), referred to as dielectrophoretic approximation, can be applied to any physical dipoles, such as a polar molecule or a polarized particle with finite size.[7] Note that this approximation demonstrates that the force on a dipole is zero in a uniform electric field, corresponding to the previous statement.

However, higher order terms in Eq. (3.3) should be taken into consideration when the characteristic dimension of the electric field nonuniformity is comparable to the dimension of the object we concern, such as the case of closely spaced particles where the dimension of the nonuniformity of the local electric field induced by the particles is comparable to the particle size. Herein the effective moment method is introduced to approximate the $\vec{p}$ in Eq. (3.4) more

accurately for the calculation of the DEP force of a particle. The idea of this method is to hypothesize that the DEP force of a particle can be expressed by the effective moments $\vec{p}_{eff}$ derived from solving the induced electrostatic field due to the particle.[7] The reasons for this choice are that its ease of implementation and validity in many cases where is hard to employ the derivations based on the Maxwell stress tensor.[7]

Here the derivation of the effective moment in the simplest case is reviewed first since this can derive the effective moments of other more general cases simply by adjusting some parameters to the corresponding situations. Subsequently, the general expression of effective moment and the limitation of this method are stated.

Let's consider a homogeneous lossless dielectric particle of radius R and permittivity ε_p is suspending in a lossless dielectric fluid of permittivity ε_m under a uniform electric field E_0 in z direction, as illustrated in Figure 3-6. Assume that the particle does not significantly disturb the source of the applied electric field.

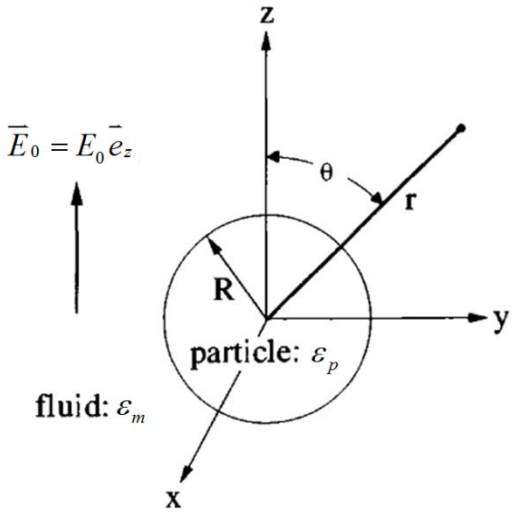

Figure 3-6 A dielectric particle with radius R and permittivity ε_p suspending in a fluid with permittivity ε_m under a uniform electric field $\vec{E}_0$ in z direction. [Jones, T. B., *Electromechanics of Particles.* Cambridge University Press: New York City, NY, 1995.][7] (Used under fair use, 2013)

We know Gauss's law is $\nabla \cdot \vec{E} = \frac{\rho}{\varepsilon_0}$, where ρ is the volume charge density and ε_0 is permittivity of free space (8.854×10^{-12} F/m). The scalar electric potential ϕ (Volts) can be

related to the vector electric field by $\vec{E} = -\nabla\phi$. Thus, we can get $\nabla\phi^2 = -\frac{\rho}{\varepsilon_0}$, which is referred to as Poisson's equation. As the charge density is zero, we obtain $\nabla\phi^2 = 0$, which is termed Laplace's equation. Due to the conservation of an electrostatic field[26] and no existence of free charge (i.e., both the particle and the medium are lossless) in this case, the curl and the divergence of the electric field are zero. As a result, the electric potential satisfies Laplace's equation everywhere for this case. Assume the dipole moment is the dominate contribution compared with other multipoles, which can be ignored. Hence the general solutions for Laplace's equation are assumed[7]

$$\phi_m(r,\theta) = -E_0 r\cos\theta + \frac{A\cos\theta}{r^2}, \quad r > R \tag{3.5}$$

$$\phi_p(r,\theta) = -Br\cos\theta, \quad r < R \tag{3.6}$$

where ϕ_m and ϕ_p are the potential within the fluid and the sphere, respectively and A and B are unknown constants. The first term on the right hand side of Eq. (3.5) represent the applied electric field and the second term represents the induced dipole due to the particle.

To specify the solutions, we need to find out the boundary conditions at the particle surface (i.e., $r = R$). The first boundary condition is the continuity of the normal electric field components across the particle-fluid boundary, which can be rewritten as

$$\phi_m(r = R,\theta) = \phi_p(r = R,\theta) \tag{3.7}$$

The second boundary condition is the continuity of the normal components of the electric flux density (or electric displacement) $\vec{D}$ (Cm^{-2}) across the boundary. $\vec{D}$ is defined as $\vec{D} = \varepsilon\vec{E}$. Thus the second boundary condition can be written as

$$\varepsilon_m E_{rm}(r = R,\theta) = \varepsilon_p E_{rp}(r = R,\theta) \tag{3.8}$$

where $E_{rm} = -\frac{\partial\phi_m}{\partial r}$ and $E_{rp} = -\frac{\partial\phi_p}{\partial r}$ are the normal electric field components in the fluid and the particle, respectively. Substituting Eq. (3.5) and (3.6) into Eq. (3.7) and (3.8), we obtain

$$A = \frac{\varepsilon_p - \varepsilon_m}{\varepsilon_p + 2\varepsilon_m} R^3 E_0 \text{ and } B = \frac{3\varepsilon_m}{\varepsilon_p + 2\varepsilon_m} E_0 \tag{3.9}$$

Based on the concept of the effective moment method, the effective dipole moment of the polarized particle in this case can be taken as an equivalent, free-charge, point dipole offering the same dipolar electric potential ϕ_{dipole} [II], which is

$$\phi_{dipole} = \frac{p_{eff} \cos\theta}{4\pi\varepsilon_m r^2} \tag{3.10}$$

Table 3-2 Mathematical expressions for the moment, electric potential, and z-directed force due to the linear multipoles, or any axisymmetric charge distribution. [Jones, T. B., *Electromechanics of Particles*. Cambridge University Press: New York City, NY, 1995.][7] (Used under fair use, 2013)

Multipolar term	Moment: $p^{(n)}$	Potential: Φ_n	Force: $\bar{F}_n$
Monopole: $n = 0$	$p^{(0)} = q_0$	$\frac{q_0}{4\pi\varepsilon_1 r}$	$q_0\bar{E}$
Dipole: $n = 1$	$p^{(1)} = q_1 d_1$	$\frac{q_1 d_1}{4\pi\varepsilon_1 r^2}(\cos\theta)$	$(q_1\bar{d}_1 \cdot \nabla)\bar{E}$
Quadrupole: $n = 2$	$p^{(2)} = 2q_2 d_2^2$	$\frac{2q_2 d_2^2}{4\pi\varepsilon_1 r^3}\left(\frac{3\cos^2\theta - 1}{2}\right)$	$q_2(\bar{d}_2 \cdot \nabla)^2\bar{E}$
Octupole: $n = 3$	$p^{(3)} = 6q_3 d_3^3$	$\frac{6q_3 d_3^3}{4\pi\varepsilon_1 r^4}\left(\frac{5\cos^3\theta - 3\cos\theta}{2}\right)$	$q_3(\bar{d}_3 \cdot \nabla)^3\bar{E}$
General nth-order multipole	$p^{(n)} = n!q_n d_n^n$	$\Phi_n = \frac{p^{(n)}}{4\pi\varepsilon_1 r^{n+1}} P_n(\cos\theta)$	$\bar{F}_n = q_n(\bar{d}_n \cdot \nabla)^n\bar{E}$

Comparing the second term on the right hand side of Eq. (3.5) with Eq. (3.10), we can get

[II] The expressions of the electric potential by linear multipoles are summarized in Table 3-2 and the detailed derivations by Legendre polynomials can be found in Ref. 7 and 26. Here we directly use the derived results.

$$p_{eff} = 4\pi\varepsilon_m A = 4\pi\varepsilon_m R^3 E_0 \frac{\varepsilon_p - \varepsilon_m}{\varepsilon_p + 2\varepsilon_m} = 4\pi\varepsilon_m K R^3 E_0 \tag{3.11}$$

$$K(\varepsilon_p, \varepsilon_p) = \frac{\varepsilon_p - \varepsilon_m}{\varepsilon_p + 2\varepsilon_m} \tag{3.12}$$

K is known as the Clausius-Mossotti function, representing the strength of the effective polarization of a spherical particle.[7] Note that K can point out the relative direction of the applied electric field and the effective dipole moment. As $K > 0$ (i.e., $\varepsilon_p > \varepsilon_m$), the dipole and applied electric field point in the same direction; however, as $K < 0$ (i.e., $\varepsilon_p < \varepsilon_m$), the dipole points toward the opposite direction to the electric field, corresponding to the statement in section 3.1.1.

Finally, substituting Eq. (3.11) into Eq. (3.4), dielectric approximation gives

$$\vec{F}_{DEP} = 2\pi\varepsilon_m R^3 \left(\frac{\varepsilon_p - \varepsilon_m}{\varepsilon_p + 2\varepsilon_m}\right) \nabla E_0^2 \tag{3.13}$$

However, Eq. (3.13) only can be applied to the case we specified. Table 3-3 summarizes the effective moments, Calusius-Mossotti function, electric potentials, and forces for more general cases. The detailed derivations of these expressions can be found in Ref. 7. Note that these mathematical formulas look very similar to Eq. (3.11) and (3.13) and they all can be derived by the equations in Table 3-2. As for lossy materials, the permittivities should be in the complex form, which is represented by underlining $\underline{\varepsilon}$, so does Calusius-Mossotti function. In addition, the lossy properties of materials are significant under an AC electric field; thus the DEP behaviors of lossy materials under an AC field are discussed, so do that in Table 3-2. Thus the concept of phasor, a representation of a complex number in terms of a complex exponential by Euler formula, is introduced to rewrite time-varying parameters, such as electric field and potential for the connivance of calculation. For example, $\vec{E}_0 = E_0 \cos\omega t \vec{e}_z = \mathrm{Re}[E_0 \exp(j\omega t)]\vec{e}_z$ and $\underline{\vec{E}}_0 = E_0 \exp(j\omega t)\vec{e}_z$ is the vector phasor expression of a sinusoidal AC electric field. Only the real part, which is denoted Re[…], is meaningful. That is why the real part of the force is considered in Table 3-3. Furthermore, the force under an AC electric field consists of a constant (average) term and a time-varying term. Since the motion due to the time-varying term is usually

damped heavily by the viscosity of the suspension medium for the particle size range from 1 to 1000 μm[7], Table 3-3 only pays attention on the time-average term, which is designated <…>. However, the medium we used in our study is air so the time-varying term should be studied as well. We will discuss the time-varying term in detail in Chapter 6.

Note that the effective moment method is not rigorous for lossy dielectrics since potential energy arguments are not legitimate.[7] Even so, the effective moment method is still very useful because in most circumstance, dielectric loss is negligible and there is no much difficulty to adjust the method when dielectric loss cannot be neglected.

3.2.2 Frequency-Dependent DEP

Let's now consider the case of a homogenous particle with ohmic loss but no dielectric loss suspended in a dielectric medium under an electric field. Eq. (T3.4) and (T3.10) point out

Table 3-3 Summary of some mathematical expressions based on the effective moment method for some specific cases.[7]

	Only consider dipole moment	Consider both dipole and other mutipoles
Lossless dielectric homogeneous sphere	$p_{eff} = 4\pi\varepsilon_m K R^3 E_0$ (3.11) $K(\varepsilon_p, \varepsilon_p) = \frac{\varepsilon_p - \varepsilon_m}{\varepsilon_p + 2\varepsilon_m}$ (3.12) $\phi_{dipole} = \frac{p_{eff}\cos\theta}{4\pi\varepsilon_m r^2}$ (3.10) $\vec{F}_{DEP} = 2\pi\varepsilon_m R^3 (\frac{\varepsilon_p - \varepsilon_m}{\varepsilon_p + 2\varepsilon_m})\nabla E_0^2$ (3.11)	$p^{(n)} = \frac{4\pi\varepsilon_m K^{(n)} R^{2n+1}}{(n-1)!}\frac{\partial^{n-1}E_z}{\partial z^{n-1}}$ (T3.5) $K^{(n)} = \frac{\varepsilon_p - \varepsilon_m}{n\varepsilon_p + (n+1)\varepsilon_m}$ (T3.6) $\phi_n = -\frac{\partial^n E_z}{\partial z^n} = \frac{(n+1)!q}{4\pi\varepsilon_m \zeta^{n+2}}$ (T3.7) ζ : the distance between the electric field source and the center of the particle $\vec{F}_n = q_n(\vec{d}_n\cdot\nabla)^n\vec{E} = \frac{p^{(n)}}{n!}\frac{\partial^n E_z}{\partial z^n}\vec{e}_z$ $= \frac{2\pi\varepsilon_m K^{(n)} R^{2n+1}}{n!(n-1)!}\frac{\partial}{\partial z}\left[\frac{\partial^{n-1}E_z}{\partial z^{n-1}}\right]^2\vec{e}_z$ (T3.8)
Ohmic lossy dielectric homogeneous sphere	$\vec{\underline{p}}_{eff} = 4\pi\varepsilon_m \underline{K} R^3 \vec{\underline{E}}_0$ (T3.1) $\underline{K}(\omega) = \frac{\underline{\varepsilon}_p - \underline{\varepsilon}_m}{\underline{\varepsilon}_p + 2\underline{\varepsilon}_m} = \frac{\sigma_p - \sigma_m}{\sigma_p + 2\sigma_m}\left[\frac{j\omega\tau_0 + 1}{j\omega\tau_{MW} + 1}\right]$ (T3.2) $\tau_{MW} = \frac{\varepsilon_p + 2\varepsilon_m}{\sigma_p + 2\sigma_m},\ \tau_0 = \frac{\varepsilon_p - \varepsilon_m}{\sigma_p - \sigma_m}$ (T3.3) $\left\langle \vec{F}(t)\right\rangle = \frac{1}{2}\mathrm{Re}[\vec{\underline{p}}_{eff}\cdot\nabla\vec{\underline{E}}^*] = 2\pi\varepsilon_m R^3\,\mathrm{Re}[\underline{K}(\omega)]\nabla E_{rms}^2$ (T3.4)	$\underline{K}^{(n)} = \frac{\underline{\varepsilon}_p - \underline{\varepsilon}_m}{n\underline{\varepsilon}_p + (n+1)\underline{\varepsilon}_m}$ (T3.9) $\left\langle F_z^{(n)}\right\rangle = \frac{2\pi\varepsilon_m R^{2n+1}}{n!(n-1)!}\mathrm{Re}[\underline{K}^{(n)}]\frac{\partial}{\partial z}\left[\frac{\partial^{n-1}E_{z,rms}}{\partial z^{n-1}}\right]^2$ (T3.10)

that $\mathrm{Re}[\underline{K}]$ is the factor to determine the frequency dependence of the time-averaged DEP force. To study the frequency-dependent DEP, we can merely focus on $\mathrm{Re}[\underline{K}]$. From Eq. (T3.2), we can get

$$\mathrm{Re}[\underline{K}] = \frac{\varepsilon_p - \varepsilon_m}{\varepsilon_p + 2\varepsilon_m} + \frac{3(\varepsilon_m \sigma_p - \varepsilon_p \sigma_m)}{\tau_{MW}(\sigma_p + 2\sigma_m)^2 (1 + \omega^2 \tau_{MW}{}^2)} \tag{3.14}$$

where τ_{MW} depicts the decay of a dipolar distribution of free charge at the surface of the particle.[7] Applying two frequency-limitations to the $\underline{K}(\omega)$ gives

$$\lim_{\omega\tau_{MW}\to 0} \mathrm{Re}[\underline{K}] = \frac{\sigma_p - \sigma_m}{\sigma_p + 2\sigma_m} \tag{3.15}$$

$$\lim_{\omega\tau_{MW}\to \infty} \mathrm{Re}[\underline{K}] = \frac{\varepsilon_p - \varepsilon_m}{\varepsilon_p + 2\varepsilon_m} \tag{3.16}$$

Eq. (3.15) and (3.16) confirm two different DEP behaviors at low and high frequencies, respectively, that is, the conductivities of the sphere and medium govern the low-frequency DEP

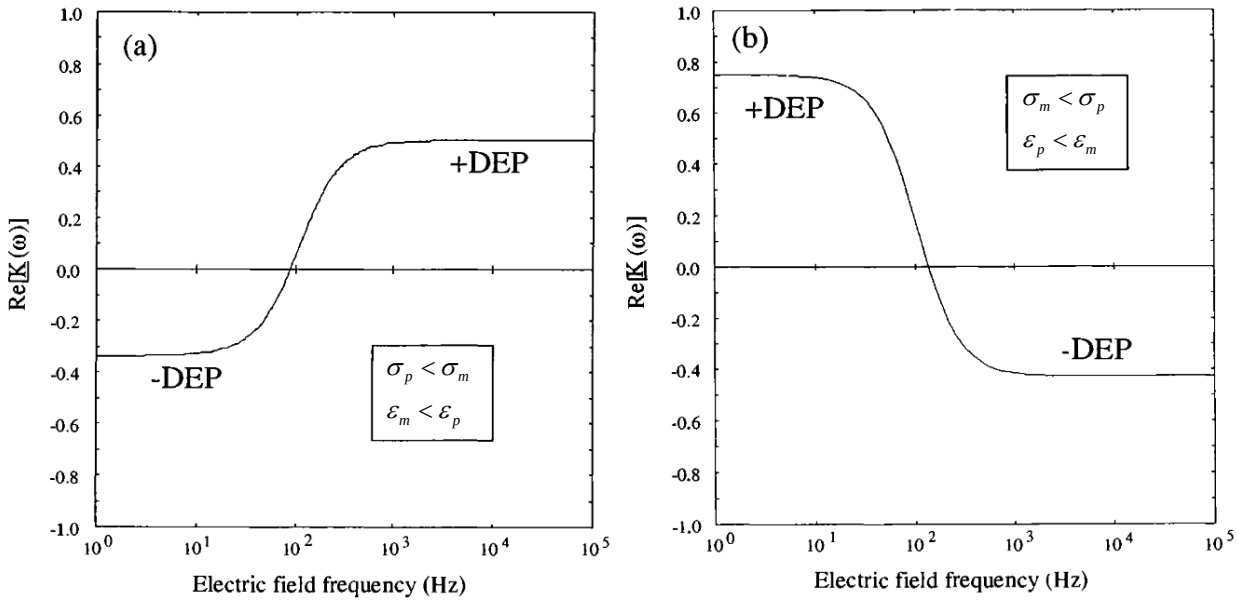

Figure 3-7 Calculated DEP spectra of homogeneous dielectric spheres with ohmic loss but no dielectric loss when (a) $\varepsilon_m / \varepsilon_0 = 2.5$, $\varepsilon_p / \varepsilon_0 = 10.0$, $\sigma_m = 4\times10^{-8}$ S/m, $\sigma_p = 10^{-8}$ S/m and $R = 5$ μm, and (b) $\varepsilon_m / \varepsilon_0 = 10.0$, $\varepsilon_p / \varepsilon_0 = 1.0$, $\sigma_m = 10^{-8} S/m$, $\sigma_p = 10^{-7}$ S/m and $R = 5$ μm. [Jones, T. B., *Electromechanics of Particles.* Cambridge University Press: New York City, NY, 1995.][7] (Used under fair use, 2013)

behavior and the permittivities of the sphere and medium governs the high-frequency DEP behavior. Figure 3-7 shows the variation of $\mathrm{Re}[\underline{K}]$ versus the applied electric field frequencies in different conditions. Note that at a certain frequency, $\mathrm{Re}[\underline{K}]$ becomes zero and there is no F_{DEP}. This frequency is so-called crossover frequency since the force has opposite sign on either side of this frequency.[29] For the work in this thesis, the medium is always air, so the dielectric constant and conductivity of the particles is always greater than the medium.

3.2.3 Models for Layered Spherical Particles

So far, we have only concerned homogeneous spheres. As for heterogeneous spheres, we briefly introduce the particle with shell structure here. The principle of the model for layered spherical particles is to replace a layered spherical particle with an equivalent homogeneous particle of the same radius but with the effective permittivity, as shown in Figure 3-8 (a), so that the mathematical expressions for a homogenous sphere above are still valid for the layered sphere as long as the permittivity of the homogeneous sphere is replaced by the effective permittivity of the layered sphere.[7] So the general expression of the effective permittivity is

$$\underline{\varepsilon}_N^{'} = \underline{\varepsilon}_N \left\{ \frac{a^3 + 2\left(\dfrac{\underline{\varepsilon}_{N+1} - \underline{\varepsilon}_N}{\underline{\varepsilon}_{N+1} + 2\underline{\varepsilon}_N} \right)}{a^3 - \left(\dfrac{\underline{\varepsilon}_{N+1} - \underline{\varepsilon}_N}{\underline{\varepsilon}_{N+1} + 2\underline{\varepsilon}_N} \right)} \right\} \tag{3.17}$$

where $a = R_N / R_{N+1}$ and N+1 indicates the most inner layer so N represents the layer shells the most inner layer. Eq. (3.17) can be applied repeatedly for multilayer structure. As shown in Figure 3-8 (a), we can use ε_3 and ε_4 to calculate the effective permittivity $\varepsilon_3^{'}$ first and then use $\varepsilon_3^{'}$ and ε_2 to calculate $\varepsilon_2^{'}$. In addition, Eq. (3.17) is for a sphere with ohmic loss but no dielectric loss and Maxwell-Wagner relaxation happens for each interface. For a lossless sphere, we can just replace the complex form of permittivities by the real form of permittivies. In fact, the derivation of Eq. (3.17) is similar to that in section 3.2.1 so it is valid only for a uniform or nearly uniform electric field since only the dipole is concerned. For a layered sphere with ohmic loss but no dielectric loss in a nonuniform field, higher mutilpolar terms should be concerned, which gives

$$(\underline{\varepsilon}_2)'_n = \left\{ \frac{a^{2n+1}(n+1)\underline{K}^{(n)}}{a^{2n+1} - n\underline{K}^{(n)}} \right\} \tag{3.18}$$

where $\underline{K}^{(n)}$ is defined as Eq.(T3.9). Similarly, for a lossless sphere, we can just replace $\underline{K}^{(n)}$ by $K^{(n)}$ defined as Eq. (T3.6).

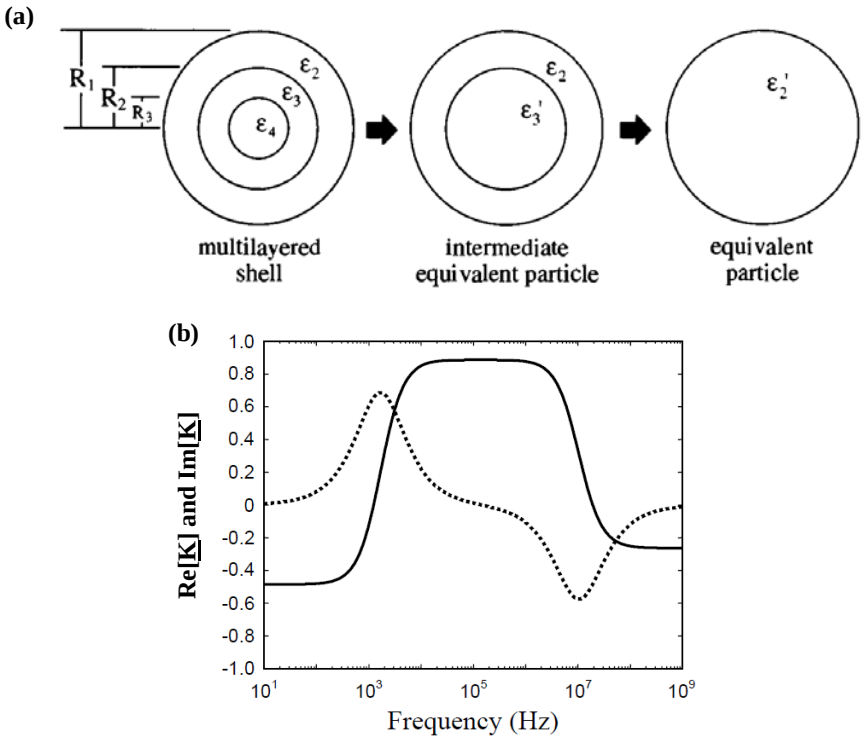

Figure 3-8 (a) Schematic of the replacement of multilayered spherical particle with an equivalent homogeneous sphere of the same radius but with the effective permittivity. [Jones, T. B., *Electromechanics of Particles.* Cambridge University Press: New York City, NY, 1995.][7] (Used under fair use, 2013) (b) The DEP spectrum of the tow-layered spherical particle. The solid line represents $\mathrm{Re}[\underline{K}]$ and the dot line represents $\mathrm{Im}[\underline{K}]$. [Morgan, H.; Green, N. G., *AC Electrokinetics: colloids and nanoparticles*. Research Studies Press: Philadelphia, PA, 2003.][27] (Used under fair use, 2013)

It is noteworthy that Eq. (3.17) is the same as Maxwell's classic mixture formula for the effective permittivity of a mixture consisting of noninteracting spherical particles in a medium with very low volume fraction (i.e., $\varphi << 1$)[7,27], which is usually written as

$$\underline{\varepsilon}_{mix} = \underline{\varepsilon}_m \left\{ \frac{1 + 2\varphi\left(\frac{\underline{\varepsilon}_p - \underline{\varepsilon}_m}{\underline{\varepsilon}_p + 2\underline{\varepsilon}_m}\right)}{1 - \varphi\left(\frac{\underline{\varepsilon}_p - \underline{\varepsilon}_m}{\underline{\varepsilon}_p + 2\underline{\varepsilon}_m}\right)} \right\} \tag{3.19}$$

3.3Maxwell-Wagner Model of Interparticle Force in AC-DC Electric Fields

Maxwell-Wagner Model is the simplest model to simulate the electric-field interparticle force resulting from both the perimittivites and condcutivities of identical dielectric spheres with ohmic loss and an ohmic lossy dielectric medium by combining the effective moment method with the point-dipole approximation.[5] The derivation of this model starts at solving Laplace's equation of an isolated dielectric sphere with ohmic loss in a uniform AC electric field and assuming the induced dipole moment is the dominate contribution of the particle polarization, like the derivation in section 3.2.1. Combining the concept of the point-dipole approximation, the time-averaged force on a sphere i at the origin due to another identical sphere j at (r_{ij}, θ_{ij}) as, shown in Figure 3-9 (a), can be expressed

$$\vec{F}_{ij}(r_{ij}, \theta_{ij}) = \frac{12\pi\varepsilon_m R^6}{r^4} \beta_{eff}^2(\omega) E_{rms}^2 [(3\cos^2\theta_{ij} - 1)\vec{e}_r + (\sin 2\theta_{ij})\vec{e}_\theta] \tag{3.20}$$

where $E_{rms} = E_0 / \sqrt{2}$, and the effective relative polarizability β_{eff} is

$$\beta_{eff}^2 = \frac{\beta_c^2 + \beta_d^2(\omega\tau_{mw})^2}{1 + (\omega\tau_{mw})^2} \tag{3.21}$$

where

$$\beta_d = \frac{\varepsilon_p - \varepsilon_m}{\varepsilon_p + 2\varepsilon_m}, \ \beta_c = \frac{\sigma_p - \sigma_m}{\sigma_p + 2\sigma_m} \tag{3.22}$$

Interestingly, if we apply two frequency limits to Eq. (3.21), we can find similar results to Eq. (3.15) and (3.16). That is,

$$\lim_{\omega\tau_{MW} \to \infty} \beta_{eff}^2(\omega) = \beta_d^2 \tag{3.23}$$

$$\lim_{\omega\tau_{MW} \to 0} \beta_{eff}^2(\omega) = \beta_c^2 \tag{3.24}$$

which also demonstrate that the conductivities of particles and medium govern the field-induced force in a DC and/or low-frequency AC electric fields and the permittivities of particles and medium govern the force in a high-frequency AC fields. Likewise, to see the frequency dependence of the electric field-induced interparticle force, we merely focus on the variation of $\beta_{eff}^2(\omega)$ with frequency, which is plotted in Figure 3-9 (b).

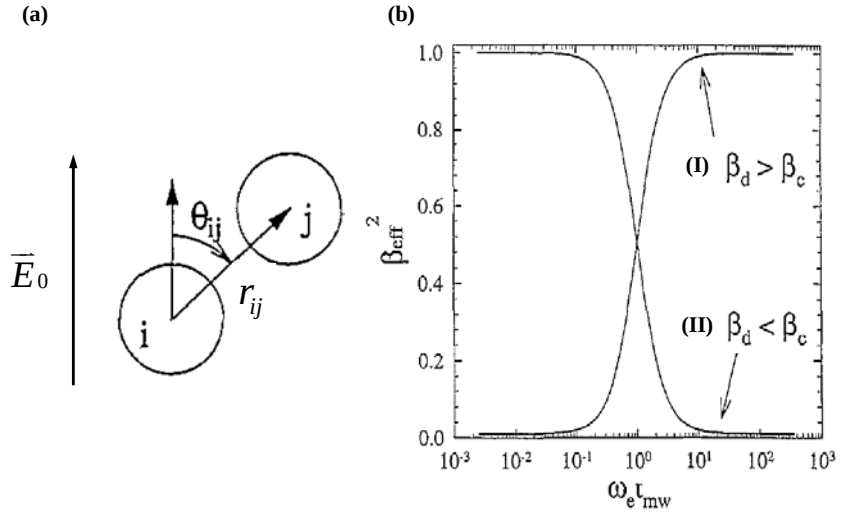

Figure 3-9 (a) Electric field-induced interaction between two identical spheres i and j in an electric field. r_{ij} is the separation between the centers of the particles and θ_{ij} is the angle between the line-of-center and the electric field. (b) Calculated square of the effective relative polarizability β_{eff}^2 versus dimensionless frequency in terms of the Maxwell-Wagner relaxation time: (I) $\beta_d = 10\beta_c$; (II) $\beta_d = 0.1\beta_c$. [Parthasarathy, M.; Klingenberg, D. J., Electrorheology: Mechanisms and models. *Materials Science & Engineering R-Reports* **1996**, *17* (2), 57-103.][5] (Used under fair use, 2013)

3.4 Equivalent Circuit Model of Interparticle Force in AC-DC Electric Fields

Different from the electromagnetic point of view above, Colver has employed the concept of equivalent circuits to develop an interparticle force model of for electric field stabilized gas-fluidized beds[31], as illustrated in Figure 3-10. The resistance-capacitance components in this model result in two time constants: self-particle charge relaxation time τ_p and particle-particle relaxation time τ_b for transient decay of charge within a particle and between two particles, respectively. To formulate the model, Colver came up some assumptions as follows.

(1) The concerned spherical powders are in a cubic packing.

(2) Particles are semi-insulating with a small but finite surface electrical conductivity (i.e., ohmic loss) and finite contact resistance at point of contact.

(3) Self-particle charge decay is no influenced by neighboring particles and can be evaluated using single-particle relaxation theory. The single particle charge relaxation time is

$$\tau_p^{'} = \frac{(\varepsilon_p + 2\varepsilon_0)d}{4\sigma_s} \tag{3.25}$$

where d is the particle diameter and σ_s is the surface conductivity of the particle, which can be given as

$$\sigma_s = \frac{d}{\pi\rho_p}\ln(\frac{d}{r_c}) \tag{3.26}$$

where ρ_p is the apparent (single) particle resistivity and r_c is the particle contact radius.

(4) Particle-particle charge decay can be evaluated using continuum bed relaxation theory. The bulk powder charge relaxation time is given as

$$\tau_b^{'} = \bar{\varepsilon}_p \rho_b \tag{3.27}$$

where ρ_b is the apparent bulk powder resistivity and $\bar{\varepsilon}_p$ is the corresponding bulk powder permittivity for bed voidage α, given as Eq. (3.28) and (3.29) respectively.

$$\rho_b = (9.406\times10^{48})E^{-0.69}T^{-17.71}(d)^{5.12}\times e^{-0.188RH} \tag{3.28}$$

where T is temperature (K) and RH is relative humidity (%) and this equation has been tested up to 40% RH.

$$\frac{\bar{\varepsilon}_p}{\varepsilon_0} = \frac{3\left(\frac{\varepsilon_p}{\varepsilon_0}\right) - 2\left(\frac{\varepsilon_p}{\varepsilon_0} - 1\right)\alpha}{3 + \left(\frac{\varepsilon_p}{\varepsilon_0} - 1\right)\alpha} \tag{3.29}$$

(5) The equivalent circuit is comparable small to the wavelength of the applied signals so all electrical signals travel through the circuit quickly, affecting every point in the circuit simultaneously (i.e., lumped parameter circuit theory).[30] Thus distributed capacitance and resistance over the surface of a particle can be assumed having single values.

(6) Circuit components are linear, which means any steady-state output of the circuit (e.g., voltage and current) is also a sinusoidal signal with frequency f when the input signal is a sinusoidal function with frequency f but they may not be in phase.

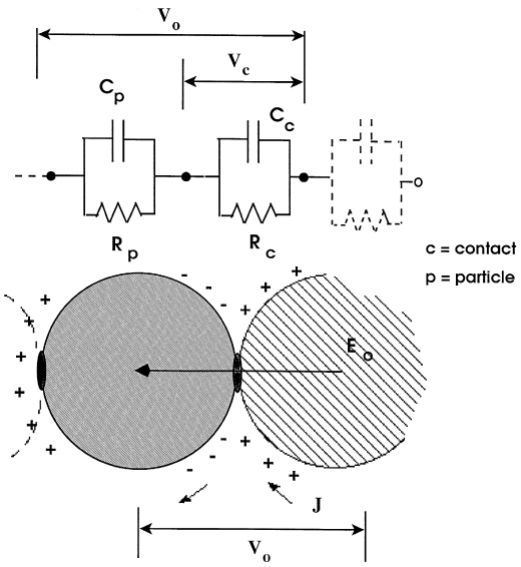

Figure 3-10 An equivalent circuit for formulating the interparticle force of a one-diemensional particle chain in AC-DC fields. [Colver, G. M., An interparticle force model for ac-dc electric fields in powders. *Powder Technology* **2000**, *112* (1-2), 126-136.][31] (Used under fair use, 2013)

Clover also assumed the capacitors in the circuit are simple parallel plate capacitors. Therefore the contact capacitance C_c at the interface between the particles and the self-particle capacitance C_p are given as

$$C_c = \frac{\varepsilon_0 A_c}{x_c} = \frac{\varepsilon_0 \pi r'^2}{x_c} K_1,\ C_p = \frac{\varepsilon_p \pi r'^2}{d} K_2 \qquad (3.30)$$

where x_c is the separation distance between the particles, A_c is the effective capacitance area, r' is the radius of A_c and the constants K_1 and K_2 account for effective capacitance area, distributed capacitance, curvature of particles, and the average contact separation distance.

For the application of the model to both AC and DC fields, a sinusoidal applied field $V(t) = V\exp(j\omega t)$ is assumed. Based on Kirchhoff's law, we can obtain the differential equation depicting the AC (or DC as $\omega \to 0$) voltage drop across the contact capacitance V_c

$$\frac{dV_c}{dt} + \frac{V_c}{\tau_b} = \frac{V_c}{\tau_{pc}}[1 + j\omega\tau_p]e^{j\omega t} \quad \text{AC or DC } (\omega \to 0) \tag{3.31}$$

where the time constants are defined as

$$\begin{aligned} \tau_b &= \left(\frac{1}{1/R_p + 1/R_c}\right)[C_p + C_c] = \frac{R_p R_c}{R_p + R_c}[C_p + C_c] \\ &= \frac{R_c}{R_p + R_c}\tau_{pc} = \frac{R_c}{R_p + R_c}\tau_p + \frac{R_p}{R_p + R_c}\tau_c \end{aligned} \tag{3.32}$$

where R_c is the particle contact resistance, R_p is the single particle resistance $\tau_{pc} = R_p[C_p + C_c] = \tau_p + R_p C_c$, $\tau_p = R_p C_p$ and $\tau_c = R_c C_c$ is the particle contact relaxation time. Solving Eq. (3.32) gives

$$V_c = A\exp\left(-\frac{t}{\tau_b}\right) + \left(\frac{\tau_b}{\tau_{pc}}\right)\left[\frac{1 + (\tau_p\omega)^2}{1 + (\tau_b\omega)^2}\right] \times V_0 \exp j(\omega t + \delta_1 - \delta_2) \tag{3.33}$$

where δ_1 and δ_2 are defined as $\tan\delta_1 = 1/\omega\tau_b$ and $\tan\delta_2 = 1/\omega\tau_p$, respectively. On the right hand side of Eq. (3.33), the first term is the transient response and the second term is the steady-periodic response. The interparticle force can be taken as the force acting on the plates of the contact capacitor. Since the transient term would diminish over time, we can ignore it and also the phase angle (i.e., $\omega t + \delta_1 - \delta_2 = 0$), obtaining the peak force per unit area

$$\begin{aligned} \frac{F_{\max}}{\overline{A}_c} &= \frac{\varepsilon_0 E_c^2}{2} = \frac{\varepsilon_0}{2}\left[\frac{1 + (\tau_p\omega)^2}{1 + (\tau_b\omega)^2}\right]\left[\frac{\tau_b}{\tau_{pc}}\frac{V_0}{x_c}\right]^2, \quad \text{AC/DC} \\ &= \frac{\varepsilon_0}{2}\left[\frac{1 + (\tau_p\omega)^2}{1 + (\tau_b\omega)^2}\right]\left[\frac{\tau_b}{\tau_{pc}}\frac{d}{x_c}E_0\right]^2 \end{aligned} \tag{3.34}$$

where $\overline{A}_c = \pi r'^2$ and the separation distance between the particles is assumed smaller than the diameter of the particle so the applied voltage can be rewritten in terms of the electric field

strength in the far-field. Further, the time-averaged interparticle force per unit area can be expressed

$$\frac{F_{avg}}{\overline{A}_c} = \frac{\varepsilon_0}{2}\left[\frac{1+(\tau_p\omega)^2}{1+(\tau_b\omega)^2}\right]\left[\frac{\tau_b}{\tau_{pc}}\frac{d}{x_c}E_{rms}\right]^2 = \frac{F_{\max}}{2\overline{A}_c}, \quad \textbf{AC} \tag{3.35}$$

where $E_{rms} = E_0/\sqrt{2}$ is the rms value for the applied sinusoidal field.

To cover both AC and DC fields, Colver further combined DC field interparticle force equation Eq. (3.36) with Eq. (3.34), giving more general AC-DC interparticle force equation Eq. (3.37).

$$F_{dc} = \delta\pi\varepsilon_0 d^2 E_{bk}^{2-\beta} E^{\beta} \quad \text{DC} \tag{3.36}$$

$$F_{\max} = \delta\pi\varepsilon_0\left[\frac{1+(\tau_p\omega)^2}{1+(\tau_b\omega)^2}\right]^{\gamma} d^2 E_{bk}^{2-\beta} E^{\beta} \tag{3.37}$$

where δ, β, and γ are constants and E_{bk} is the electric breakdown strength[III] between the spheres.

Although Colver's model is based on the concept of the equivalent circuit, some features of his model correspond or similar to some conclusions from the effective moment method and Maxwell-Wagner model, which are summarized as follows.

(1) The mathematical expressions of the electric field-induced force from these three models all show the force is proportional to the square of the rms value of the applied electric field.

(2) Colver's model also shows that the force would either increase of decrease with frequency. Colver mentioned that it is the relative magnitude of τ_p and τ_b that determines the trend of the force with the frequency. Note that Eq. (3.25) Eq. (3.27) can be used to calculate these two time constants based on the assumptions (3) and (4). In addition, the permittivity and conductivity of the particles would always greater than the

[III]Electric (or dielectric) breakdown strength is the maximum electric field strength that an insulating material can withstand without any current leakage.[25] Once the electric field strength larger than this value, the insulating material would not be insulating anymore, but conductive.

medium in Colver's model since he derived his model for air medium. Thus we can infer that the trend of the force depends on the relative magnitude of the permittivity and surface conductivity of the particles and the resistivity and the permittivity of bulk powder in Colver's model.

(3) Besides τ_p and τ_b, Colver also pointed out that C_p / C_c governs the magnitude of the forces at large values of $\tau_b \omega$ and R_c / R_p governs the force at small values of $\tau_b \omega$. Note that $C_p / C_c = (x_c / d)(\varepsilon_p / \varepsilon_0)$ as $K_1 = K_2 = K$ for simplification. Then in other words, we can interpret that the force is governed by the perimitivities of the particles and air at high frequency and by the conductivities of the particles and the air at low frequency when the separation distance between the two particles are fixed.

We will use these models to interpret our experimental results in Chapter 6.

Chapter 4 – Atomic Force Microscopy (AFM) and the Technique of Force Measurements

AFM is well-known for its ability to image surface topography at the micro- and/or nanoscale. However, what AFM can really do is far more than this by a well-designed experiment, the choice of operation modes, instrumental modification, and/or methods of data acquisition.[32] Besides imaging, AFM has used in the measurements of different surface forces (e.g., van der Waal and adhesion forces)[33,34] and nanoscale dielectric constant,[35] the quantitative study of elastic and viscoelastic properties and tribology, including friction, wear and lubrication,[36,37] picogram mass sensors,[38] nanoscale fabrication,[39] and so on, shown the versatility of this instrument. In this charter, we will focus on the technique of force measurement, which is used in the work. But in the beginning, we will briefly introduce basic concepts and modes of AFM before talking about the measurement of forces.

4.1 Basic Concepts and Modes of AFM

There are mainly five parts in AFM: 1) cantilevers and the attached tips, 2) laser beam 3) photodiode (i.e., photo dectactor), 4) piezoelectric positioner (usually shorten to piezo), and 5) a feedback loop, as shown in Figure 4-1. Before the measurement, the laser beam is focused at the end of the cantilever and deflects to the photodiode. When the tip on the cantilever feels or senses some forces between itself and the sample, the cantilever would start to bend, thus changing the position of the deflected laser beam on the photodiode. At this moment, the signal detected by the photodiode would be fed into a DC feedback amplifier in the feedback loop, comparing with the set point determined by the operator. The resulting difference (i.e., error signal) is sent to a proportional–integral–differential (PID) controller to make the piezo adjust the separation between the cantilever and the sample, keeping the deflection of the laser beam equal to the set point. The adjustment of the piezo generates the image of the sample surface.[40] Note that the stiffness of the cantilever would affect how small the force can be reflected to the photodiode. The softer the cantilever is, the smaller the force can be detected, which can be explained by Hooke's law and the stiffness of the cantilever is also called the spring constant of the cantilever. In addition, the apex radius and the geometry of the tip would affect how small the indentation and the convexity at the surface of the sample can be probed by the tip. Thus, the combination of the cantilever and tip would determine the resolution of an AFM image since the

sensitivity and the quality of the photodioe, piezo, and the feedback loop for commercial AFMs are quite similar nowadays.

The operation of AFM can be divided into several modes based on whether the cantilever oscillates or not and the types of the set point. Here, a static mode – contact mode and two dynamic modes – amplitude modulation (AM) and frequency modulation (FM) modes are introduced. Besides those three basic modes, we will also introduce a Kelvin probe force microscopy (KPFM), which is related to this work.

Contact mode

The features of the contact mode are that the cantilever does not oscillate, the tip would directly touch the sample while imaging and can be used in both ambient conditions and liquids due to its simplicity. The set point of this mode is the deflection of laser beam on the photodiode. Although this mode is mostly used, it would cause the damage either of the sample or of the tip, depending on which one is harder, thus distorting the features of generated image and not suitable for imaging soft materials, such as biomaterials and polymers.[40]

Amplitude-Modulation (AM) Mode

The principle of the AM mode is shown in Figure 4-1. First the cantilever is mechanically excited at or near its free resonant frequency (i.e., the resonant frequency without the effect of tip-sample interaction). When the tip approaches the sample and starts to sense the force, the deflection of the laser beam from the cantilever would change and is detected by the photodiode. The detected signal is sent to a lock-in amplifier to get the information of the amplitude and phase of the oscillating cantilever for comparing with the set point, a chosen amplitude of the oscillation, usually is 70-80% of the free amplitude (the amplitude at the free resonant frequency). As state before, the calculated error signal from the DC feedback amplifier is fed into the PID controller to control the piezo, keeping the detected signal from the photodiode (or the detected amplitude) is the same as the set point.[41] The adjustment of the piezo here is the topography of the sample surface as well. In addition, the difference between the detected phase and the phase from the driving force for exciting the cantilever can give the map of the material properties of the sample, such as soft or hard.[42] The AFM mode is usually used in ambient

conditions and liquids, but not in the ultra high vacuum (UHV), which would slow down the speed of imaging.[41-43]

(a)

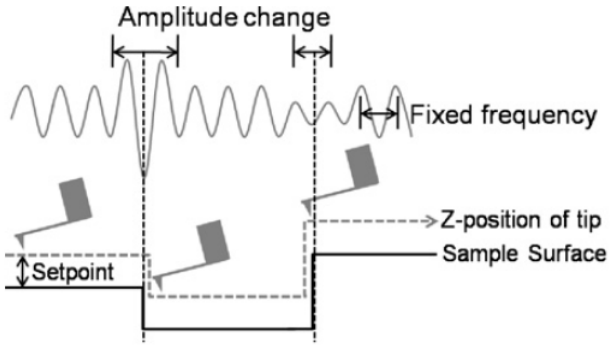

(b)

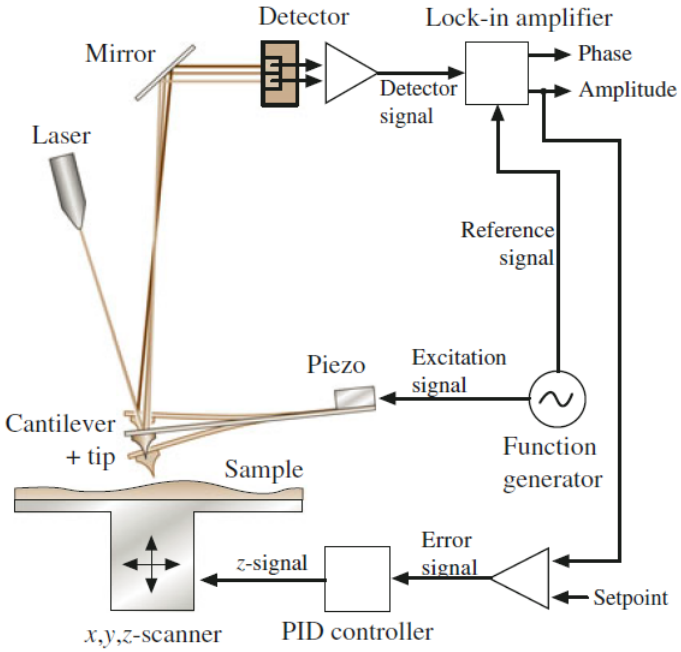

Figure 4-1 (a) The behavior of the cantilever in an AM mode [Melitz, W.; Shen, J.; Kummel, A. C.; Lee, S., Kelvin probe force microscopy and its application. *Surface Science Reports* **2011**, *66* (1), 1-27.][43] (Used under fair use, 2013) (b) Scheme of an AFM setup in the AM mode. [Schirmeisen, A.; Anczykowski, B.; Hölscher, H.; Fuchs, H., Dynamic Modes of Atomic Force Microscopy. In *Nanotribology and nanomechanics. Volume 1, Measurement techniques and nanomechanics*, Bhushan, B., Ed. Springer: Berlin ; Heidelberg ; New York 2011; pp 307-353.][41] (Used under fair use, 2013)

Conventionally, the AM-mode is also called the tapping mode since the cantilever is oscillating at or near its free resonant frequency, causing the tip touch the sample shortly but

frequently.[40] However, the AM-mode can be used in a non-contact mode as well,[42] which is confusing; thus, it is better to name the modes based on the type of the set point and the operation principle of the feedback loop.

Frequency-Modulation (FM) Mode

Similar to the AM-mode, the cantilever is excited at its free resonant frequency in the FM mode as well. Nevertheless the set point of the FM mode is the free resonant frequency of the

(a)

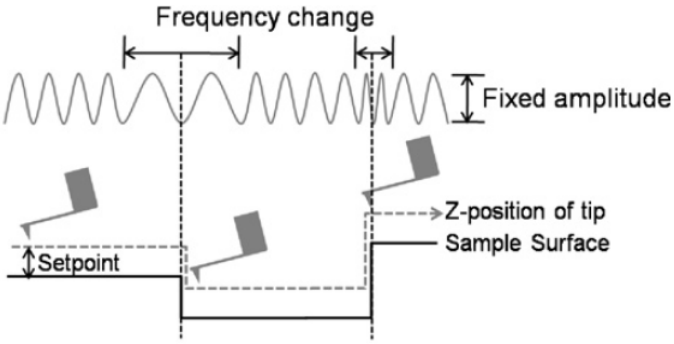

(b)

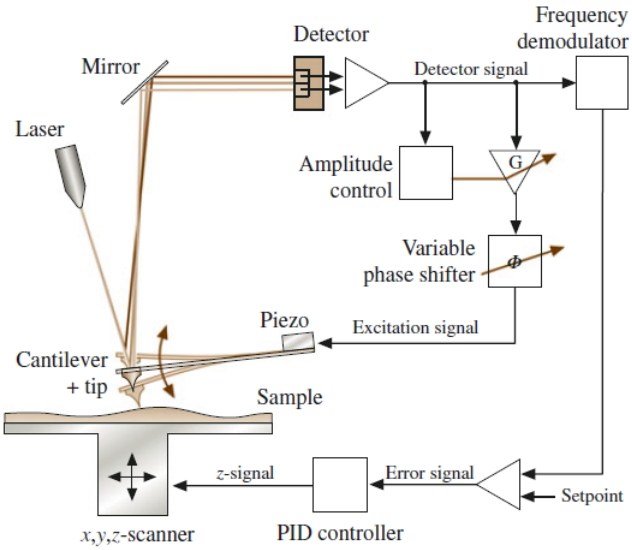

Figure 4-2 (a) The behavior of the cantilever in an FM mode. [Melitz, W.; Shen, J.; Kummel, A. C.; Lee, S., Kelvin probe force microscopy and its application. *Surface Science Reports* **2011**, *66* (1), 1-27.][43] (Used under fair use, 2013) (b) Scheme of an AFM setup in the FM mode. [Schirmeisen, A.; Anczykowski, B.; Hölscher, H.; Fuchs, H., Dynamic Modes of Atomic Force Microscopy. In *Nanotribology and nanomechanics. Volume 1, Measurement techniques and nanomechanics*, Bhushan, B., Ed. Springer: Berlin ; Heidelberg ; New York 2011; pp 307-353.][41] (Used under fair use, 2013)

cantilever. The DC feedback amplifier would calculate the difference between the detected resonant frequency and the free resonant frequency of the cantilever as the control signal to adjust the separation between the tip and sample. In addition, the FM mode has an additional feedback loop, as shown in Figure 4-2, to keep the amplitude of the oscillating cantilever constant so that the separation between the tip and the sample would not be affected by the amplitude.[41] That is why the FM-mode is also called the non-contact mode or the self-excitation mode.[41,42] The FM-mode is designed for imaging in UHV to achieve high-resolution image and to compensate the disability of the AM-mode in UHV.[41-43]

Kelvin Probe Force Microscopy (KPFM)

KPFM was derived from both the dynamic modes of AFM and the macroscopic Kelvin Probe technique, which is used to measure surface potential, to map the work function or surface potential of the sample with high-resolution at and the micro- and nanoscale.[43,44] Different from the forementioned modes, an DC-voltage (V_{DC}) is applied to compensate the contact potential difference (CPD) between the tip and the sample surface and an AC-voltage ($V_{AC}\sin(\omega_{AC}t)$) is applied to excited the tip in a KPFM. As a result, the force sensed here is mainly the electrostatic force. The electrostatic force can be derived as follows by regarding the tip-sample system as a parallel plate capacitor due to the very short distance between them.[43,44]

The energy stored in a parallel plated capacitor is $U_{el}=\frac{1}{2}CV^2$, thus the electrostatic force is given as

$$F_{el}=-\nabla U_{el}=-\frac{1}{2}\frac{\partial C}{\partial r}V^2-CV\frac{\partial V}{\partial r} \tag{4.1}$$

Since the voltages here are distance-independent and the direction of them is perpendicular to the sample surface, which is z-direction, the Eq. (5.1) can be simplified as

$$F_{el}=-\frac{1}{2}\frac{\partial C}{\partial z}V^2=-\frac{1}{2}\frac{\partial C}{\partial z}\left[V_{DC}\pm V_{CPD}+V_{AC}\sin(\omega_{AC}t)\right]^2 \tag{4.2}$$

where V_{CPD} is defined as

$$V_{CPD} = \frac{\Delta\phi}{-e} = \frac{\phi_{tip} - \phi_{smaple}}{-e} \tag{4.3}$$

where ϕ_{tip} and ϕ_{smaple} are work function of the tip and sample and e is the elementary charge. Note that the sign of V_{CPD} in Eq. (4.2) is determined by how V_{DC} is applied to the sample or the tip. Based on Eq. (4.3), we can calculate the work function of the sample by using the tip with a known work function in KPFM. Further, F_{el} can be divided into three forces by rearranging Eq. (4.2).

$$F_{DC} = -\frac{\partial C}{\partial z}\left[\frac{1}{2}(V_{DC} \pm V_{CPD})^2 + \frac{1}{4}V_{AC}^2\right] \tag{4.4}$$

$$F_{\omega} = -\frac{\partial C}{\partial z}(V_{DC} \pm V_{CPD})V_{AC}\sin(\omega_{AC}t) \tag{4.5}$$

$$F_{2\omega} = \frac{\partial C}{\partial z}\frac{V_{AC}}{4}\cos(2\omega_{AC}t) \tag{4.6}$$

The operation principle of KPFM is based these three forces, F_{DC}, F_{ω} and $F_{2\omega}$. We would also use similar concepts to explain our results in chapter 8.

Since KPFM is based on the dynamic modes of AFM, it can be operated in either AM or FM mode as well. The principles and feedback loops designs of AM- and FM-KPFM are show in Figure 4-3. In AM-KPFM, the amplitude of the oscillating cantilever at ω_{AC} is taken as control signal. Once the feedback loops get the signal of amplitude, it would adjust V_{DC} to minimize the difference between V_{DC} and V_{CPD}, thus nullifying F_{ω} and the amplitude. The adjustment of V_{DC} is can be used to map the CPD of the sample.[43] In FM-KPFM, the frequency shift of the oscillation cantilever from ω_{AC} is the control signal instead. Similarly, the feedback loops would adjust V_{DC} to reduce the frequency shift and the adjustment of V_{DC} can be converted to the image of CPD since they possess the same magnitude but opposite sign.

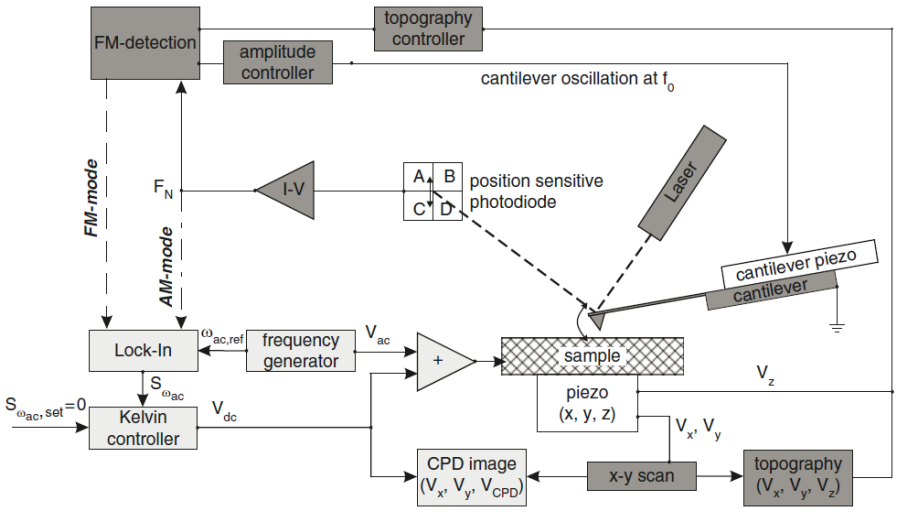

Figure 4-3 Scheme of the operation principle of a KPFM. [Sadewasser, S., Experimental Technique and Working Modes. In *Kelvin probe force microscopy: measuring and compensating electrostatic forces*, Sadewasser, S.; Glatzel, T., Eds. Springer-Verlag Berlin Heidelberg: Heidelberg ; New York, 2012; pp 7-24.][44] (Used under fair use, 2013)

4.2 Technique of Force Measurement

Both the contact mode and dynamic modes can be used in surface force measurement.[33,41] Here we only introduce the fore measurement technique in contact mode since we use this mode in this work.

The principle of surface force measurement by AFM, as shown in Figure 4-4, is different from that of imaging. For imaging, the cantilever usually with a sharp tip would scan the sample surface, which is controlled by a feedback loop. However, for force measurement, a microsphere would be attach to the end of the cantilever, used as a tip/probe, and the cantilever or the sample, depending on where the piezo is located, would approach and retract the sample surface as illustrated in the right-hand side of Figure 4-4. The cantilever with a microsphere is so-called the colloidal probe, which is developed to quantitatively measure the surface forces.[33] The reasons for using a microsphere rather than a sharp tip are as follows. First, the force between a colloidal probe and sample is larger than that between a sharp tip, which usually only has a 5-10 nm radius, and sample based on the Derjaguin approximation so the measurement can be more accurate. The Derjaguin approximation is expressed as

$$F(D) \approx 2\pi \left(\frac{R_1 R_2}{R_1 + R_2} \right) W(D) \qquad (4.7)$$

where D is the distance between the two subjects (e.g., the colloid and the sample), R_1 and R_2 the radii of the two subjects, respectively, and W the interaction free-energy.[45] Second, more quantitative analysis, such as calculating the surface energy by the Derijaguin approximation can be proceeded since the geometry of the colloidal probe is known and it is easy to determine the radius of a microsphere. Also, the surface roughness of a microsphere can be controlled and examined easier than that of a small, sharp tip during manufacturing. Furthermore, we can choose to use the microspheres made from different materials and/or coated with different chemicals/materials, such as hydrophobic functional groups and gold to study surface forces in different systems.[33]

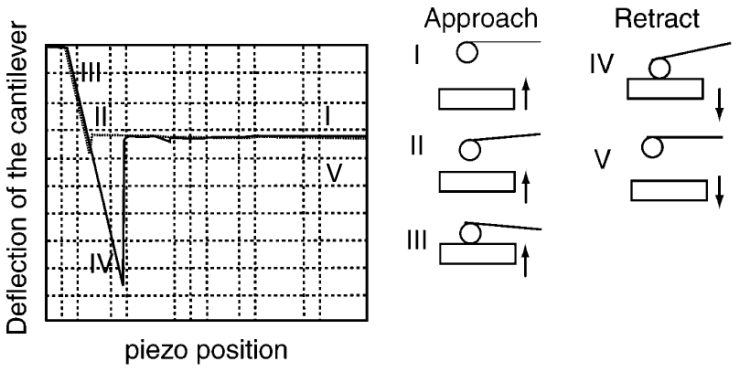

Figure 4-4 On the left, a typical raw data diagram of the deflection of the cantilever (i.e., the deflection of the laser beam for the catnielver) vs. the piezo position (i.e., the displacement of the piezo) from a force measurement by AFM is shown. On the right, the scheme of the behaviors of a cantilever with respect to a flat sample in a force measurement is illustrated. [Ralston, J.; Larson, I.; Rutland, M. W.; Feiler, A. A.; Kleijn, M., Atomic force microscopy and direct surface force measurements - (IUPAC technical report). *Pure and Applied Chemistry* **2005**, *77* (12), 2149-2170.][34] (Used under fair use, 2013)

A typical raw data curve from the force measurement by AFM is shown in the left-hand side of Figure 4-4. There are five regions in this curve corresponding to different behaviors of the cantilever which are illustrated on the right of Figure 4-4. In region I and V, the distance between the probe and the sample is so large that the colloidal probe does not sense any force and no bending of the cantilever. In region II, however, the distance is quite short; thus the colloidal probe starts to sense some forces, either attractive (in Figure 4-4) or repulsive (in Figure 4-5), and the cantilever deflection is not flat anymore. In region III, the probe contacts the

sample and moves compliantly with the piezo. This linear region is called the constant compliance region and reflects the optical sensitivity of the photodiode with respect to the cantilever deflection, which is usually used to calibrate the cantilever deflection.[34,46] In region IV, the cantilever still contacts the sample but the piezo moves in an opposite direction. Once the restoring force of the cantilever is large enough to pull off the cantilever itself from the sample surface, the cantilever would jump back to the original position (i.e., region V) since the distance between the colloidal probe and the sample is large and no surface force is sensed by the colloidal probe.

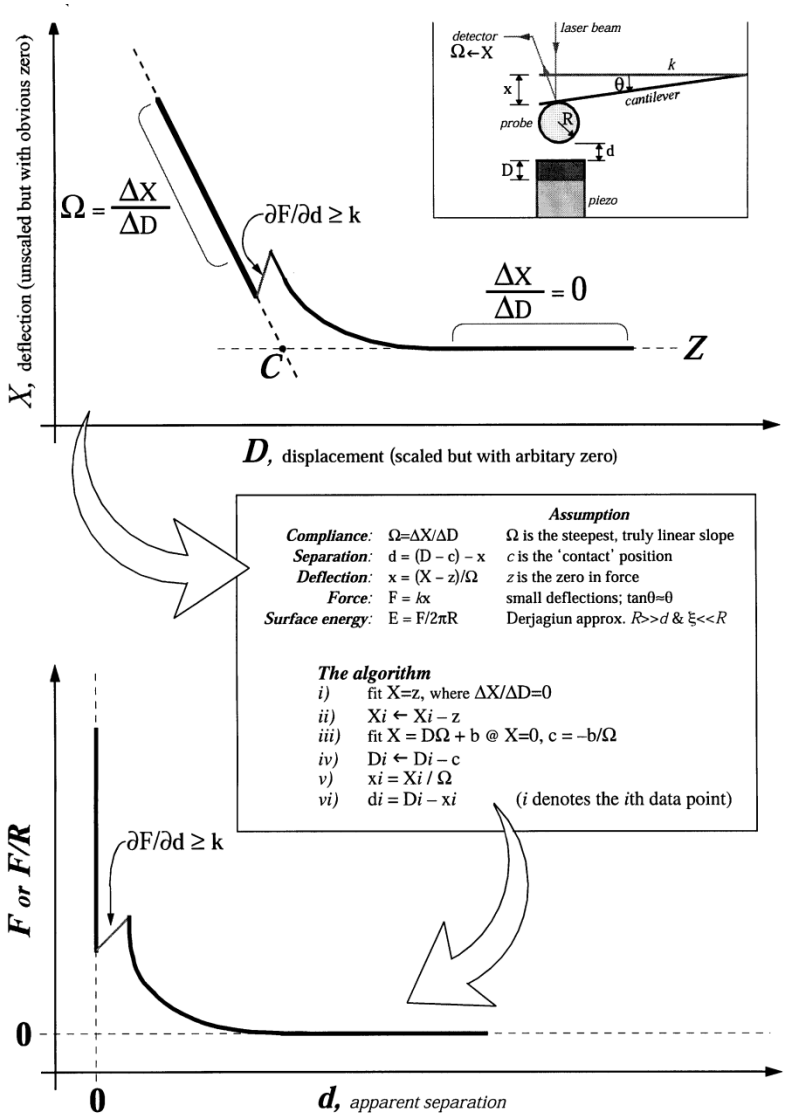

Figure 4-5 The procedure for converting a cantilever deflection vs. piezo displacement curve to a force vs. distance curve. [Senden, T. J., Force microscopy and surface interactions. *Current Opinion in Colloid & Interface Science* **2001**, *6* (2), 95-101.][46] (Used under fair use, 2013)

The standard procedure for converting the raw data to a force curve is illustrated in Figure 4-5. Usually the cantilever deflection at large distance (z in Figure 4-5) is assumed no measured surface force and is used to define the zero of cantilever deflection signal. As mentioned before, the slope of the constant compliance region (Ω) is used to calibrate and convert the cantilever deflection signal into units of distance. Then the calibrated and converted deflection signal (x) would be multiplied by the calibrated spring constant of the cantilever with the microsphere (k) to get the surface forces between the colloidal probe and the sample. The separation or distance (d) between the colloidal probe and the surface is the relative movement between the cantilever (x) and the piezo (D) and the contact position (c) is used to define the zero separation.[46] However, in this work, we modify this procedure since the electric field-induced force is a very long-range force and we need to use the data collected under no electric field to define the zero of the cantilever deflection signal. We will state our modify procedure in Chapter 6 for details.

Chapter 5 – Experimental Section

5.1 AFM Setup

This work was mainly performed with a Cypher™ AFM (Asylum Research, Santa Barbara, CA). To measure the F_{DEP} between the two particles, we modified the AFM as shown in Figure 5-1.

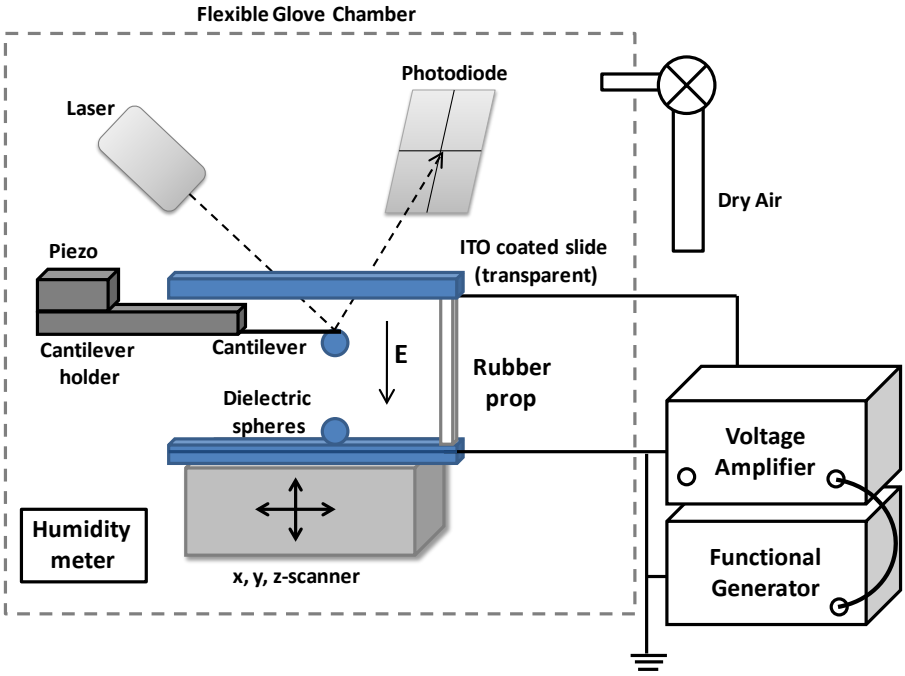

Figure 5-1 Schematic of apparatus. The sphere attached to the cantilever is referred to as the "top sphere" whereas the sphere attached to the scanner is referred to as the "bottom sphere

The electric field was created using two electrodes separated with a gap of 7.00 mm by a rubber prop. Indium tin oxide (ITO) coated slides which are transparent but highly conductive were chosen as the electrodes to allow the laser beam pass through the top electrode as shown in Figure 5-1. The applied voltage was generated by a function generator (Mode1395 100 MHz Synthesized Arbitrary Waveform Generator, Wavetek-Datron) and amplified 100× by a voltage amplifier (Model 2100HF High Frequency High-Voltage Power Amplifier, Trek Inc.). The voltage was varied from 60 to 220 V rms (root-mean-square). All voltages in this thesis are rms values. The frequency was in the range from DC to 1 MHz.

To create a low humidity environment, the whole AFM was enclosed in a flexible glove chamber (GLOVE BAG™ Inflatable Glove Chamber, Glas-Col LLC) supplied with dry air

continuously circulated. The RH can go down to less than 3% within around 1 to 2 hours but the measurement was executed after about 8 hours of continuous flow to ensure the surface of the microspheres and their surroundings are dry enough. During the measurement, dry air still circulated to maintain the low humidity environment. The air flow did not significantly affect AFM operation which has been examined by measuring the variation of the deflection of laser beam with time (Figure 5-2). The RH and temperature in the chamber was monitored by a humidity meter (THWD-3 Relative Humidity and Temperature Meter, Amprobe). All measurements of field-induced interactions between two spheres were conducted at 2 ± 1 % RH and 25 ± 3 °C.

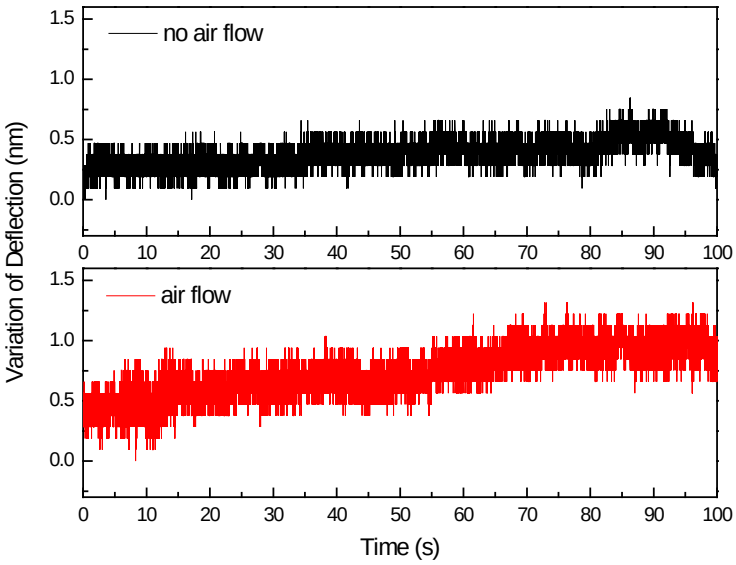

Figure 5-2 Effect of air-flow on deflection of AFM cantilever in glove bag. Plot shows deflection of cantilever as a function of time with no air flow (top) and with air flow (bottom).

5.2 Sample Preparation

A barium titanate ($BaTiO_3$) glass microsphsere (MO-SCI Specialty Products, L.L.C.) was attached to the end of a silicon rectangular shaped cantilever (tipless, NSC12/no backside metal coating, MikroMasch) with heat-softening epoxy resin (Epikote 1004) by micromanipulators under an optical microscope. The attachment was confirmed by an optical microscope. The normal spring constants and resonant frequencies of the colloidal probes and cantilevers alone were calibrated by the Hutter method[47]. The surface roughness of the microspheres on the

cantilever was examined by inverse imaging with a TGT01 grating (NT-MDT). The microspheres had a roughness less than 500 pm rms over the areas of 1 μm x 1 μm and 500 nm x 500 nm. For studying field-induced interactions between two spheres, the $BaTiO_3$ glass spheres were attached to a thin glass slide with epoxy resin by using micromanipulators. The sizes of the microspheres used in this study verified by using the camera module of the AFM were approximately 30 μm in diameter.

5.3 Alignment of Two Particles

To investigate field-induced intershpereical interaction, the two microspheres were first aligned manually using a video microscope that is part of the AFM, and then aligned more accurately by imaging the bottom sphere with the top sphere. After imaging the sphere on the glass slide on the bottom electrode by the colloidal probe, the commercial AFM software can identify and control the relative position of the top and bottom spheres. Thus, we can align the two microspheres and measure the force as a function of distance between the apexes of the spheres via the software.[34]

5.4 Force Curve Collection and Analysis

Since the electric field-induced force is a long range force, we modified the normal procedure. In the normal method, the zero of force is determined from the force (deflection) at large separation, where there is no surface force. When there is a very long range and slowly varying force, it is difficult to know at what separation zero force occurs. In addition, there is a complicating effect, the virtual deflection[48], where the signal from the deflection varied slowly with distance, even when there is no change in force.

Fortunately, the field-induced force can be conveniently turned on and off with a switch, so we have established the zero force with the field turned off. Thus, for each condition (e.g., at 60 V and 5 kHz), two successive force curves, one with and one without an applied voltage, were collected for around one second of each other. The measurement without an applied voltage was used to determine “zero deflection” as in the normal method as shown in Figure 5-3 (a). The two measurements (with and without the applied field) were each analyzed in the normal way, i.e. to produce a force–separation plot, thereby ensuring that the two curves have the same zero of separation, and were not shifted due to slight changes in temperature. The deflection signal in the

(a)

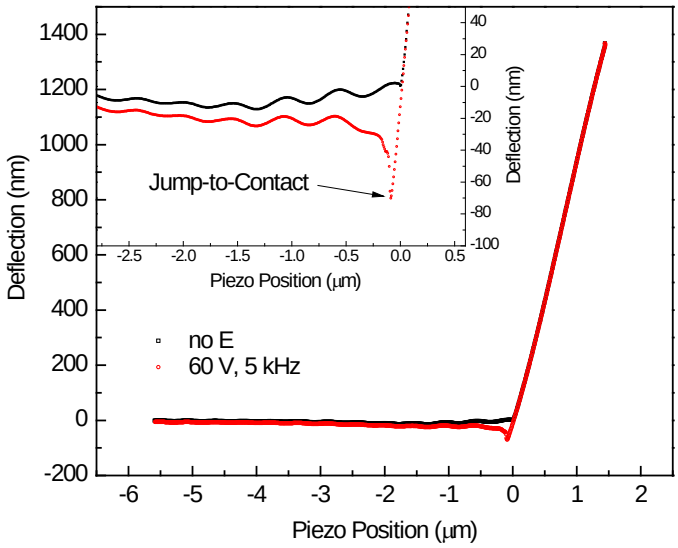

(b)

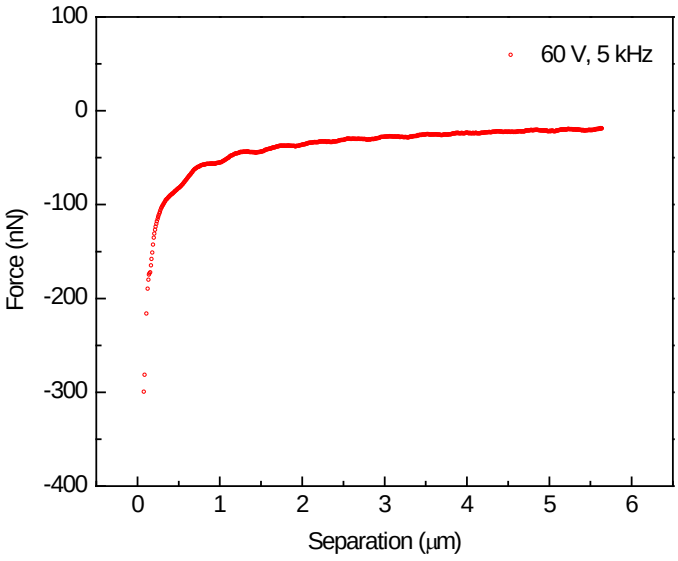

Figure 5-3 (a) Raw data showing deflection–piezo position with the field on or off. (b) Net Force as a function of separation after the zero field data has been subtracted.

absence of the field was then subtracted from the deflection signal in the field. An additional effect of this subtraction is that all other contributions to the measured force are removed. We have explicitly assumed that these other contributions are additive. These other contributions include measurement artifacts due to variation in the laser signal with separation (virtual

deflection and optical interference between reflections of light from the cantilever and sample) and real forces, such as the van der Waals force. Thus, we assume that the van der Waals force is not affected by the applied field. In practice, this is a small assumption because the van der Waals force is very weak and short range (Figure 5-3 (a)) compared to the field-induced force, and is usually only significant at separations where we are unable to measure data because of a mechanical instability.

Chapter 6 – Results and Discussions

As described in section 3.2.1, an AC electric field-induced force consists of a constant (time-averaged) term and a time-varying term. By rewriting the Maxwell-Wagner model, we can get

$$
\begin{aligned}
F &= \frac{12\pi\varepsilon_m R^6}{r^4}\beta_{eff}^2(\omega)\vec{E}_0^2[(3\cos^2\theta_{ij}-1)\vec{e}_r+(\sin 2\theta_{ij})\vec{e}_\theta] \\
&= \frac{12\pi\varepsilon_m R^6}{r^4}\beta_{eff}^2(\omega)E_0^2(\cos^2\omega t)[(3\cos^2\theta_{ij}-1)\vec{e}_r+(\sin 2\theta_{ij})\vec{e}_\theta] \\
&= \frac{12\pi\varepsilon_m R^6}{r^4}\beta_{eff}^2(\omega)E_0^2\frac{(1+\cos 2\omega t)}{2}[(3\cos^2\theta_{ij}-1)\vec{e}_r+(\sin 2\theta_{ij})\vec{e}_\theta] \\
&= \frac{12\pi\varepsilon_m R^6}{r^4}\beta_{eff}^2(\omega)\left[E_0^2/2+E_0^2(\cos 2\omega t)/2\right][(3\cos^2\theta_{ij}-1)\vec{e}_r+(\sin 2\theta_{ij})\vec{e}_\theta] \\
&= \frac{12\pi\varepsilon_m R^6}{r^4}\beta_{eff}^2(\omega)\left[E_{rms}^2+E_{rms}^2(\cos 2\omega t)\right][(3\cos^2\theta_{ij}-1)\vec{e}_r+(\sin 2\theta_{ij})\vec{e}_\theta]
\end{aligned}
$$

When the two particles align with the direction of the applied electric field (i.e., $\theta_{ij}=0$), the AC electric field-induced force between two identical particles can be expressed as

$$
F = \frac{24\pi\varepsilon_m R^6}{r^4}\beta_{eff}^2(\omega)E_{rms}^2+\frac{24\pi\varepsilon_m R^6}{r^4}\beta_{eff}^2(\omega)E_{rms}^2(\cos 2\omega t) \qquad (6.1)
$$

The first term on the right hand side of Eq. (6.1) is referred to as static component[49, IV] of F_{DEP} (i.e., the time-averaged term) which is related to the translation behavior of particles under an electric field. The second term is called dynamic component[IV] of F_{DEP} (i.e., the time-varying term) representing the vibration behavior of particles under an AC electric field. Note that the amplitude of the dynamic component is the same as the static component. Most studies pay attention on the static component of F_{DEP} and scarcely discuss the dynamic component due to the heavy damping effect for small particles in liquid media or no obvious oscillation for large particles with large mass inertia in gas media.[7] In this study, we have developed a special

[IV] The static component is also called DC component or DC offset, which is the average value of a signal.[49] And the dynamic component is called AC component.[49] To avoid confusion DC and AC will only be used to describe the applied field, while "static" and "dynamic" are used to describe the resultant force .

experimental setup and measurement techniques by AFM to observe the translation and vibration behaviors of a microparticle in air simultaneously. In addition to study the time-averaged electric field-induced force between two closely spaced spherical dielectric microparticles, we have also found that the vibration behavior of small particles would affect their translation behaviors while they are close enough in air. Therefore, we also describe and discuss the interesting dynamic component. We believe both static and dynamic components of the electric field-induced force of two closely spaced microparticles are important for better understanding the interfacial and surface phenomena under an electric field.

Our analyses and discussion are divided into several sections as follows. The contribution from the cantilever to the total force measured by AFM will be introduced and discussed first in section 6.1. Then, we will discuss the static and dynamic behavior of the colloidal probe to determine the behavior of small particles in air under an AC electric field in section 6.2. We will then discuss how the electric field affects the time-averaged electric field-induced force in section 6.3 and field-induced adhesion in section 6.4.

6.1 Cantilever Contribution to the Total Measured Electric Field-Induced Force

The main objective of this thesis is to understand how an external electric field affects the forces between two spherical particles. However, our measurement necessitates the use of an AFM cantilever to determine the force, and this cantilever can also be polarized and can affect the polarization of the spheres, so it was necessary to first characterize the behavior of the cantilever. The behavior of the cantilever is interesting in its own right because an applied filed can be used to drive the oscillation of a cantilever.

The three experimental systems are shown in Figure 6-1: (a) cantilever with sphere attached (colloidal probe) interacting with sphere; (b) cantilever only and (c) cantilever interacting with sphere. When comparing results from these three systems, our objective is to finally understand the two sphere experiment, so we always describe a range of separations that are relevant to that system. Thus the cantilever is always the same distance from the lower plate when we compare different experiments. For example, if the range of separations of interest is 0–6 μm in a sphere-sphere (diameter 30 μm) experiment, then the cantilever is 60–66 μm from the

plate during the experiment. Thus the relevant separation for the cantilever in the cantilever-only experiment is also 60–66 μm from the plate.

Figure 6-2 (a) shows the forces between the cantilever and the bottom electrode under an electric field and no electric field, respectively. The results demonstrate that even when the separation is quite large (from 60 to ~66 μm), the cantilever still can be polarized and sense a strong attractive force, implying the field-induced force is a strong long-range force. In addition, force for system (c) is greater than (b) so the cantilever interacts significantly with the bottom sphere.

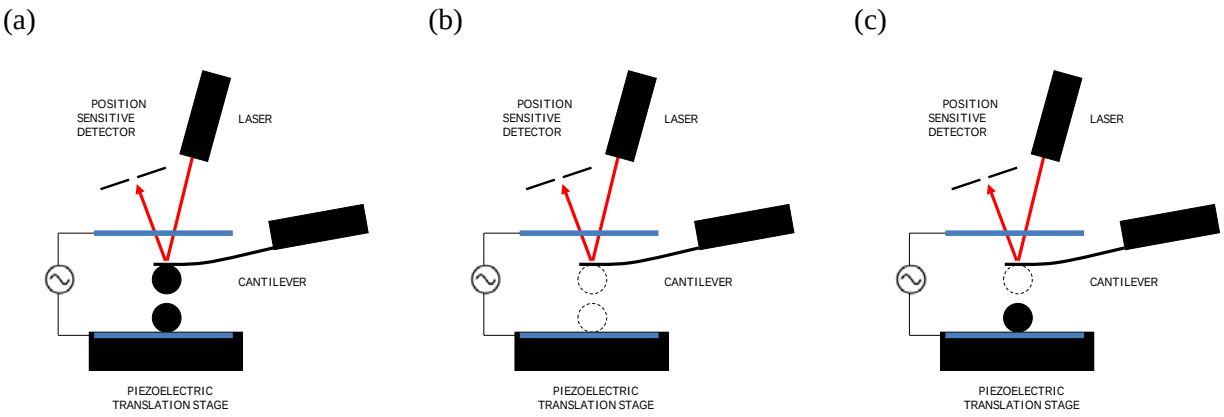

Figure 6-1 The three different systems considered here (a) Two spheres system: The field-induced force between two $BaTiO_3$ glass microspheres was measured. Note that the measured force in this system contains the contribution from the cantilever. (b) Cantilever-only system. This is used to determine the effect of the field on the cantilever. (c) Cantilever-bottom sphere system. This is used to determine the interaction between the cantilever and bottom sphere. The dash circles represent the locations of the spheres in the two spheres system, which means the separations between the cantilever and the bottom electrode in these three systems are the same.

In more detail, the field-forces of the cantilever-only system and the cantilever-bottom sphere system (Figure 6-2 (b)) have no significant separation dependence. This shows that there is little variation in the field at this large separation and/or that the force has a short range. This is useful because the shape of the sphere-sphere force curve is not affected by the cantilever. When we bring the cantilever much closer to the bottom plate (separation 0–5 μm), the force decreases exponentially with distance.

Figure 6-2 (b) displays the comparison of the forces of three different systems at 60 V and 5 kHz. As expected, the force of the two spheres system is the largest since it contains the

(a)

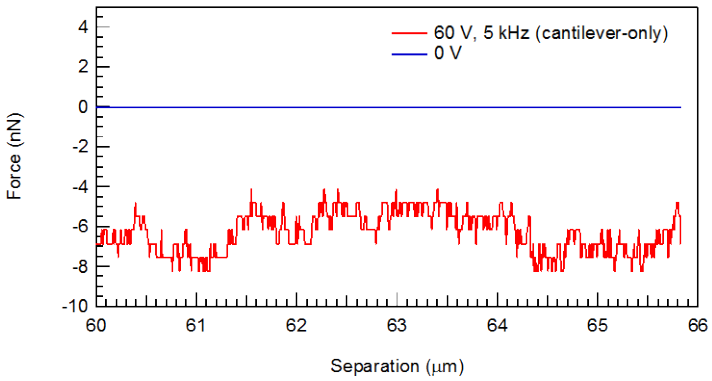

(b)

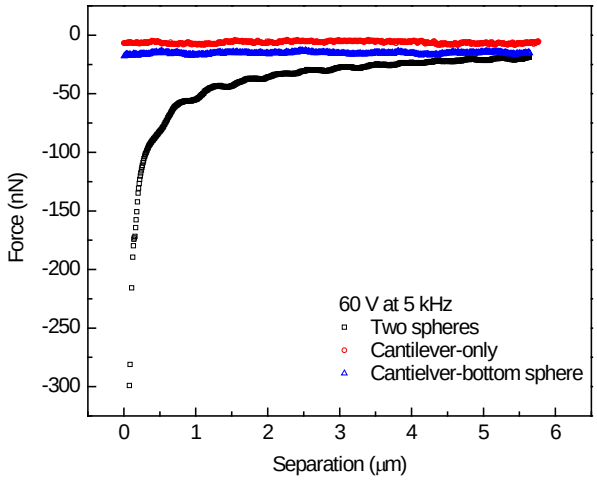

Figure 6-2 (a) Comparison of the force under an electric field (at 60 V and 5 kHz) to the force without applying electric filed from the cantilever-only system. The separation here is the distance between the cantilever and the bottom electrode. (b) The comparisons of three separation-dependent forces from three different systems at 60 V and 5 kHz. Note the separation here is the distance between two spheres in the two spheres system. For the cantilever-only system, the separation should be "separation + 60 μm"; for the cantilever-bottom system, it should be "separation + 30 μm."

contributions from the cantilever and spheres. As the separation is large (e.g., 5 μm in the two spheres system), the field-induced force of the cantilever-bottom system (- 13.33 nN at 5 μm) is larger than half that of the two spheres system (-20.78 nN at 5 μm), indicating that the contribution from the cantilever to the measured field-induced force is significant at large separation. However, the field-induced force of the cantilever-bottom system is equal to and/or less than half the forces of the two spheres while the separation is equal to and/or smaller than 3 μm. Similar results were obtained from a series of different applied voltages and frequencies.

Thus, we would not consider the forces at the separation larger than 3 μm in the following discussion.

6.2 AC Electric Field-Induced Oscillation Behavior of a Colloidal Probe

To study the vibration behaviors, we collected time series of the deflection signal at sample rate 5 MHz while the colloidal probe was approached to and retracted from the bottom $BaTiO_3$ glass microsphere with different applied voltages and frequencies. The small data blocks (40000 samples) at the separation from around 2 μm to 1.85 μm while the probe was approached to the bottom sphere were chosen to convert to amplitude-frequency spectra by fast Fourier transformation (FFT) with the application of a Hanning window (IGOR Pro 5.02, WaveMetrics, Portland, OR) so that the effect of cantilever can be neglected in the data analyses.

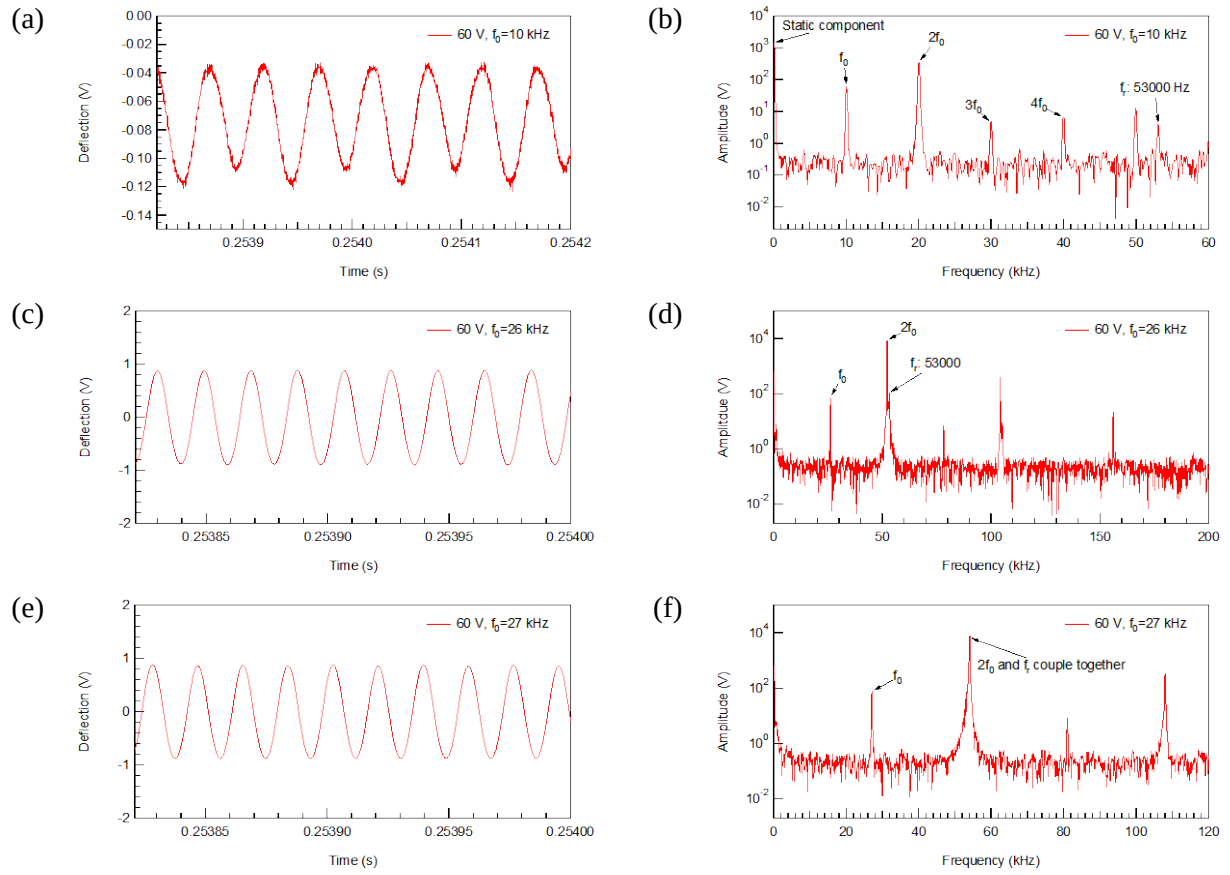

Figure 6-3 Time series data of the deflection signal of the two spheres system when the applied voltage is 60 V and the applied frequency is: (a) 10 kHz; (c) 26 kHz; (e) 27 kHz and the corresponding FFT spectra (b), (d) and (f) respectively. The resonant frequency of the colloidal probe is 53 kHz.

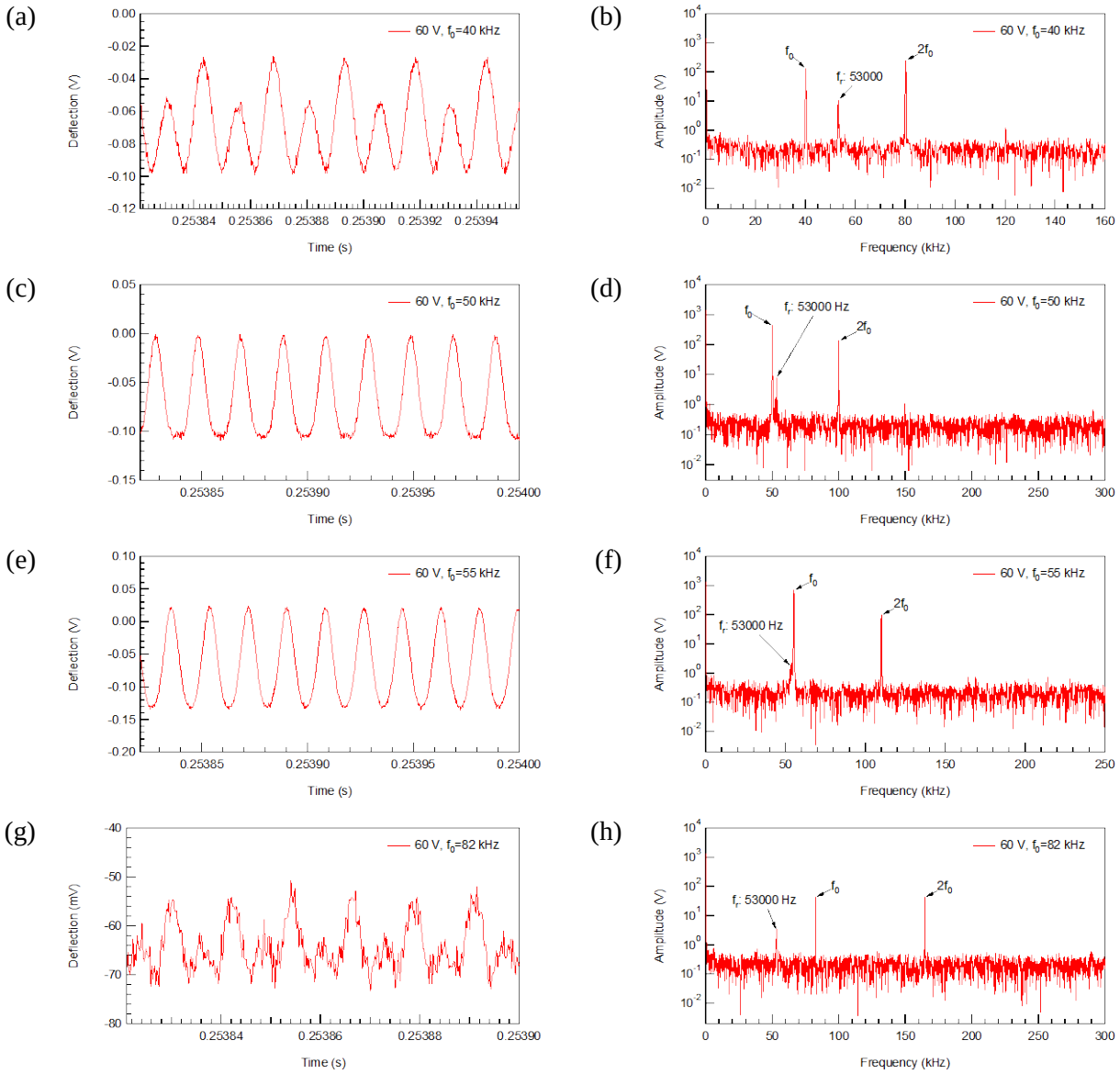

Figure 6-4 Time series data of the deflection signal of the two spheres system when the applied voltage is 60 V and the applied frequency is: (a) 40 kHz; (c) 50 kHz; (e) 55 kHz; (g) 82 kHz and the corresponding FFT spectra (b), (d), (f) and (h) respectively. The resonant frequency of the colloidal probe is 53.0 kHz.

From equation 6.1, we expect that the time series data will show a peak at two times the drive frequency ($2f_0$). The measured time series of the deflection data is shown in Figure 6-3 Figure 6-4, along with Fourier transforms. The measured data can be more complex, because (i) the cantilever has its own response function and (ii) there could be other forces. The response function of the colloid probe can be determined from the thermal noise spectrum, which shows that the cantilever resonance (f_r) is at 53 kHz. Thus, we always expect a constant response

function below 53 kHz, a stronger response at 53 kHz and a weaker response at higher frequencies. The thermal noise is present during all experiments so we always expect to see a peak at 53 kHz regardless of the drive frequency. This can be seen in Figure 6-3 and Figure 6-4. We also see the response at $2f_0$ in all data, confirming the applicability of Eq. (6.1). However, there are also other harmonics (f_0, $3f_0$, $4f_0$, etc.). The amplitude of different peaks at different applied frequency is summarized in Figure 6-5.

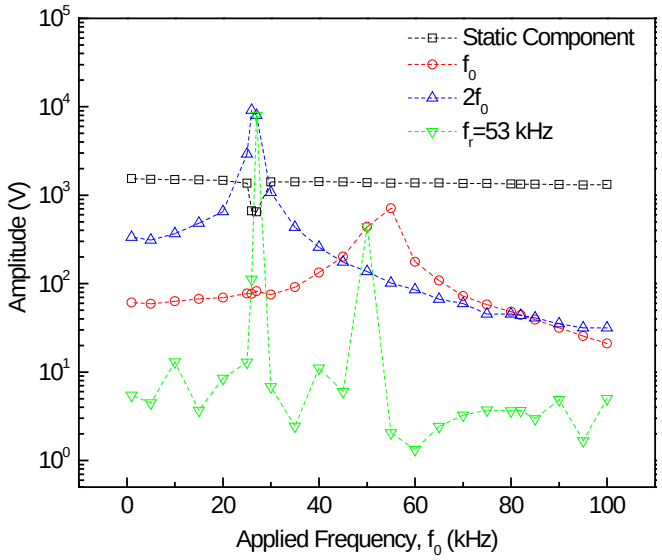

Figure 6-5 The comparison of the magnitude of different peaks that response at 0 (i.e., static component), f_0, $2f$ and f_r at different applied frequencies (f_0).

Both the Maxwell-Wagner Model (Eq. 3.3.24) and Colver's equivalent circuit model (Eq. 3.3.39) point out that the electric field-induced force is proportional to the square of the electric field. By rearranging the equations (e.g., Eq. (6.1)), we can conclude that particles under an AC electric field would vibrate at $2f_0$ in theory. In addition, the cantilever would vibrate under an AC electric field at $2f_0$ as well. The reason for the cantilever vibration is the cooperation of the mechanical spring force from the cantilever itself and the AC electric field-induced force between the cantilever and the electrodes. Take the electrodes and the cantilever as two parallel-plate capacitors in series as illustrated in Figure 6-6 and assume that they have the same area and the fringing fields can be neglected.[50,51] Since the cantilever is polarized by the electrodes,

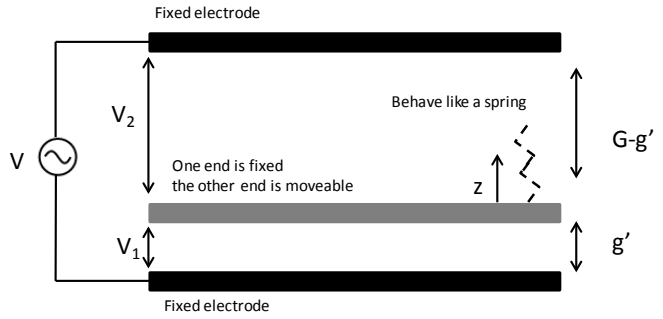

Figure 6-6 The scheme of the configuration of the cantilever and electrodes, where g is the gap between the cantilever and bottom electrode, G is the gap between the two electrodes, g' is the gap between the cantilever and the bottom electrode, z is the displacement of the cantilever, V is the applied voltage, V_1 is the voltage between the cantilever and bottom electrode, and V_2 is the voltage between the cantilever and top electrode. Note that $V=V_1+V_2$. The bottom electrode was totally fixed. Although the top electrode was fixed at one end, it still can be taken as "totally fixed" due to its large mass inertia. The cantilever was only fixed at one end.

electric fields would be built between the cantilever and the top and bottom electrodes respectively. Assuming that the voltage between the cantilever and the bottom electrode is $V_1 = V_{1,0}\cos(\omega_0 t)$ and that between the cantilever and the top electrode is $V_2 = V_{2,0}\cos(\omega_0 t)$; thus $V = V\cos(\omega_0 t) = V_1 + V_2$. As a result, the net force of the configuration illustrated in Figure 6-3 can be expressed as[50,51]

$$\begin{aligned} F_{net} &= -\frac{1}{2}\frac{\varepsilon A'}{(g'-z)^2}V_1^2 + \frac{1}{2}\frac{\varepsilon A'}{(G-g'+z)^2}V_2^2 + kz \\ &= -\frac{1}{2}\frac{\varepsilon A'}{(g'-z)^2}V_{1,0}^2\cos^2(\omega_0 t) + \frac{1}{2}\frac{\varepsilon A'}{(G-g'+z)^2}V_{2,0}^2\cos^2(\omega_0 t) + kz \end{aligned} \tag{6.2}$$

where A' represents the area of the electrode plate and the cantilever respectively and the positive sign is for the forces that increase the gap between the cantilever and the bottom electrode. On the right hand side of Eq. (6.2), the first term is the electrostatic force between the cantilever and bottom electrode, the second term is the electrostatic force between the cantilever and top electrode and the third term is the spring force of the cantilever. In Eq. (6.2), the magnitude of the electrostatic forces change with the applied frequency and time at a fixed magnitude of the applied voltage, thus changing the corresponding spring force according to the Newton's third law. Therefore, the frequency of the net force "waveform" would be equal to $2f_0$ theoretically.

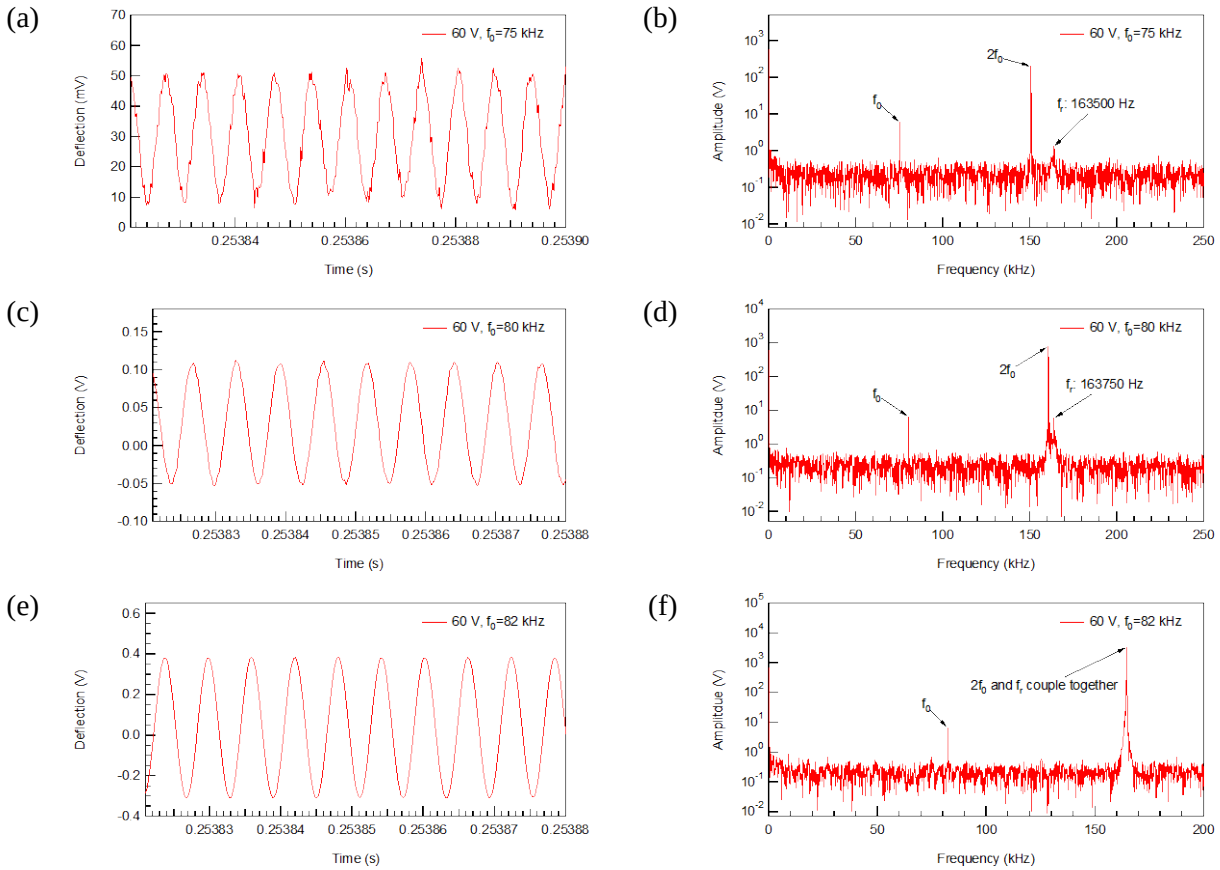

Figure 6-7 Time series data of the deflection signal of the cantilever-only system when the applied voltage is 60 V and the applied frequency is: (a) 75 kHz; (c) 80 kHz; (e) 82 kHz and the corresponding FFT spectra (b), (d) and (f) respectively. The resonant frequency of the cantilever is 164 kHz.

Our results (Figure 6-3, Figure 6-4 and Figure 6-5) demonstrate that the AC electric field-induced force indeed response at $2f_0$. Nevertheless, we found that the force would also response at f_r and other nf_0 (n is a non-zero positive integer) as well, which cannot be explained by the above theories. We also collected time series of the deflection signal of the cantilever-only system as shown in Figure 6-7. Similar phenomena can be observed in the cantilever-only system as well even if the f_r of the cantilever without mounted sphere is 164 kHz, which is quite different from that of the colloidal probe. The detected peak at f_r is quite small and mostly is buried in the noise floor as shown in Figure 6-7 (b) and (f). Besides, no peak prevails above the noise floor at $3f_0$ and $4f_0$ in the cantilever-only system, which may be buried in the noise floor as well. The magnitude of different peaks at different response frequencies and different applied frequencies is summarized in Figure 6-8. Likewise, the magnitude of the static

component is always the largest except at around half f_r of the cantilever (i.e., 82 kHz). As for the dynamic component, the peak that responses at $2f_0$ is the largest, especially at half f_r. The magnitude of the peak at f_0 has no big difference at different f_0, for f_0 does not cover f_r of the cantilever.

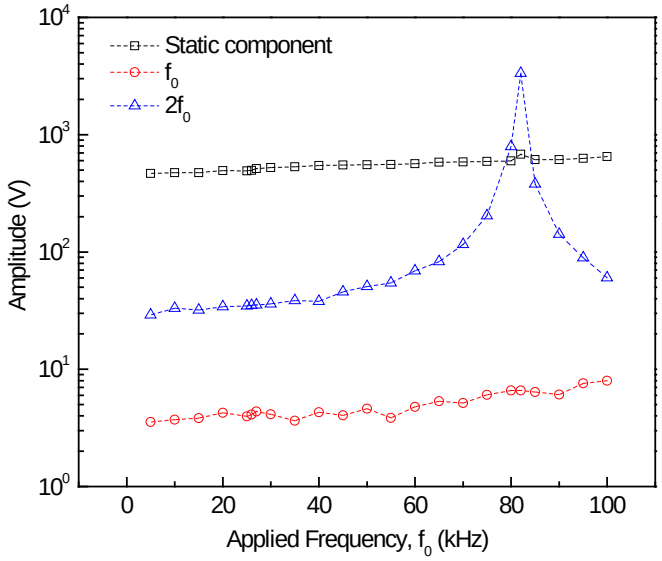

Figure 6-8 The comparison of the magnitude of different peaks that response at 0 (i.e., static component), f_0 and $2f_0$ at different applied frequencies (f_0).

The possible reason for the appearance of the peak at $4f_0$ in the two sphere system may be the local electric field around the spheres due to the polarized charge on the two spheres. Since the top sphere mainly oscillates at $2f_0$, the bottom sphere would sense a field with frequency $2f_0$ due to the polarized charges on the top sphere and thus has polarized charges alternating at $2f_0$. Likewise, the top sphere would sense a field with frequency $2f_0$ due to the polarized charge on the bottom sphere and thus would response at twice the $2f_0$; that is, $4f_0$. Note that the peak at $4f_0$ is smaller than the peak at $2f_0$ in Figure 6-3 (b), (d) and (f) since the polarized charges induced AC local field is much smaller than the externally applied field. This also explains why no peak prevails above the noise floor at $6f_0$ in the two spheres system. In the

cantilever-only system, only a cantilever is under an electric field so no local field induced from the polarized charge on other objects and hence no peak prevails at $4f_0$.

(a)

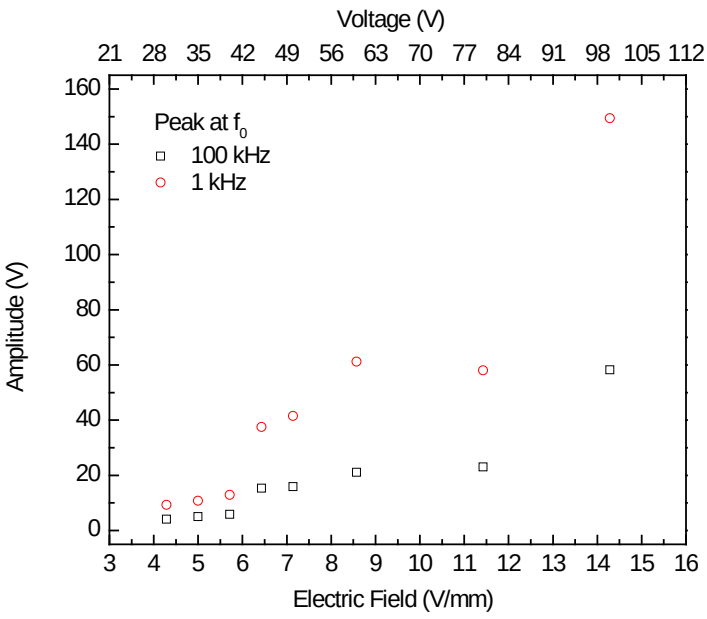

(b)

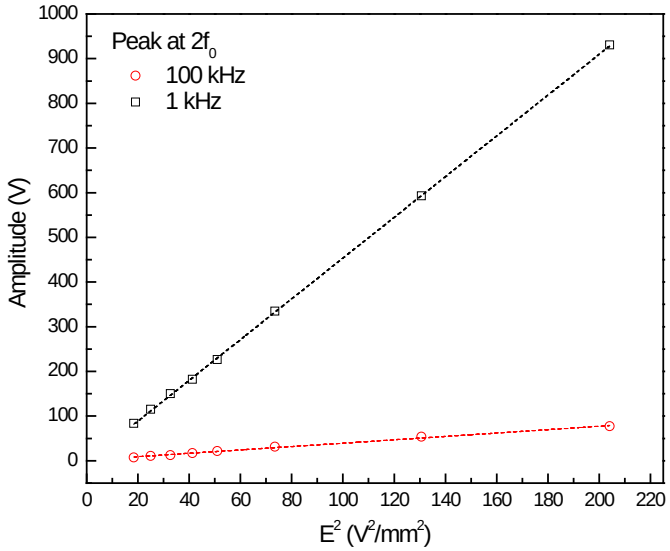

Figure 6-9 The correlation between the applied electric field strength and the amplitude of the peak at (a) the applied frequency f_0 and (b) twice the applied frequency $2f_0$ in the two spheres system.

As for the peak at f_0 in the FFT spectra of both the two spheres system and the cantilever-only system, Kaler *et al.* have reported similar results for a 45-μm-diameter protoplasted tobacco plant cell suspended in sorbitol solution under a low-frequency electric field.[52] They suggest that the peak at f_0 is attributed to the Coulomb interaction between the

(a)

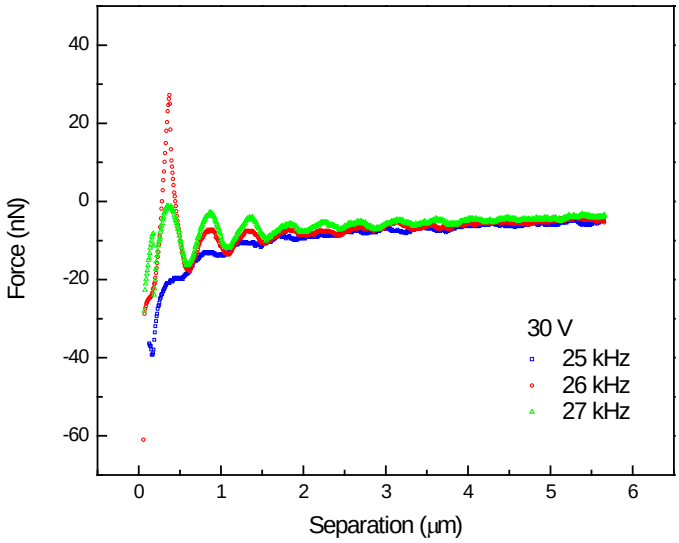

(b)

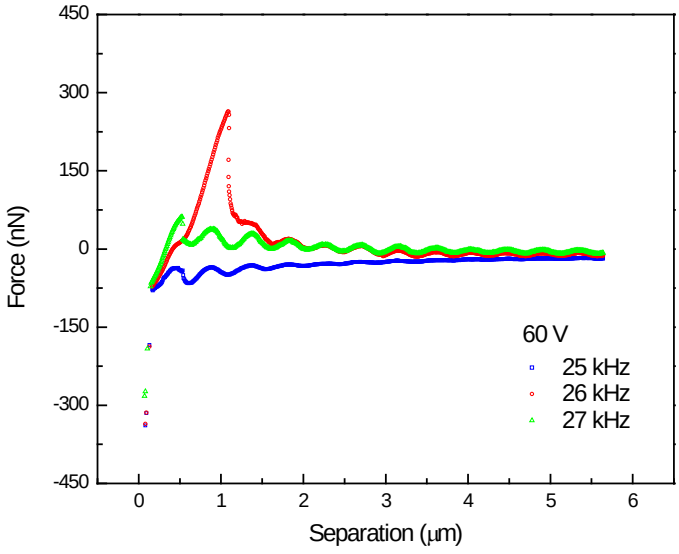

Figure 6-10 The variation of the AC electric field-induced force with the separation between two $BaTiO_3$ glass microspheres at the applied voltage: (a) 30 V and (b) 60 V when the applied frequency is around half the resonant frequency of the colloidal probe (i.e., 53 kHz).

surface charges on the cells in the aqueous medium and the external electric field (i.e., electrophoresis). Based on their results, they found that the magnitude of the oscillation is proportional to the applied voltage at frequency above ~10 Hz when the applied frequency is ranged from ~1 to ~1000 Hz. Nevertheless, based on our results, we do not find any correlation between the applied field strength and the amplitude of the peak at f_0 (Figure 6-8 (a)) whereas the amplitude of the peak at $2f_0$ is proportional to the square of the applied field strength, agreeing with the Maxwell-Wagner and Colver's models (Figure 6-8 (b)). We are not sure whether the peak at f_0 is attributed to the surface charge or not. It may also result from the nonlinearity of our systems. Further study is necessary to understand these phenomena.

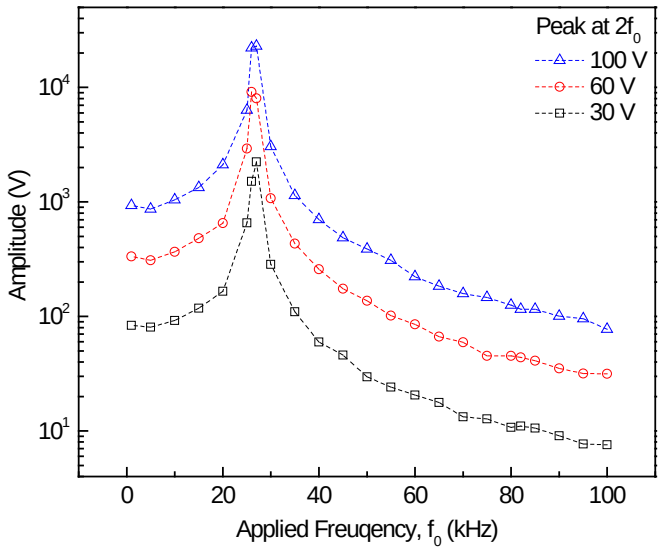

Figure 6-11 The comparison of the magnitude of the colloidal probe vibration responses at twice the applied frequency when the applied voltages are 30, 60 and 100 V.

Note that the peak at $2f_0$ abruptly increases and become the largest peak (larger than the static component) when f_0 is equal to half f_r in the two sphere system and cantilever-only system. This is because the colloidal probe/cantilever vibrates at $2f_0$ and when f_0 is equal to half f_r of the colloidal probe/cantilever, $2f_0$ is equal to f_r and resonance of the colloidal probe/cantilever happens. Figure 6-10 shows the force curves of the static component of the two

sphere system when the applied frequency is around half the resonance frequency. As shown in Figure 6-10, the colloidal probe is not able to measure the force due to its resonance. Therefore, while the colloidal probe resonates (i.e. the applied frequency is at 25, 26, or 27 kHz), the measured forces are not legitimate and we would not concern these into our discussion.

We also study the effect of the applied electric voltage on the amplitude of the deflection signal at different applied frequency. Figure 6-11 shows the comparison of the peak at $2f_0$ at different applied voltages and applied frequencies. The magnitude of the amplitude increases with the applied voltage. As the applied voltage increases, the resonance still occurs when the applied frequency is half f_r of the colloidal probe. This indicates that no electrostatic spring softening/hardening effect happens, which would decrease/increase the resonant frequency of the resonator.[53]

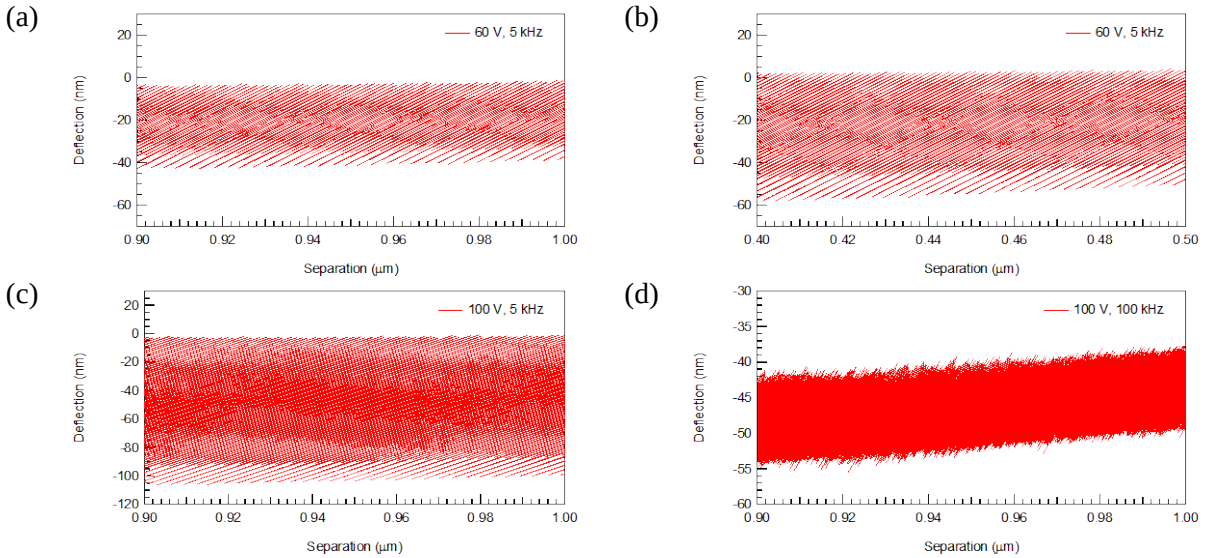

Figure 6-12 The variation of the deflection signal at the separation between the two $BaTiO_3$ glass microspheres ranged from (a) 0.90 to 1.00 μm; (b) 0.40 to 0.50 μm as the applied voltage is 60 V and the applied frequency is 5 kHz and at the separation ranged from 0.90 to 1.00 μm when the applied voltage is 100 V and the applied frequency is (c) 5 kHz; (d) 100 kHz.

In addition to the time series of the deflection signal, we also analyze the variation of the deflection signal with the separation between the two $BaTiO_3$ glass microspheres. Figure 6-12 (a) and (b) show the variation of the deflection signal at two different regions of the separation between the two $BaTiO_3$ glass microspheres when the applied voltage is 60 V and the applied frequency is 5 kHz. As the range of the separation is between 0.90 and 1.00 μm, the amplitude of

the deflection is around 40 nm. However, the amplitude becomes around 60 nm as the range of the separation is between 0.40 and 0.50 μm. This may be because the local electric field between the two spheres becomes stronger while the separation between the spheres decreases. When the two spheres get closer with each other, the degree of the polarization increases since the polarized spheres can polarize each other as well, causing the electric field around the closely spaced spheres in fact is stronger than the applied one. The amplitude is proportional to the AC electric field-induced force so the amplitude would increase with the increase of the local electric field strength. Also, the amplitude would incrase with the applied voltage (Figure 6-12 (a) and (c)) and change with the applied frequency (Figure 6-12 (c) and (d)), following the trend of the curves in Figure 6-11 due to the nature of vibration.

Since the colloidal probe under an AC electric field would vibrate while it is approaching to the bottom sphere, it would bounce back when the separation between the two spheres is comparable to the amplitude of the colloidal probe vibration as shown in Figure 6-13 (a) and (b). The increase of the amplitude of the deflection signal with the decrease of the separation

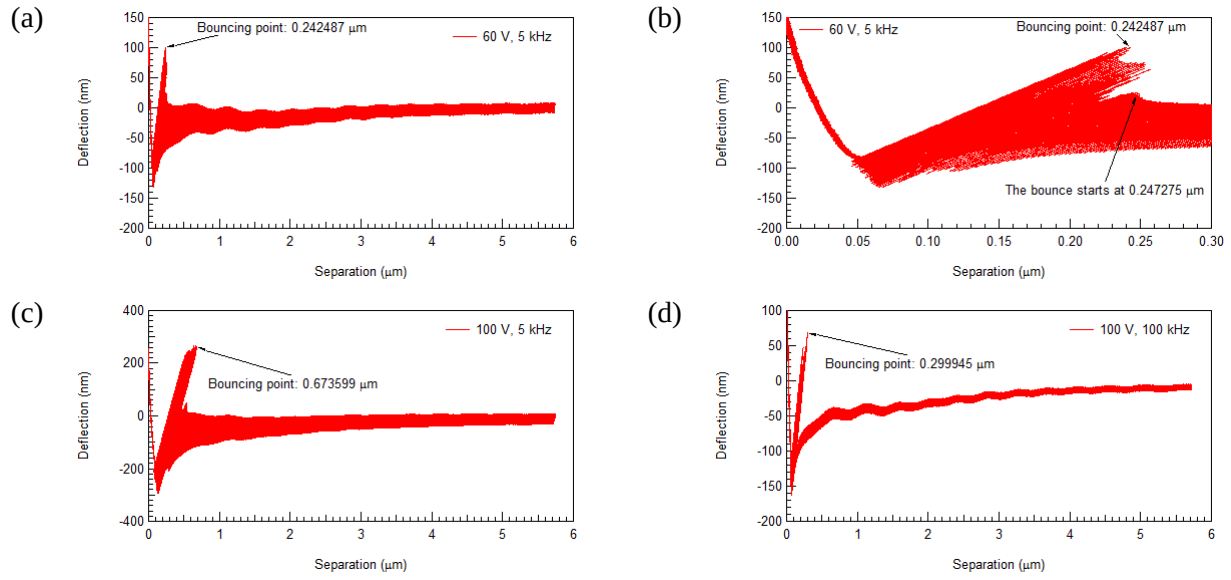

Figure 6-13 The variation of the deflection signal with the separation between the two $BaTiO_3$ glass microspheres at different applied voltages and frequencies: (a) 60 V, 5 kHz; (b) the enlargement of the bouncing point of (a); (c) 100 V, 5 kHz; (d) 100 V, 100 kHz.

between the two microspheres would aggravate this phenomenon, giving rise to the electric field dependency of the bounce (Figure 6-13 (a) and (c)). Furthermore, the bounce is applied

frequency-dependent as well due to the frequency-dependent amplitude as shown above. In Figure 6-12, we point out where the colloidal probe would bounce back, which is referred to as "bouncing point" and summarize them at some conditions in Table 6-1. At a fixed applied frequency, the bouncing point increases with the applied voltage. At a fixed applied voltage, the bouncing point would increase with the applied frequency when it is below or equal to the resonant frequency of the colloidal probe but decrease with the applied frequency when it is above the resonant frequency, like the trend of curves in Figure 6-11. Note that there is no apparent bounce as the applied frequency is 100 kHz. For example, the bouncing point is 295 nm as the applied voltage is 100 V and the applied frequency is 100 kHz. Thus, we would discuss the data at 100 kHz from 100 V to 30 V for the static components in the following sections since this set is affected by the vibration of the colloidal probe much less. Also the smallest separation we would concern is 300 nm.

Table 6-1 Brief summary of the bouncing point at different applied voltages and frequencies.

Applied Voltage and Frequency	bouncing point (nm)
120, 100 kHz	869.54
100 V, 5 kHz	673.60
100 V, 100 kHz	299.95
60 V, 5 kHz	242.49
60 V, 100 kHz	153.89
30 V, 5 kHz	None
30 V, 100 kHz	None

6.3 Electric Field-Induced Force between Two Dielectric Microspheres

We measured the variation of the AC electric field-induced force (F_{in}) with different separations between the two $BaTiO_3$ glass microspheres and different applied voltages/applied electric field strengths (E_0) at different frequencies. Figure 6-14 shows the frequency dependence of the field-induced force and the negative sign of the force means the measured force is an attractive force. In Figure 6-14 (a), the field-induced force does not change with frequency at different separations. In Figure 6-14 (b), there is no obvious variation of the field-induced force from 1 kHz to 100 kHz at difference voltages. Thus, our results demonstrate that the AC field-induced force between two dielectric microspheres at 1-100 kHz is independent of

(a)

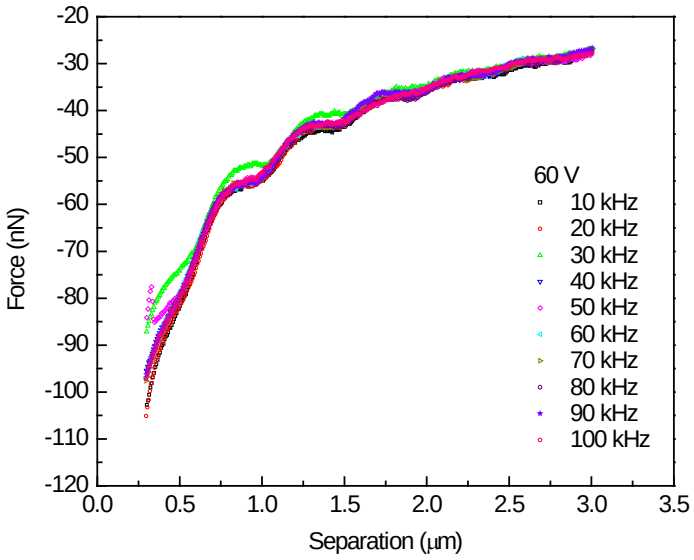

(b)

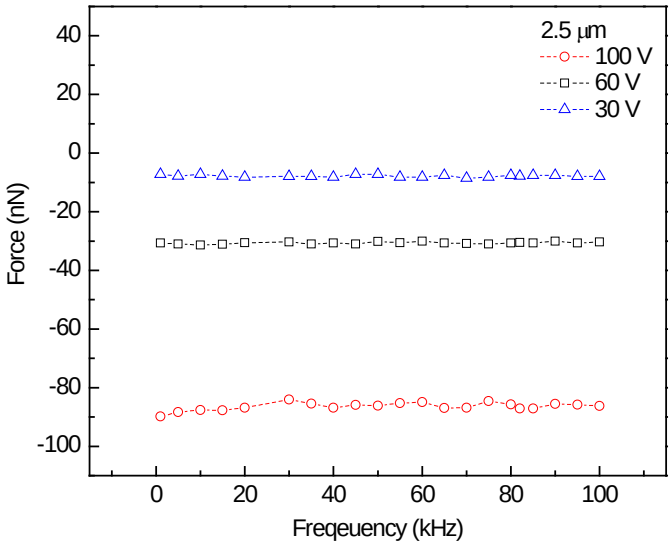

Figure 6-14 (a) The variation of the AC electric field-induced forces with the separation between two $BaTiO_3$ glass microspheres at different frequencies when the applied voltage is 60 V. (b) The variation of the AC electric field-induced forces with frequencies at different applied voltages when the separation between the two dielectric microspheres is 2.5 μm.

the frequency. Based on the Maxwell-Wagner model,[5,12] the frequency-dependent term in the Maxwell-Wagner model can be expressed by combining Eq. (3.21) and Eq. (3.22)

$$\beta_{eff}^2 = \frac{(\sigma_p - \sigma_m)^2 + \omega^2(\varepsilon_p - \varepsilon_m)^2}{(\sigma_p + 2\sigma_m)^2 + \omega^2(\varepsilon_p + 2\varepsilon_m)^2} \tag{6.3}$$

Since the dielectric constant of $BaTiO_3$ glass microspheres[25, 54,V] and the range of the frequency we used are quite high, we can ignore the terms of conductivity in Eq. (6.4), resulting in β_{eff}^2 independent of the frequency. In addition, the frequency-dependent terms in Colver's model[31] (Eq. (3.35)) can be neglected as well due to the large dielectric constant of $BaTiO_3$ and applied frequencies. Hence, our results about frequency dependence of the AC field-induced force agree not only with Maxwell-Wagner model but also with Colver's model. Although some research results[31,10] demonstrate that the AC field-induced force is frequency-dependent, the range of the frequencies they used is so small that the conductivity would dominate the field-induced force, not the dielectric constant. Some charges would easily accumulate at the material surfaces under a low-frequency or DC field; that is the Maxwell-Wagner interfacial Relaxation,[7,27] causing the time-varying field-induced force even if the humidity is well-controlled.

To verify that our results do not have the Maxwell-Wagner interfacial relaxation, we measured the variation of the field-induced force with time when the colloidal probe was positioned around 6 μm above the bottom microsphere and hovered for over 100 seconds.[18] We also measured the force without any electric field as a reference. Figure 6-15 shows our results of examining on Maxwell-Wagner Relaxation effect. In Figure 6-15 (a) and (b), the force varies with time as a DC field is applied but the force maintains constant as 1 kHz electric field is applied. This examination points out that the permittivities of the particles and the medium dominate the field-induced force, not their conductivities under the applied AC field in our experiment, implying the crossover frequency is lower than the 1 kHz for our system. We also study the effect of the electric field strength on the rate of the charge accumulation by comparing the variation of the normalized force with time (Figure 6-15 (c)). Surprisingly, there is no big difference when the applied voltage is doubled. The above examination and analysis of the Maxwell Wagner Relaxation effect suggests that AFM has potential to quantitatively study this

[V] The $BaTiO_3$ glass microspheres we used are not made of $BaTiO_3$. The composition (by weight) of the microspheres is SiO_2 (1~20%), B_2O_3 (1~20%), ZrO_2 (1~10%), BaO (40~70%), and TiO_2 (40~70%).[54(a)] Thus the relative permittivity of the particle we used may be less than 80[54(b)] but still much higher than that of air and of cantilever. And the electrical conductivity of oxides are usually quite low (< ~10^{-3} S/m)[54(c)]. Further, BaTiO3 is ferroelectric so the special phenomena of the ferroelectric materials under an electric field are not taken into account here since the microspheres are not made of ferroelectric materials.

effect at micro- and/or nanoscale, which may help the study of high-dielectric electronic materials.[55]

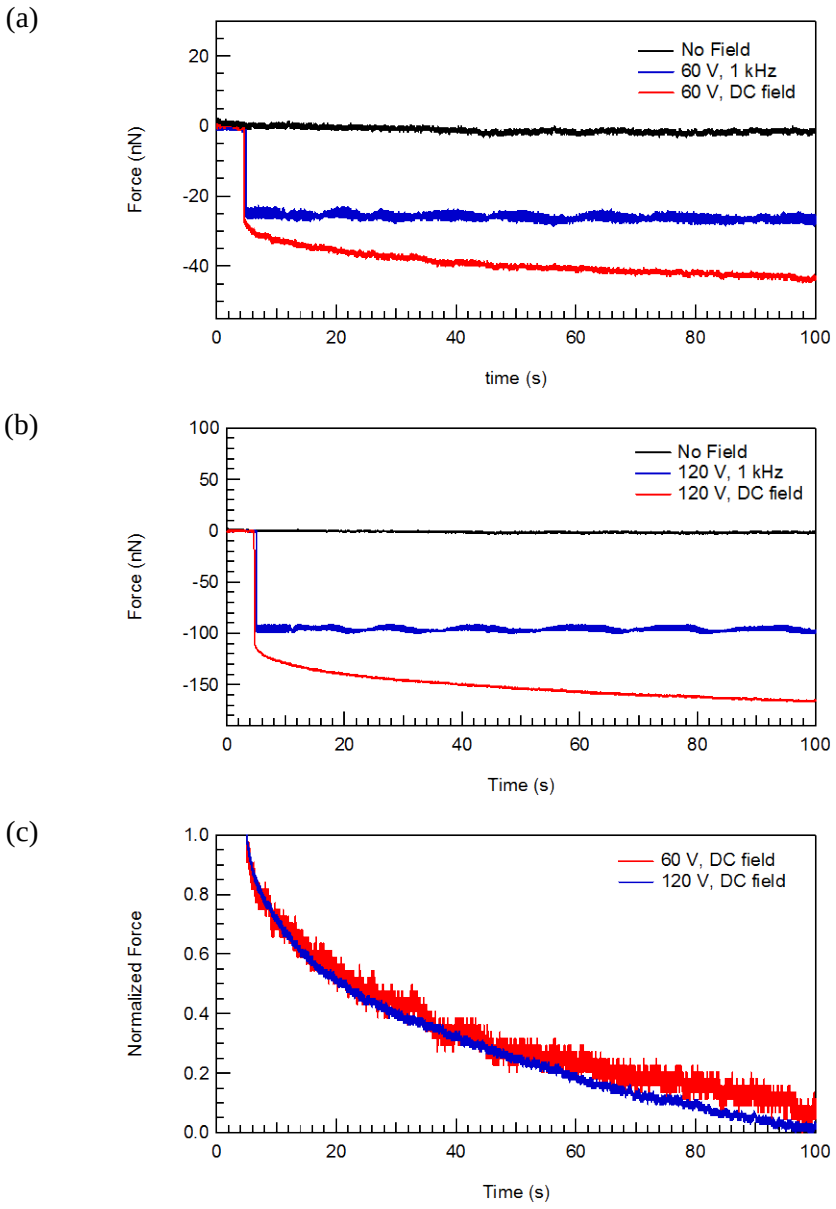

Figure 6-15 The variations electric field-induced force between two dielectric microspheres with time when the applied voltage is (a) 60 V and (b) 120 V and the distance between the two spheres is around 6 μm. The electric fields were applied after AFM started to record the data for about 5 seconds. (c) The variation of normalized DC electric field-induced force with time at difference applied voltages.

Beside the frequency dependence, we have also studied the relationship between the field-induced force and the applied electric field strength at different separations as shown in Figure 6-16. Our analyses manifest that the field-induced force would increase with the applied

voltage/electric field strength. In addition, the shorter the separation between the two microspheres is, the lager the field-induced force is. To elucidate the relationship between the filed-induced force and the electric field strength for two closely spaced dielectric microspheres, we choose to plot the field-induced force versus the square of the applied electric field strength (Figure 6-16). Surprisingly, the plotted curves exhibit linearity even when the separation is two orders smaller than the diameter of the microsphere. Although according to the Maxwell-Wagner model (Eq. (3.20)) the field-induced force should be proportional to the square of the applied electric field strength, the model is , however, derived from the concept of the point-dipole approximation, which is legitimate when the separation between the spheres is more than one diameter.[56]

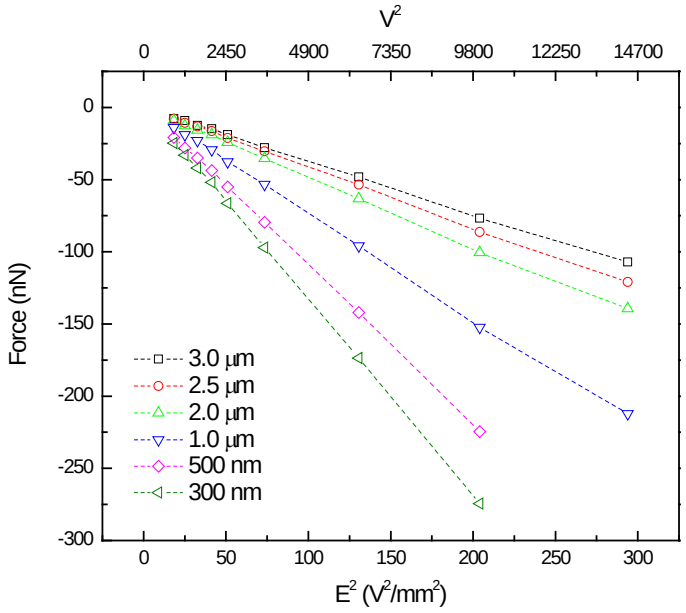

Figure 6-16 Relationship of the electric field-induced forces between two $BaTiO_3$ glass microspheres with the square of the applied electric field at different separation as the applied frequency is 100 kHz.

To further study this, we also compare our results with the theoretical calculation from two analytical models, the Maxwell-Wagner model and Colver's equivalent circuit model as shown in Figure 6-17. The calculated forces are smaller than the experimental results. The discrepancy is expectable since the local electric field (i.e., the electric-field distribution around the region where spheres are going to contact each other) for the closely spaced spheres is much

higher than the applied electric field (E_0).[57] Therefore, we conclude that the electric field around the microsphere is indeed distorted and enhanced due to the small separation between the two spheres.

(a)

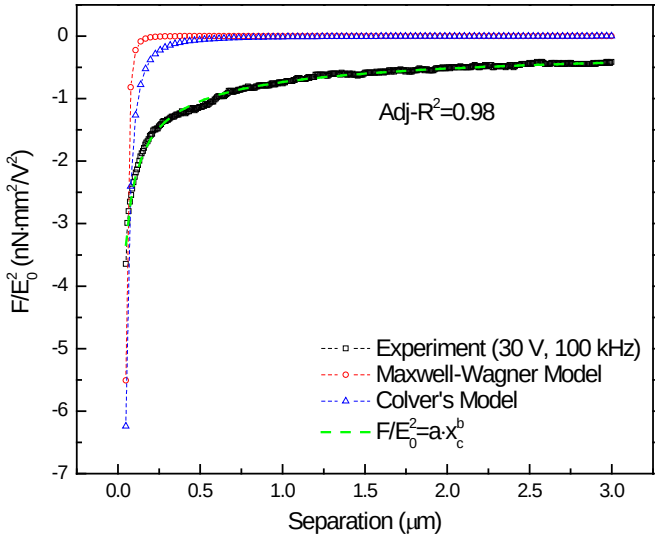

(b)

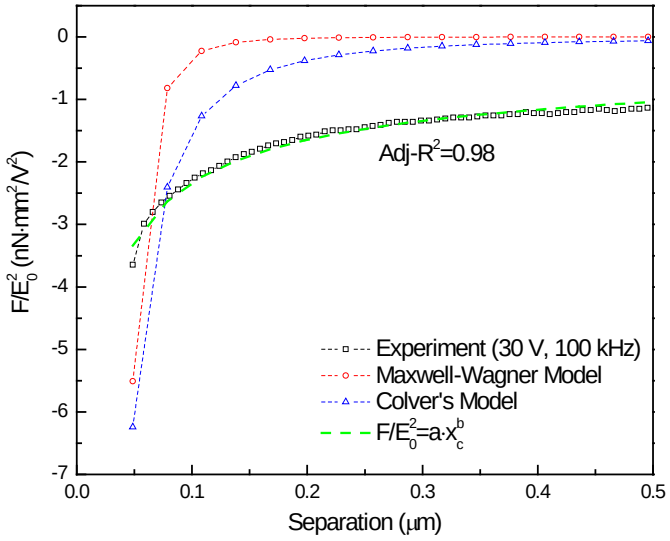

Figure 6-17 (a) Comparison of the measured electric field-induced force with calculated results from different models and the fit to a simple power law, $F / E_0^2 = a \cdot x_c^{-b}$, where a and b are constants and b=0.5671. (b) The enlargement of (a) at small separation.

Note that the simulated curve from Colver's model is closer to the experimental data than that from the Maxwell-Wagner model when the separation is around 350 nm. The main difference between these two models is that the field-induced force is inversely proportional to the fourth power of the distance between the centers of the two spheres in the Maxwell-Wagner model but in Colver's model, the field-induced force is inversely proportional to the square of the separation between the two spheres (i.e, from the bottom of the sphere to the top of the other sphere).

Although we do not have a good theoretical model for the force, we have examined the fit to a simple power law, $F / E_0^2 = a \cdot x_c^{-b}$ where a and b are fitting constants. A good fit is obtained when $b = 0.5671$, even at small separation, as shown in Figure 6-18.

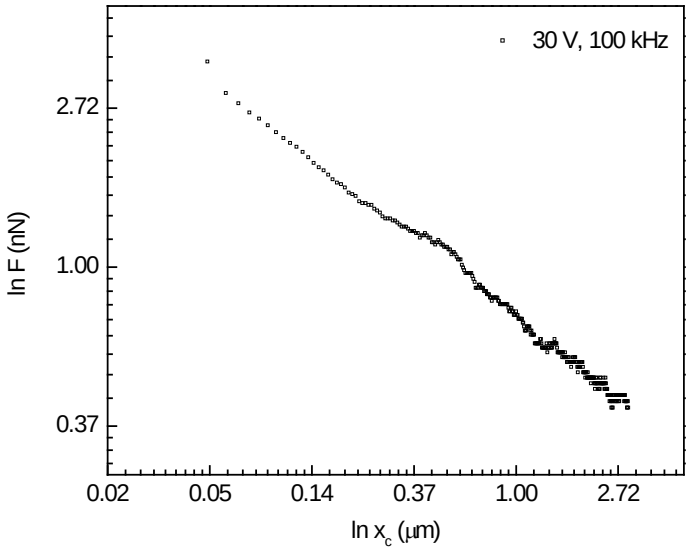

Figure 6-18 The linearity between $\ln F$ and $\ln x_c$.

6.4 Electric Field-Induced Adhesion Force

The field induced force increases in magnitude as the separation decreases but we are unable to measure the force at very small separations because the spring becomes mechanically unstable. One additional point that is experimentally accessible is the force at zero separation, which can be obtained by bringing the spheres into contact and measuring the force required to

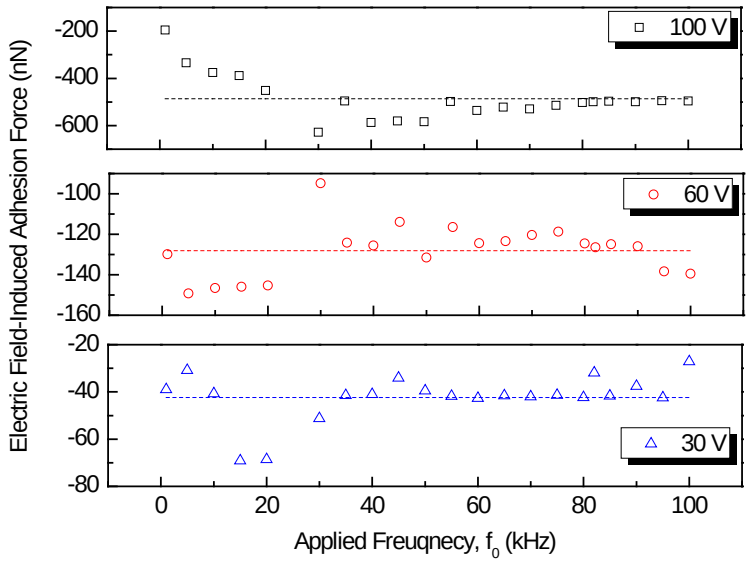

Figure 6-19 The variation of the AC electric field-induced adhesion with different applied frequencies when the applied voltages are 100, 60 and 30, respectively. The dash lines represent the average values of each set of data.

pull them apart. This is the adhesion force, which has many applications in particle removal, friction, resistance to disruption of particle aggregates, etc. We measured the adhesion for both the DC force and the AC force. First, we examined the frequency dependence of the AC force. The oscillatory response makes interpretation of this measurement more complicated because the oscillation will make it easier for the particle to pull off the surface. Figure 6-19 shows that the force is mainly independent of frequency, as for the forces at finite separation. There is a large amount of scatter at low frequency, but we could not determine a consistent trend.

Figure 6-20 (a) shows the adhesion forces with and without field. When the field was off, the measured adhesion force can range from -700 nN to -1200 nN. The possible reasons for such large deviation are that the contact charges were generated while the colloidal probe was used to scan the bottom sphere for finding the apex of the bottom sphere and the two spheres contected during the force measurement no matter the field was on or off. Bunker *et al.* have studied the electrostatic force between a lactose microsphere and a glass slide by AFM in these two situations at different humidity: i) repeatedly contacting the particle with the glass slide in the

(a)

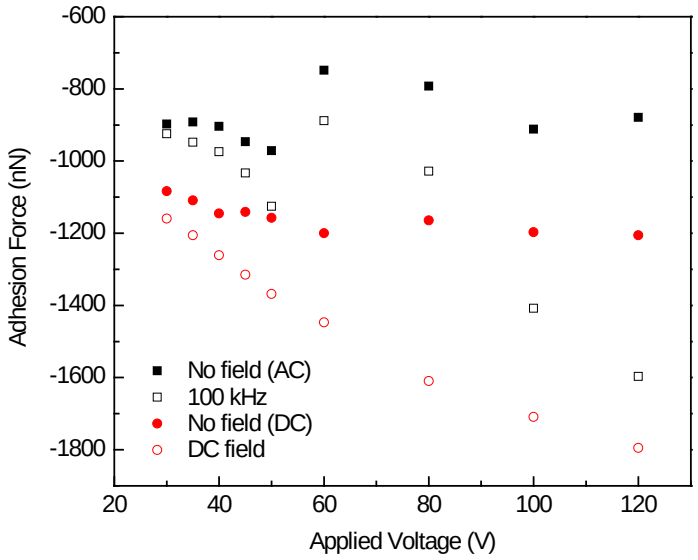

(b)

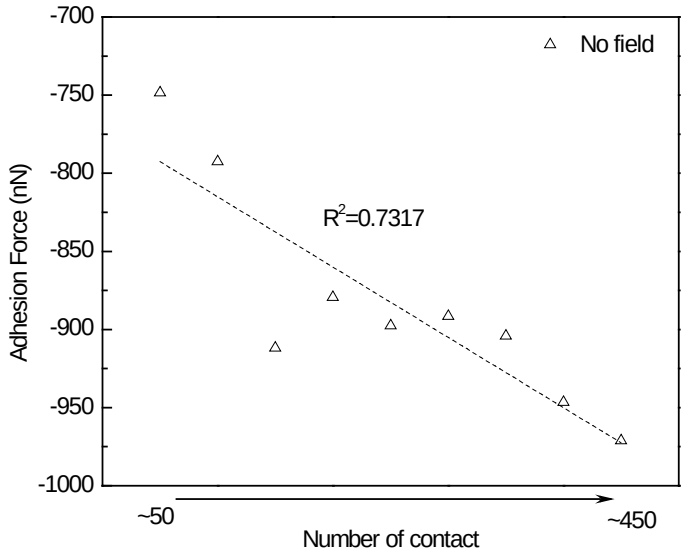

Figure 6-20 (a) Adhesion force with field on and off. The solid spots means field off and the hollow spot means field on. (b) Correlation between the number of time of two spheres contact and the adhesion force.

normal direction by taking force-distance curves (contact charging) and ii) scanning the particle across the surface of glass slide in contact mode imaging (tribocharging).[58] They found both the contact charging and tribocharing would generate contact charge at the surface at 0.1% RH. In addition, the more the time that two spheres contacted, the higher the electrostatic force is. We

also found similar qualitative results in our system as shown in Figure 6-19 (b). This hypothesis corresponds to the existence of the peak at f_0 in the FFT spectra of dynamic component as well. Due to the possible existence of contact charges at the sphere surface, we subtract the adhesion force without the field from the adhesion force with the field to get the field-induced adhesion force as shown in Figure 6-21. Figure 6-21 shows the electric field dependence of the electric field-induced adhesion force for the AC applied field and for the DC applied field. For both of these fields, the adhesion is proportional to the square of the field strength, as for the force at a finite separation, which implies that its origin is DEP (Figure 6-16). The important point is that the adhesion can be systematically varied by the application of an electric field, and increased greatly compared to the adhesion in the absence of a field. Note also that the DC-induced adhesion is greater than the AC-induced adhesion. This result plus the dependence on the square of the field is again consistent with results at finite separation so we again attribute the force to accumulation of charges at the surface (the Maxwell-Wagner relaxation effect).

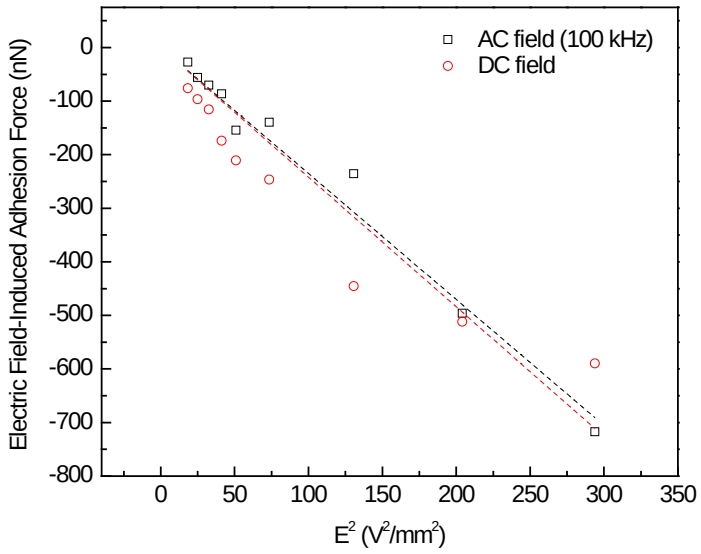

Figure 6-21 Relationship between the electric field-induced adhesion force and the square of the applied electric field strength under a DC and an AC electric field, where the frequency of the AC field is 100 kHz. The dash lines are the linear fitting results.

Chapter 7 – Conclusions

We developed a quantitatively technique to measure the forces of two dielectric microspheres induced by an external electric field in a low humidity environment by AFM. Different from other proposed techniques, AFM can precisely control the relative position of the microspheres, thus able to study the relationship between electric field-induced force and the separation between two spheres, which is scarcely studied due to the limitation of the measurement technique.

By the technique we developed, we measured the electric field-induced force and electric field-induced adhesion force between two $BaTiO_3$ glass microspheres under a DC and an AC electric field in a very low humidity environment (less than 5% RH). We found that the DC electric field-induced force of two spheres at a fixed separation would increase with time, demonstrating the existence of the Maxwell-Wagner relaxation effect in a novel method and exhibiting the potential of AFM to study dielectric properties of dielectric materials at micro- and/or nanoscale. In addition, our results show that the AC electric field-induced force would not change with the applied frequency ranged from 1 to 100 kHz, implying the crossover frequency of the system we studied is below 1 kHz and the permittivities of the $BaTiO_3$ glass microspheres and the medium (i.e., dry air) dominate the field-induced force. Surprisingly, the AC electric field-induced force is still proportional to the square of the applied electric field strength even when the separation between two spheres is much smaller than the diameter of the microsphere at which the local electric field would be distorted. Compared to the calculated results from the Maxwell-Wagner model that is derived from the concept of the point-dipole approximation, the measured AC field-induced force is much larger especially when the separation between the spheres is very small, indicating that the local electric field around the closely spaces spheres is indeed distorted. We also compared experimental results with other calculated results from Colver's equivalent circuit model. Interestingly, the results from Colver's model are closer to the experimental results than those from the Maxwell-Wagner model while the separation between the spheres is small, implying the field-induced force is a very long-range force than the present theories predict.

There is also an oscillatory component to the field-induced force. This force occurs at a frequency of twice the field frequency and scales with the square of the field amplitude. It is therefore consistent with a DEP force. The amplitude also grows as the separation decreases.

Finally, there is a large adhesion between the particles both in the absence of the field and in the presence of the field. The additional force caused by the field has similar properties to the force at a distance: it is independent of the frequency and scales with the square of the field amplitude. The field is thus a useful method of controllably holding particles together in air.

References

1. Feng, J. Q.; Hays, D. A., Relative importance of electrostatic forces on powder particles. *Powder Technology* **2003,** *135*, 65-75.

2. Rosensweig, R. E., PROCESS CONCEPTS USING FIELD-STABILIZED 2-PHASE FLUIDIZED FLOW. *Journal of Electrostatics* **1995,** *34* (2-3), 163-187.

3. Andres, U., Dielectric separation of minerals. *Journal of Electrostatics* **1996,** *37* (4), 227-248.

4. Hao, T., Electrorheological suspensions. *Advances in Colloid and Interface Science* **2002,** *97* (1-3), 1-35.

5. Parthasarathy, M.; Klingenberg, D. J., Electrorheology: Mechanisms and models. *Materials Science & Engineering R-Reports* **1996,** *17* (2), 57-103.

6. Pethig, R., Review Article-Dielectrophoresis: Status of the theory, technology, and applications. *Biomicrofluidics* **2010,** *4* (2).

7. Jones, T. B., *Electromechanics of Particles*. Cambridge University Press: New York City, NY, 1995.

8. Tombs, T. N.; Jones, T. B., DIGITAL DIELECTROPHORETIC LEVITATION. *Review of Scientific Instruments* **1991,** *62* (4), 1072-1077.

9. Wang, Z. Y.; Peng, Z.; Lu, K. Q.; Wen, W. J., Experimental investigation for field-induced interaction force of two spheres. *Applied Physics Letters* **2003,** *82* (11), 1796-1798.

10. Wang, Z. Y.; Shen, R.; Niu, X. J.; Lu, K. Q.; Wen, W. J., Frequency dependence of a field-induced force between two high dielectric spheres in various fluid media. *Journal of Applied Physics* **2003,** *94* (12), 7832-7834.

11. Wang, Z. Y.; Shen, R.; Niu, X. J.; Sun, G.; Lu, K. Q.; Hou, B.; Wen, W. J., Dielectric dependence of field-induced interspherical force. *Journal of Physics D-Applied Physics* **2005,** *38* (8), 1325-1329.

12. Rankin, P. J.; Klingenberg, D. J., The electrorheology of barium titanate suspensions. *Journal of Rheology* **1998,** *42* (3), 639-656.

13. Mittal, M.; Lele, P. P.; Kaler, E. W.; Furst, E. M., Polarization and interactions of colloidal particles in ac electric fields. *Journal of Chemical Physics* **2008,** *129* (6).

14. Wei, M. T.; Junio, J.; Ou-Yang, H. D., Direct measurements of the frequency-dependent dielectrophoresis force. *Biomicrofluidics* **2009,** *3* (1).

15. Hong, Y.; Pyo, J. W.; Baek, S. H.; Lee, S. W.; Yoon, D. S.; No, K.; Kim, B. M., Quantitative measurements of absolute dielectrophoretic forces using optical tweezers. *Optics Letters* **2010,** *35* (14), 2493-2495.

16. Jonas, A.; Zemanek, P., Light at work: The use of optical forces for particle manipulation, sorting, and analysis. *Electrophoresis* **2008,** *29* (24), 4813-4851.

17. Neuman, K. C.; Nagy, A., Single-molecule force spectroscopy: optical tweezers, magnetic tweezers and atomic force microscopy. *Nature Methods* **2008,** *5* (6), 491-505.

18. Mizes, H. A., ADHESION OF SMALL PARTICLES IN ELECTRIC-FIELDS. *Journal of Adhesion Science and Technology* **1994,** *8* (8), 937-951.

19. Mizes, H.; Ott, M.; Eklund, E.; Hays, D., Small particle adhesion: measurement and control. *Colloids and Surfaces a-Physicochemical and Engineering Aspects* **2000,** *165* (1-3), 11-23.

20. Kwek, J. W.; Vakarelski, I. U.; Ng, W. K.; Heng, J. Y. Y.; Tan, R. B. H., Novel parallel plate condenser for single particle electrostatic force measurements in atomic force microscope. *Colloids and Surfaces a-Physicochemical and Engineering Aspects* **2011,** *385* (1-3), 206-212.

21. Gouveia, R. F.; Galembeck, F., Electrostatic Charging of Hydrophilic Particles Due to Water Adsorption. *Journal of the American Chemical Society* **2009,** *131* (32), 11381-11386.

22. Shamai, R.; Andelman, D.; Berge, B.; Hayes, R., Water, electricity, and between ... On electrowetting and its applications. *Soft Matter* **2008,** *4* (1), 38-45.

23. Gomez-Monivas, S.; Saenz, J. J.; Calleja, M.; Garcia, R., Field-induced formation of nanometer-sized water bridges. *Phys. Rev. Lett.* **2003,** *91* (5).

24. Kao, K. C., *DIELECTRIC PHENOMENA IN SOLIDS: With Emphasis on Physical Concepts of Electronic Processes*. Academic Press: Amsterdam ; Boston, 2004.

25. Laughton, M. A.; Warne, D. F., *Electrical Engineer's Reference*. Newnes: Boston, 2003.

26. Lorrain, P.; Corson, D. R.; Lorrain, F., *Fundamentals of Electromagnetic Phenomena*. W.H. Freeman: New York, 2000.

27. Morgan, H.; Green, N. G., *AC Electrokinetics: colloids and nanoparticles*. Research Studies Press: Philadelphia, PA, 2003.

28. Hao, T.; Kawai, A.; Ikazaki, F., Mechanism of the electrorheological effect: Evidence from the conductive, dielectric, and surface characteristics of water-free electrorheological fluids. *Langmuir* **1998,** *14* (5), 1256-1262.

29. Hughes, M. P., *Nanoelectromechanics in Engineering and Biology*. CRC Press: Boca Raton, Fla, 2003.

30. Nilsson, J. W.; Riedel, S., *Electric Circuits*. 7th ed.; Pearson/Prentice Hall: Upper Saddle River, N.J., 2005.

31. Colver, G. M., An interparticle force model for ac-dc electric fields in powders. *Powder Technology* **2000,** *112* (1-2), 126-136.

32. Bhushan, B.; Fuchs, H., *Applied Scanning Probe Methods*. Springer: Berlin ; New York, 2009; Vol. I-XIII.

33. Butt, H. J.; Cappella, B.; Kappl, M., Force measurements with the atomic force microscope: Technique, interpretation and applications. *Surface Science Reports* **2005,** *59* (1-6), 1-152.

34. Ralston, J.; Larson, I.; Rutland, M. W.; Feiler, A. A.; Kleijn, M., Atomic force microscopy and direct surface force measurements - (IUPAC technical report). *Pure and Applied Chemistry* **2005,** *77* (12), 2149-2170.

35. (a) Fumagalli, L.; Ferrari, G.; Sampietro, M.; Gomila, G., Quantitative Nanoscale Dielectric Microscopy of Single-Layer Supported Biomembranes. *Nano Letters* **2009,** *9* (4), 1604-1608; (b) Gramse, G.; Casuso, I.; Toset, J.; Fumagalli, L.; Gomila, G., Quantitative dielectric constant measurement of thin films by DC electrostatic force microscopy. *Nanotechnology* **2009,** *20* (39).

36. Attard, P., Measurement and interpretation of elastic and viscoelastic properties with the atomic force microscope. *Journal of Physics-Condensed Matter* **2007,** *19* (47).

37. Bhushan, B., *Nanotribology and Nanomechanics*. Springer: Berlin, 2011; Vol. I & II.

38. Sone, H.; Fujinuma, Y.; Hosaka, S., Picogram mass sensor using resonance frequency shift of cantilever. *Japanese Journal of Applied Physics Part 1-Regular Papers Short Notes & Review Papers* **2004,** *43* (6A), 3648-3651.

39. (a) Dagata, J. A.; Perez-Murano, F.; Martin, C.; Kuramochi, H.; Yokoyama, H., Current, charge, and capacitance during scanning probe oxidation of silicon. I. Maximum charge density and lateral diffusion. *Journal of Applied Physics* **2004,** *96* (4), 2386-2392; (b) Dagata, J. A.; Perez-Murano, F.; Martin, C.; Kuramochi, H.; Yokoyama, H., Current, charge, and capacitance during scanning probe oxidation of silicon. II. Electrostatic and meniscus forces acting on cantilever bending. *Journal of Applied Physics* **2004,** *96* (4), 2393-2399.

40. Jalili, N.; Laxminarayana, K., A review of atomic force microscopy imaging systems: application to molecular metrology and biological sciences. *Mechatronics* **2004,** *14* (8), 907-945.

41. Schirmeisen, A.; Anczykowski, B.; Hölscher, H.; Fuchs, H., Dynamic Modes of Atomic Force Microscopy. In *Nanotribology and nanomechanics. Volume 1, Measurement techniques and nanomechanics*, Bhushan, B., Ed. Springer: Berlin ; Heidelberg ; New York 2011; pp 307-353.

42. Garcia, R.; Perez, R., Dynamic atomic force microscopy methods. *Surface Science Reports* **2002,** *47* (6-8), 197-301.

43. Melitz, W.; Shen, J.; Kummel, A. C.; Lee, S., Kelvin probe force microscopy and its application. *Surface Science Reports* **2011,** *66* (1), 1-27.

44. Sadewasser, S., Experimental Technique and Working Modes. In *Kelvin probe force microscopy: measuring and compensating electrostatic forces*, Sadewasser, S.; Glatzel, T., Eds. Springer-Verlag Berlin Heidelberg: Heidelberg ; New York, 2012; pp 7-24.

45. Israelachvili, J., *Intermolecular & surface Forces*. Academic Press London: London ; San Diego 1991.

46. Senden, T. J., Force microscopy and surface interactions. *Current Opinion in Colloid & Interface Science* **2001,** *6* (2), 95-101.

47. Hutter, J. L.; Bechhoefer, J., CALIBRATION OF ATOMIC-FORCE MICROSCOPE TIPS. *Review of Scientific Instruments* **1993,** *64* (7), 1868-1873.

48. Honig, C. D. F.; Ducker, W. A., Squeeze Film Lubrication in Silicone Oil: Experimental Test of the No-Slip Boundary Condition at Solid-Liquid Interfaces. *J. Phys. Chem. C* **2008,** *112* (44), 17324-17330.

49. Figliola, R. S.; Beasley, D. E., *Theory and Design for Mechanical Measurements*. 5th ed.; John Wiley: Hoboken, NJ 2011.

50. Senturia, S. D., *Microsystem Design*. Kluwer Academic Publishers: Boston, 2001.

51. Kaajakari, V., *Practical MEMS: Design of microsystems, accelerometers, gyroscopes, RF MEMS, optical MEMS, and microfluidic systems*. Small Gear Publishing: 2009.

52. Kaler, K.; Jones, T. B.; Paul, R., LOW-FREQUENCY MICROMOTIONS OF DEP-LEVITATED PLANT-PROTOPLASTS .1. *Journal of Colloid and Interface Science* **1995,** *175* (1), 108-117.

53. Zhao, J. H.; Bridges, G. E.; Thomson, D. J., Direct evidence of "spring softening" nonlinearity in micromachined mechanical resonator using optical beam deflection technique. *Journal of Vacuum Science & Technology A* **2006,** *24* (3), 732-736.

54. (a) Data sheet of barium-titanate spheres. Mo-Sci Corporation: Rolla, MO; (b) Robertson, J., High dielectric constant oxides. *European Physical Journal-Applied Physics* **2004,** *28* (3), 265-291.

55. Lunkenheimer, P.; Bobnar, V.; Pronin, A. V.; Ritus, A. I.; Volkov, A. A.; Loidl, A., Origin of apparent colossal dielectric constants. *Physical Review B* **2002,** *66* (5).

56. Whittle, M.; Bullough, W. A.; Peel, D. J.; Firoozian, R., DEPENDENCE OF ELECTRORHEOLOGICAL RESPONSE ON CONDUCTIVITY AND POLARIZATION TIME. *Physical Review E* **1994,** *49* (6), 5249-5259.

57. Chen, Y.; Sprecher, A. F.; Conrad, H., ELECTROSTATIC PARTICLE-PARTICLE INTERACTIONS IN ELECTRORHEOLOGICAL FLUIDS. *Journal of Applied Physics* **1991,** *70* (11), 6796-6803.

58. Bunker, M. J.; Davies, M. C.; James, M. B.; Roberts, C. J., Direct observation of single particle electrostatic charging by atomic force microscopy. *Pharmaceutical Research* **2007,** *24* (6), 1165-1169.